Computer-Aided Measurement of Microwave Circuits

Thesis by

Wyman L. Williams

In Partial Fulfillment of the Requirements

for the Degree of

Doctor of Philosophy

California Institute of Technology

Pasadena, California

1989

(Submitted November 22, 1988)

To my Mother

Acknowledgements

Many thanks to my advisor, Dave Rutledge, for his wealth of ideas, his encouragement and support. His guidance has been of inestimable value in making my time at Caltech interesting and productive.

I would also like to thank the Fannie and John Hertz Foundation for support during my graduate study.

For many stimulating ideas of both a technical and highly non-technical nature, my thanks go to Wade Regehr, Rick Compton, Matt Johnson, Doug Johnson, Scott Wedge and Dean Neikirk. Thanks to Kent Potter for his ideas and advice on fabrication and measurement techniques. For their helpful discussions on a wide range of engineering topics, my thanks to Arthur Sheiman, Bobby Weikle, Zoya Popović, Phil Stimson and Dayalan Kasilingam. Thanks to Fred Charette for his guidance in the business aspects of engineering.

I am indebted to Barry Allen for introducing me to the microwave game, and for many interesting discussions over the years. Thanks to Sandy Weinreb for a very educational summer at NRAO, and for his helpful discussions since.

For their friendship and help in maintaining my sanity during my stay at Caltech, I thank Rich Rand, Pete and Patty Felker, Jim Garvey, Kerry Walzl, Ruth Erlanson, Charlie and Barbara Lawrence and Clint Dodd.

Thanks to Marcy Levinson for all she has shared with me, and thanks to my mother and sister for their love and encouragement always.

Computer-Aided Measurement of Microwave Circuits

Abstract

Instruments that measure the scattering parameters of microwave circuits generally have large systematic errors due to unavoidable parasitics in the instruments. These errors can be modeled analytically, however, and removed through a calibration procedure. A personal computer is well suited to the performance of the required calculations. Combining a personal computer with a microwave network analyzer results in a flexible and accurate automatic instrument. Two such automatic network analyzers are presented here. A new type of network analyzer, known as a sampled-line network analyzer is presented. It is an extension of the six-port network analyzer concept developed at the National Bureau of Standards. It is a particularly simple implementation and shows promise for the construction of relatively low-cost microwave network analyzers. The sampled-line network analyzer is analyzed theoretically and several experimental versions of it are presented. Another personal computer-controlled network analyzer is presented in which a Pascal program automates an HP 8410 network analyzer. The result is an instrument which can measure S-parameters from 0.5 to 18 GHz with a measurement error vector ranging in magnitude from 0.01 in the low frequency range to about 0.03 at 18 GHz.

Contents

List of Figures

List of Tables

Chapter 1

Introduction

The microwave frequency range of the electromagnetic spectrum is generally considered to extend from 300 MHz to 30 GHz. Microwaves propagate through the Earth's atmosphere with little attenuation or ionospheric refraction and their short wavelengths (1 m to 1 cm) allow reasonably small antennas to form highly directional microwave beams.

For these reasons, microwaves are used in a wide variety of communications systems and radars. A large fraction of the USA's domestic long distance telephone traffic goes by terrestrial microwave radio, and microwave satellite relays link the continents. Ground-based microwave radars are instrumental in the safe conduct of civilian aviation, and airborne radars in military aircraft allow them to operate in low-visibility hostile environments. Microwaves are also used to track and communicate with spacecraft in Earth orbit and in deep space.

In addition, fiber optic communications systems and some high speed digital computers have achieved data rates so high that microwave design techniques must be used in laying out their circuits. The now-ubiquitous microwave oven has brought microwave technology into the home.

The design of microwave circuits to serve these applications presents the engineer with problems not encountered at lower frequencies. Parasitic reactances can load the circuits heavily, so it is generally not feasible to probe a circuit at an arbitrary point, as with an oscilloscope. Also, a circuit board might be several

wavelengths across at the design frequency, so propagation delays and transmission line effects cannot be neglected, even at the board level. The microwave engineer must consider signals as travelling wave quantities propagating around the circuit on wave guiding structures.

Components to be used in a microwave circuit are thus best characterized in terms of their interactions with travelling waves and transmission lines. The scattering- or S-parameters describe networks in these terms. A network analyzer measures the S-parameters of unknown devices.

Figure 1.1 shows a microwave two-port and the definition of its S-parameters. S-parameters are defined in terms of normalized travelling voltage waves, as outlined in the figure caption.

$$b_1 = S_{11}a_1 + S_{12}a_2$$
$$b_2 = S_{21}a_1 + S_{22}a_2$$

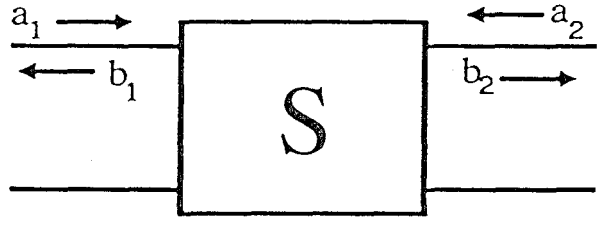

Figure 1.1 S-parameters of a linear two-port network. The S-parameters are defined in terms of the travelling wave quantities a and b where $a \equiv V^+/\sqrt{2\,\mathrm{Re}\,Z_0}$ and $b \equiv V^-/\sqrt{2\,\mathrm{Re}\,Z_0}$. V^+ and V^- are the travelling voltage wave amplitudes. Thus $|a|^2$ gives the power propagating in the + direction on the line, and $|b|^2$ gives that in the − direction.

1.1 Historical Perspective

In 1888, Heinrich Hertz performed the first known microwave measurement. Hertz used a spark discharge in a tuned circuit to generate and radiate $\sim 100\,\mathrm{MHz}$ electromagnetic waves. He placed a parabolic reflector some distance from this source. A receiving loop with a second spark gap was his test probe, and with it he observed the standing wave pattern between the source and reflector as he walked between them. With the data from this experiment, Hertz showed that electromagnetic energy propagates as waves in space at the velocity of light, giving experimental support to Maxwell's electromagnetic wave theory, published in 1864.

Hertz's basic experimental technique, measuring the maxima and minima of a standing wave pattern, was the primary method of microwave network measurement until the mid 1950's. The device used was the slotted transmission line. In the slotted line, a small probe inserted through a slot in the wall of a waveguide or coaxial line capacitively samples the standing wave pattern as it moves along the line. By comparing this pattern to that resulting from a known standard such as a short circuit at the reference plane, the reflection coefficient of the network connected at the reference plane was calculated.

During WW II, work was done on waveguide directional couplers for microwave frequencies, as described by Kyhl [1] in the MIT Radiation Laboratory series. In the mid 1950's, Hewlett-Packard used such couplers to construct a family of microwave reflectometers, as described by Hunton and Pappas [2]. These reflectometers measured only the magnitude of the reflection coefficient, but they gave a direct reading of this magnitude, allowing swept frequency measurements of reflection coefficients to be made easily.

In the late 1950's and early 1960's, workers in several laboratories [3–5] presented systems that used heterodyning schemes to measure both the magnitude and phase of reflection and transmission coefficients. These instruments gave

direct readings of the measured complex quantities and were capable of swept frequency measurement.

In 1967, Hewlett-Packard introduced such a system commercially. Known as the 8410, it used a sampling mixer and a phase-locked loop to track the frequency of the test and reference signals. The two signals were mixed down in frequency, and magnitude and phase comparisons were performed directly by analog circuitry. These ratios could be displayed in several formats on a CRT. When used with a precision network of directional couplers and switches, the 8410 performed swept frequency S-parameter measurements, with accuracy limited by the performance of the directional coupler network. The 8410 won wide acceptance in the microwave engineering community, making complex S-parameter measurement available in a large number of laboratories for the first time.

The HP 8410 was also sold bundled with a digital computer and software. This package, known as the 8409, allowed calibration of the systematic errors in the network analyzer. It was the first commercial instrument to use computer error-corrected measurement techniques to give highly accurate S-parameter measurements.

In 1984, Hewlett-Packard introduced the 8510 network analyzer. This unit uses the same heterodyning scheme as in the 8410, but incorporates several powerful digital processors to allow the calibration and error correction functions to be performed by the instrument itself. Other manufacturers, including Wiltron and EIP, have since introduced similar products.

While work on these network analyzers was proceeding in the mid 1970's, workers at the National Bureau of Standards [6–8] introduced the "six-port" network analyzer technique. This technique allowed the measurement of the complex S-parameters of a network without the use of a heterodyning scheme. The six-port, in fact, uses only a passive linear network and an ensemble of power

detectors. The simplicity of the six-port makes possible the characterization of all its sources of error in a fairly straightforward calibration procedure. With these calibration coefficients stored in a digital computer, the six-port can make highly accurate error-corrected measurement. Workers at NBS have developed a number of ingenious algorithms that allow calibration of the six-port with a minimum of precisely known impedance standards. The NBS six-ports are the standard network analyzers against which other analyzers are compared.

The six-port type of network analyzer was first actually discussed as long ago as 1947 [9]. At that time, though, the digital computers needed to realize the full potential of the approach did not exist.

The sampled-line network analyzer discussed in this thesis is an outgrowth of the six-port network analyzer. It uses a simpler circuit configuration than that used in the NBS analyzer, and a larger number of detectors. The larger number of detectors increases system reliability, provides new options for the calibration and measurement algorithms, and holds the potential for very high accuracy.

1.2 Organization of the Thesis

The thesis is broken up into two sections. The first section, including chapters 2–4, is the theoretical section. The second section, consisting of the remaining chapters, presents experimental results.

Chapter 2 presents the theoretical background for the four-port network analyzer, of which the HP 8410 and 8510 are examples. Some results of interest for all network analyzers are developed here and are carried forward in the following chapters.

Chapter 3 presents six-port network analyzer theory. Since the sampled-line analyzer is an extension of the six-port concept, this chapter provides background for description of the sampled-line.

In Chapter 4 a theoretical analysis of the sampled-line analyzer is presented. Extensions of the six-port theory are given, as well as analyses of the sampled-line structure itself as it applies to construction of a network analyzer.

Chapter 5 describes the Elf network analyzer system. Elf consists of an HP 8410 network analyzer, an IBM personal computer, some interface circuitry and a 3000-line Pascal program. The Elf program controls the network analyzer and a signal generator, allowing calibration of the network analyzer and error correction of the measured data.

In Chapter 6, the various versions of the sampled-line network analyzer that have been built to date are presented. Designs and characterizations of the analyzers, as well as sample measurements are presented.

In Chapter 7, suggestions for further work on the sampled-line network analyzer are presented.

References

[1] C.C. Montgomery, Ed., *Technique of Microwave Measurements* (MIT Radiation Laboratory Series, vol. 11) New York: McGraw-Hill, 1947, chap. 11

[2] J.K. Hunton and N.L. Pappas, "The H-P microwave reflectometers," *Hewlett-Packard J.*, vol. 6, nos. 1–2, Sept.–Oct. 1954

[3] P. Lacy, "Automated measurement of phase and transmission characteristics of microwave amplifiers," in *IEEE Int. Conv. Rec.*, pt. 3, Mar. 1963, pp. 119-125

[4] D. Leed and O. Kummer, "A loss and phase set for measuring transistor parameters and two-port networks between 5 and 250 mc," *Bell Sys. Tech. J.*, vol. 40, no. 3, pp. 841–884, May 1961

[5] S.B. Cohn and N.P. Weinhouse, "An automatic microwave phase measurement system," *Microwave J.*, vol. 7, no. 2, pp. 49–56, Feb. 1964

[6] C.A. Hoer and K.C. Roe, "Using an arbitrary six-port junction to measure complex voltage ratios," *IEEE Trans. Microwave Theory Tech.*, vol. MTT-23, pp. 978–984, Dec. 1975

[7] C.A. Hoer, "Using six-port and eight-port junctions to measure active and passive circuit parameters," *Nat. Bur. Stand. Tech. Note* 673, Sept. 1975

[8] G.F. Engen, "The six-port reflectometer: An alternative network analyzer," in *1977 IEEE Mtt-S Int. Microwave Symp. Dig.*, June 1977, pp. 44–45, 53–55

[9] A.L. Samuel, "An oscillographic method of presenting impedances on the reflection coefficient plane," *Proc. IRE,* vol. 35, pp. 1279–1283, Nov. 1947

[10] S.F. Adam, "Microwave instrumentation: An historical perspective," *IEEE Trans. Microwave Theory Tech.*, vol. MTT-32, no. 9, pp. 1157–1161, Sept. 1984

[11] H. Sobol, "Microwave communications–An historical perspective," *IEEE Trans. Microwave Theory Tech.*, vol. MTT-32, no. 9, pp. 1170–1181, Sept. 1984

Chapter 2

Four-Port Network Analyzer Theory

The job a network analyzer must perform can be stated quite simply. The parameters are shown in figure 2.1. Two travelling voltage waves, a and b, propagate in opposite directions on a transmission line. At a particular point on the line, known as the reference plane, the network analyzer measures the amplitude ratio and phase difference between these two (sinusoidal) waves.

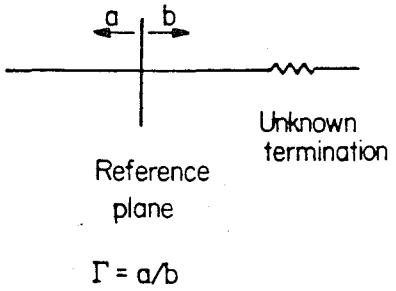

Figure 2.1 The normalized scattering waves a and b are related to the forward-going and reverse-going voltage waves V^+ and V^- on the transmission line by $a = V^+/\sqrt{2Z_0}$ and $b = V^-/\sqrt{2Z_0}$ where Z_0 is the characteristic impedance of the transmission line. Thus, Γ is the voltage reflection coefficient, $\Gamma = V^+/V^-$.

The ability to measure this complex ratio, for a set of transmission lines connected to the ports of an unknown microwave network, allows the network analyzer to determine the complete S-parameters of that network. The machinations required to derive all the S-parameters from a given set of measurements,

however, become more elaborate as the number of ports on the unknown network increases.

Machines that measure the complex ratio of travelling waves fall into two categories. The first type is built by combining a linear four-port network with a vector voltmeter, and the second uses a six-port network and several power detectors.

The four-port network analyzer was the first developed, and forms the basis of most of the currently available commercial network analyzers. In this chapter, the theory of operation of the four-port network analyzer will be presented. The theories of operation of the six-port and sampled-line network analyzers build upon this theory, and assumptions made in developing the four-port theory are germane to comparisons of performance of the various network analyzer approaches.

2.1 Reflection Measurements with the 4-Port Network Analyzer

The reflection measurement is the simplest network analyzer measurement. As shown in figure 2.1, only an unknown impedance and two travelling wave quantities are involved. The unknown impedance is connected to the end of a transmission line. The voltage wave a, travelling on the line impinges on the unknown device. The travelling wave b, resulting from the impedance mismatch between the unknown device and the transmission line, is reflected back along the line. By measuring the amplitude ratio and phase difference between the incident and reflected waves at a fixed reference plane, the complex reflection coefficient, Γ of the unknown device is determined. This, along with knowledge of the characteristic impedance of the transmission line, is sufficient to determine the unknown impedance.

Figure 2.2 shows schematically how a vector voltmeter and a pair of matched directional couplers can be combined to yield a four-port reflectometer (the box containing the two couplers forms the "four-port" for which the analyzer is named). The vector voltmeter is a frequency-tracking heterodyne receiver that indicates the complex ratio of the two microwave signals presented at its inputs.

One directional coupler samples the forward-going wave, and the other the reflected wave. If the directional couplers are matched and have perfect directivity, and if port 2 presents a source impedance of exactly Z_0 to the device under test, then $b_3/b_4 = a_2/b_2 = \Gamma$ and the value indicated by the vector voltmeter will be the true reflection coefficient.

These conditions are stringent, however, and even with the best designs imperfections in the components give rise to large errors. With the Hewlett-Packard 8743B reflection-transmission test unit, for example, in the 2–8 GHz frequency range, magnitude errors of ± 0.15 are possible when measuring reflection coefficients of unity magnitude.

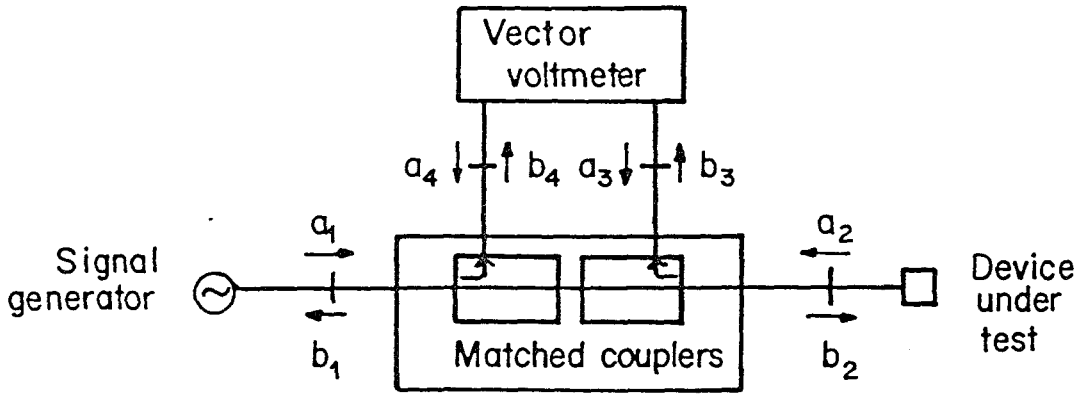

Figure 2.2 The four-port network analyzer, uses a vector voltmeter and a pair of matched directional couplers to measure the reflection coefficient.

These large errors, however, are systematic and can be calibrated out by measuring known calibration standards. The calibration procedure and the number of standards required are determined by the relationship between the true and indicated values of Γ. This relationship can be found in a straightforward way by adapting Middlebrook's extra element theorem [1] to travelling wave network parameters.

Consider the four-port network analyzer of figure 2.3. Here the dual directional couplers of figure 2.2 have been replaced by an arbitrary linear four-port. Also, offset and gain terms have been added to the response of the vector voltmeter.

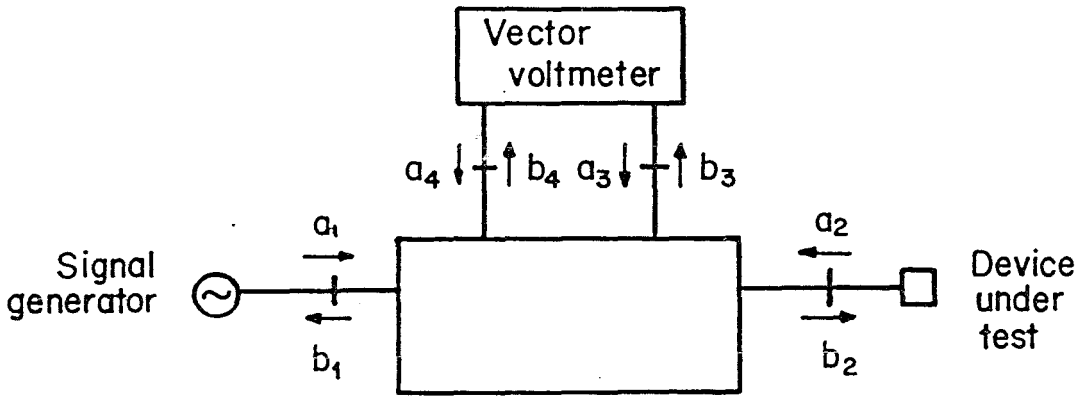

Figure 2.3 This four-port network analyzer uses a vector voltmeter and an arbitrary linear four-port network to measure the reflection coefficient. If b_3/b_4 exists, it is just a bilinear transform of Γ.

By superposition,

$$b_4 = K_1 a_1 + K_2 a_2 \tag{2.1}$$

$$b_3 = L_1 a_1 + L_2 a_2 \tag{2.2}$$

$$b_2 = M_1 a_1 + M_2 a_2 \tag{2.3}$$

By definition, $a_2 = \Gamma b_2$. Inserting this in (2.1–2.3) and solving (2.3) for b_2 gives

$$b_4 = K_1 a_1 + K_2 \Gamma b_2 \tag{2.4}$$

$$b_3 = L_1 a_1 + L_2 \Gamma b_2 \tag{2.5}$$

$$b_2 = \frac{M_1}{1 - M_2 \Gamma} a_1 \tag{2.6}$$

Substituting (2.6) into (2.4) and (2.5) gives

$$b_4 = \frac{K_1 + (M_1K_2 - M_2K_1)\Gamma}{1 - M_2\Gamma} a_1 \tag{2.7}$$

$$b_3 = \frac{L_1 + (M_1L_2 - M_2L_1)\Gamma}{1 - M_2\Gamma} a_1 \tag{2.8}$$

Dividing (2.8) by (2.7) gives

$$\frac{b_3}{b_4} = \frac{L_1 + (M_1L_2 - M_2L_1)\Gamma}{K_1 + (M_1K_2 - M_2K_1)\Gamma} \tag{2.9}$$

Finally, including the response of the vector voltmeter, $\Gamma' = c_0 + c_1 b_3/b_4$ and dividing the numerator and denominator through by the coefficient of Γ in the numerator gives

$$\Gamma' = \frac{\Gamma + A}{B\Gamma + C} \tag{2.10}$$

So the final result is that the value Γ' indicated on the vector voltmeter is a bilinear transform of the actual value of Γ. The bilinear transform has three complex constants, so three known standards must be measured in order to determine the calibration coefficients, and thereafter correct the measured data.

The calibration procedure is straightforward. Multiplying (2.10) through by the denominator of the right side gives

$$-A + \Gamma\Gamma'B - \Gamma'C = -\Gamma \tag{2.11}$$

which is a linear equation in A, B, and C. By observing Γ' for three different known values of Γ, the coefficients of three such equations are determined, and the values of A, B, and C can be determined. The true value of Γ is then found by inverting the transform:

$$\Gamma = \frac{C\Gamma' - A}{1 - B\Gamma'} \tag{2.12}$$

The above result is interesting in several respects. The first is its generality. Any four-port network that is linear, and for which the ratio of (2.10) exists, can

be used as a network analyzer and calibrated by measuring three known standards. Also, the fact that Γ' is a ratio measurement makes the result independent of the level of the test signal injected at port 1 and thus the source impedance of the generator.

The fact that Γ' is a bilinear transform of Γ allows the systematic errors of the system to be modeled in a simple way. Figure 2.4 shows the error model. It consists of an ideal network analyzer with an "error two-port" between the ideal analyzer's reference plane and the device under test. The fact that this gives rise to the same relationship between observed and actual values as that derived above can be seen by considering the T-parameters of the error two-port.

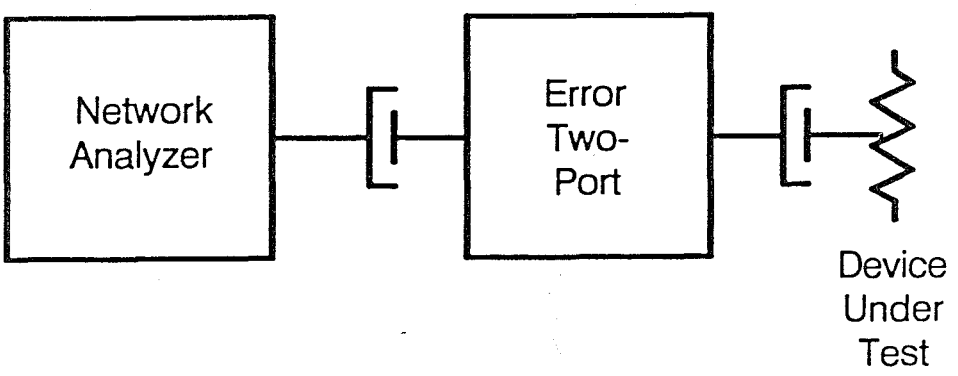

Figure 2.4 Errors in the reflection measurement can be modeled by an error 2-port between the reflectometer and the device under test.

$$b_1 = T_{11}a_2 + T_{12}b_2 \tag{2.13}$$

$$a_1 = T_{21}a_2 + T_{22}b_2 \tag{2.14}$$

$$\Gamma' = \frac{b_1}{a_1} = \frac{T_{11}a_2 + T_{12}b_2}{T_{21}a_2 + T_{22}b_2} \tag{2.15}$$

$$= \frac{T_{11}\Gamma + T_{12}}{T_{21}\Gamma + T_{22}} \tag{2.16}$$

For a practical system $T_{11} \neq 0$ and dividing the numerator and denominator of (2.16) through by T_{11} gives (2.10).

This error model can be represented by the signal flow graph of figure 2.5. The graph is labeled with three error terms that are often quoted for reflectometers. They are related to the physical sources of error in the dual-coupler type reflection test set. E_D is the directivity error, related to the imperfect directivity of the couplers in the test set. E_S is the source match error, related to the impedance mismatch at the measurement port of the test set. Lastly, E_R is the frequency response error, related to differences in the frequency responses of the two directional couplers.

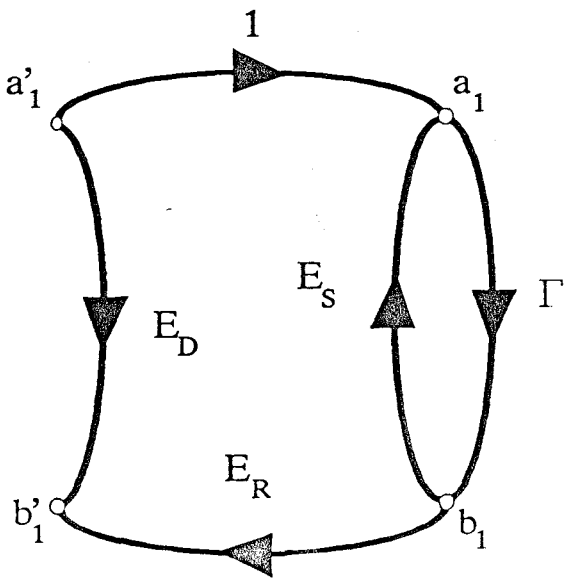

Figure 2.5 Signal flow graph for errors in the reflection measurement.

In terms of these quantities, the relation between Γ and Γ' can be found through Mason's gain rule as

$$\Gamma' = E_D + \frac{E_R\Gamma}{1 - E_S\Gamma} \tag{2.17}$$

$$= \frac{E_D + (E_R - E_SE_D)\Gamma}{1 - E_S\Gamma} \tag{2.18}$$

In practical systems, the greatest errors typically arise from the source mismatch error, when Γ is near unity in magnitude.

In modern network analyzers, built-in computers store the calibration constants and perform the bilinear transform to display the corrected reflection coefficient. Specifications are still often quoted, however, in terms of *effective* directivity, source match, etc. This method of specification makes sense due to a property of the bilinear transform: if Γ' is a bilinear transform of Γ, and Γ'' is a bilinear transform of Γ', then Γ'' is a bilinear transform of Γ. Thus, if there are errors in determination of the calibration coefficients above, and the transform is applied to the measured data, one may still be assured that the result is a bilinear transform of the true Γ, and *this* bilinear transform can be classified in terms of the quantities on a signal flow graph like that of figure 2.5.

If it is assumed that perfect calibration standards are used, and the terms of the bilinear transform are found without error, then the only sources of error remaining in the system are those due to noise and nonlinearities in the vector voltmeter.

In the vector voltmeter, the test and reference microwave signals are down-converted to intermediate frequencies of a few MHz or hundreds of kHz by a sampling mixer. At the i-f, the test signal is split into two components, one in phase with the reference signal and one in quadrature with it. From these two components, the real and imaginary parts of the complex ratio are derived. If the gains of the two channels for the test signal are not precisely matched, or if the

quadrature signal is not truly orthogonal to the in-phase signal, then errors will result which cannot be calibrated out by the linear procedures described above.

Since the i-f circuitry needs only to be adjusted for operation at a single frequency, however, sufficient precision can be achieved. In modern computer-corrected network analyzers, the errors due to these nonlinearities are less than the errors resulting from lack of repeatability of the microwave connectors used to connect the device under test to the network analyzer. This lack of repeatability — the inability to exactly match all the connectors on all the calibration standards — is the factor limiting accuracy of reflection measurements with these analyzers.

2.2 S-Parameter Measurements with the 4-Port Network Analyzer

The situation is a bit more complicated when the S-parameters of an unknown two-port are to be measured. Transmission as well as reflection must be measured. A setup for making this measurement is shown in figure 2.6. This is the configuration used in the Hewlett-Packard 8743B reflection-transmission test set, and in the Elf system, which will be discussed in a later chapter.

The test set contains a reflectometer like that described above. Port 1 of the device under test is connected to this reflectometer test port. Another port, the "transmission return" receives the signal emerging from port 2. A coaxial relay selects which signal is presented to the vector voltmeter for the complex ratio measurement. To perform a full S-parameter measurement, the unknown two-port must be flipped end-for-end once during the measurement, and the coaxial relay switched each time to observe the reflection at both the network's ports, and the transmission through it in both directions.

This gives a total of four measurements. Expressions will be derived here for the values indicated by the vector voltmeter for each of these measurements in terms of the S-parameters of the device under test. These will then be inverted to yield expressions for these S-parameters in terms of the measured quantities.

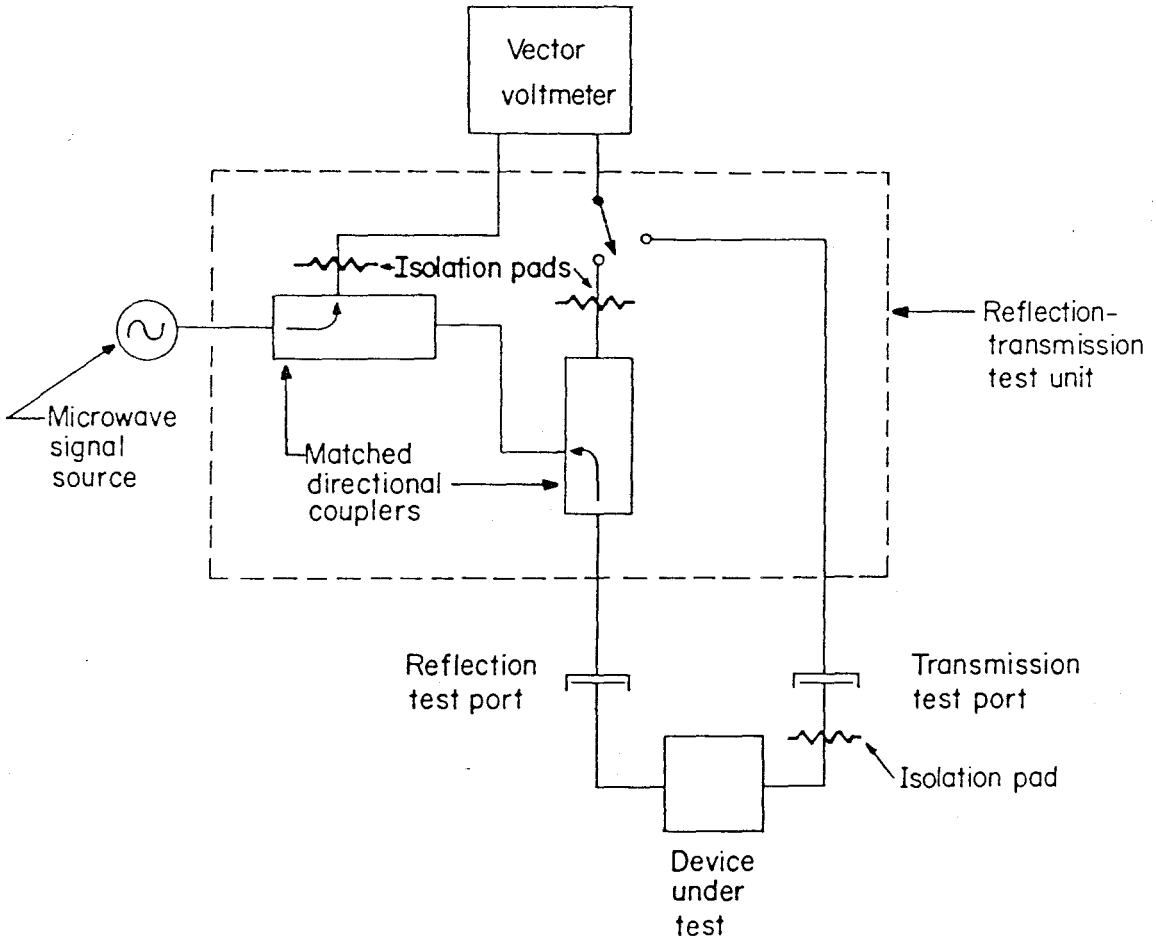

Figure 2.6 A reflection-transmission test set for full S-parameter measurements using a 4-port network analyzer

The reflection measurement is the same as that described in the previous section, except that here the measurement is of the reflection coefficient of port 1 of the two-port with its port 2 terminated in Γ_L, the impedance of the transmission return. This reflection coefficient, Γ_1 is given by

$$\Gamma_1 = S_{11} + \frac{S_{12}S_{21}\Gamma_L}{1 - S_{22}\Gamma_L} \tag{2.19}$$

where the S-parameters are those of the 2-port that is being measured. Substituting this into equation (2.10) yields

$$S'_{11} = \frac{(S_{11} + \frac{S_{12}S_{21}\Gamma_L}{1-S_{22}\Gamma_L}) + A}{B(S_{11} + \frac{S_{12}S_{21}\Gamma_L}{1-S_{22}\Gamma_L}) + C} \tag{2.20}$$

$$= \frac{(S_{11} - \Gamma_L\Delta) + A(1 - S_{22}\Gamma_L)}{B(S_{11} - \Gamma_L\Delta) + C(1 - S_{22}\Gamma_L)} \tag{2.21}$$

where S'_{11} is the value indicated by the vector voltmeter and $\Delta \equiv S_{11}S_{22} - S_{12}S_{21}$ is the system determinant of the two-port being measured.

When performing the transmission measurement, port 2 of the device under test is connected directly to the vector voltmeter, so the meter measures b_5/b_4. To derive an expression for b_5/b_4, equation (2.6) is first rearranged to give

$$a_1 = \frac{1 - M_{2T}\Gamma}{M_{1T}} b_2 \tag{2.22}$$

The subscript "T" is added to the coefficients of this expression because, in general, when the coaxial switch is moved from the reflection to the transmission position, the values of the K's, L's and M's in equations (2.1–2.8) will change, due to a change in the reflection coefficient seen looking out port 3 of the four-port network. The value of Γ_L, the reflection coefficient of the transmission return, will also change in general when this switch is moved, to a value of Γ_{LT}.

This noted, the derivation of b_5/b_4 continues by substituting (2.22) into (2.4) to give

$$b_4 = \frac{1}{M_{1T}}[K_{1T} + (M_{1T}K_{2T} - M_{2T}K_{1T})\Gamma]b_2 \tag{2.23}$$

$$= P(B_T\Gamma + C_T)b_2 \tag{2.24}$$

where B_T and C_T have the same functional form as B and C in equation (2.10), but with T subscripts on the L's and M's.

The value of Γ in (2.22–2.24) above is the reflection coefficient looking into port 1 of the two-port being measured when its second port sees Γ_{LT}. Using (2.19), the expression for b_4 can be expanded to give

$$b_4 = P[B_T(S_{11} + \frac{S_{12}S_{21}\Gamma_{LT}}{1 - S_{22}\Gamma_{LT}}) + C_T]b_2 \tag{2.25}$$

An expression for b_5 can be written in terms of b_2, as well:

$$b_5 = \frac{NS_{21}}{1 - S_{22}\Gamma_{LT}}b_2 \tag{2.26}$$

where N is the gain of the path from the transmission return port to the vector voltmeter's port.

Dividing (2.26) by (2.25) gives

$$\frac{b_5}{b_4} = \frac{1}{P}\frac{\frac{NS_{21}}{1-S_{22}\Gamma_{LT}}}{B_T(S_{11} + \frac{S_{12}S_{21}\Gamma_{LT}}{1-S_{22}\Gamma_{LT}}) + C_T} \tag{2.27}$$

$$= \frac{1}{P}\frac{NS_{21}}{B_T(S_{11} - \Gamma_{LT}\Delta) + C_T(1 - S_{22}\Gamma_{LT})} \tag{2.28}$$

Applying the offset and gain terms of the vector voltmeter ($S'_{21} = c_0 + c_1 b_5/b_4$) gives

$$S'_{21} = D + \frac{ES_{21}}{B_T(S_{11} - \Gamma_{LT}\Delta) + C_T(1 - S_{22}\Gamma_{LT})} \tag{2.29}$$

where S'_{21} is the value indicated by the vector voltmeter when the coaxial switch is in the transmission measurement position. Equations (2.21) and (2.29) are two equations in the unknown S-parameters resulting from the measurements. Flipping the two-port under test end for end and measuring it in the reverse direction yields two more equations.

$$S'_{22} = \frac{(S_{22} - \Gamma_L\Delta) + A(1 - S_{11}\Gamma_L)}{B(S_{22} - \Gamma_L\Delta) + C(1 - S_{11}\Gamma_L)} \tag{2.30}$$

$$S'_{12} = D + \frac{ES_{12}}{B_T(S_{22} - \Gamma_{LT}\Delta) + C_T(1 - S_{11}\Gamma_{LT})} \tag{2.31}$$

Equations (2.21) and (2.29–2.31) give four equations in the four unknown S-parameters. Unfortunately, these equations are nonlinear, and cannot be inverted in closed form to give the S-parameters [2]. This difficulty is removed, however, if Γ_L, B and C do not change when the vector voltmeter is switched from reflection to transmission measurement. Taking $\Gamma_{LT} = \Gamma_L$, $B_T = B$ and $C_T = C$ the above equations can be solved (see Appendix). This inversion yields expressions for the true S-parameters in terms of the measured values:

$$S_{11} = \frac{E^2(A - CS'_{11})(BS'_{22} - 1) - \Gamma_L(AB - C)^2(S'_{12} - D)(S'_{21} - D)}{E^2(BS'_{11} - 1)(BS'_{22} - 1) - \Gamma_L^2(AB - C)^2(S'_{12} - D)(S'_{21} - D)} \quad (2.32)$$

$$S_{12} = \frac{E(AB - C)(S'_{12} - D)[(BS'_{11} - 1) - \Gamma_L(A - CS'_{11})]}{E^2(BS'_{11} - 1)(BS'_{22} - 1) - \Gamma_L^2(AB - C)^2(S'_{12} - D)(S'_{21} - D)} \quad (2.33)$$

$$S_{21} = \frac{E(AB - C)(S'_{21} - D)[(BS'_{22} - 1) - \Gamma_L(A - CS'_{22})]}{E^2(BS'_{11} - 1)(BS'_{22} - 1) - \Gamma_L^2(AB - C)^2(S'_{12} - D)(S'_{21} - D)} \quad (2.34)$$

$$S_{22} = \frac{E^2(A - CS'_{22})(BS'_{11} - 1) - \Gamma_L(AB - C)^2(S'_{12} - D)(S'_{21} - D)}{E^2(BS'_{11} - 1)(BS'_{22} - 1) - \Gamma_L^2(AB - C)^2(S'_{12} - D)(S'_{21} - D)} \quad (2.35)$$

In order to use these closed-form solutions and avoid an iterative calculation at each frequency point of the measurement, the hardware of the system is engineered to isolate the detector switch from the RF measurement ports of the analyzer. Attenuators are placed between the four-port network and the vector voltmeter, and between port 2 of the device under test and the transmission return port, as indicated in figure 2.6. Also, the input port of the vector voltmeter is matched to the line as well as possible, and switches that terminate unselected lines in 50-Ω are used.

With the assumption of switch-independence, then, only six complex constants, A, B, C, D, E, and Γ_L are required to model the linear systematic errors of the reflection-transmission test set. The error model for the test set can again be drawn as a signal flow graph, as shown in figure 2.7. The three error terms noted above have not changed, but three new ones have been added. E_L is the

load mismatch term, related to the mismatch of the transmission return port of the analyzer. E_T is the gain of the transmission return path. E_X is related to the vector voltmeter's offset term. The results above can be rewritten in terms of this error model to give

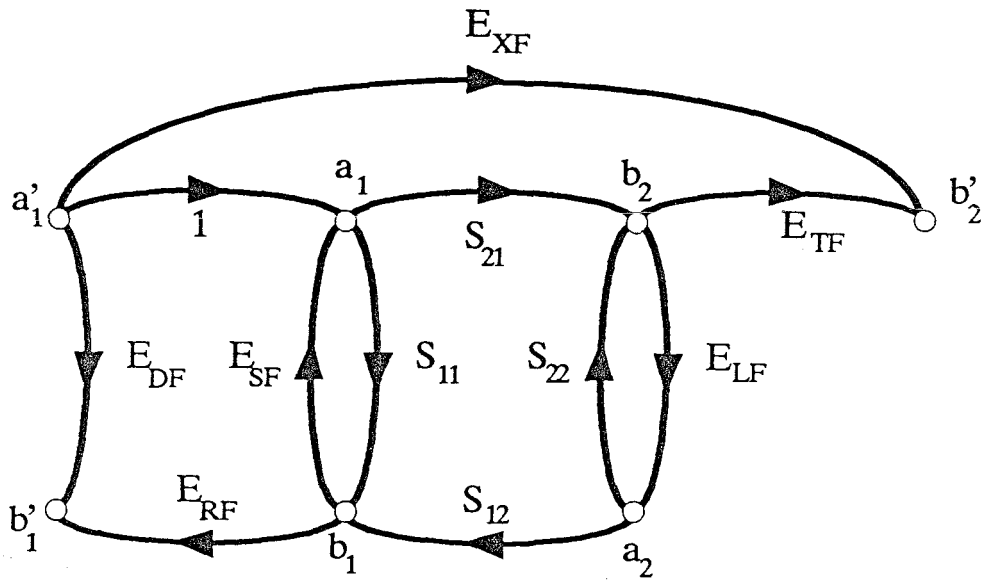

Figure 2.7 This flow graph shows the error model for the reflection-transmission test set.

$$S_{11} = \frac{\{(\frac{S'_{11}-E_D}{E_R})[1+(\frac{S'_{22}-E_D}{E_R})E_S]\} - [(\frac{S'_{21}-E_X}{E_T})(\frac{S'_{12}-E_X}{E_T})E_L]}{[1+(\frac{S'_{11}-E_D}{E_R})E_S][1+(\frac{S'_{22}-E_D}{E_R})E_S] - [(\frac{S'_{21}-E_X}{E_T})(\frac{S'_{12}-E_X}{E_T})E_L^2]} \quad (2.36)$$

$$S_{21} = \frac{[1+(\frac{S'_{22}-E_D}{E_R})(E_S-E_L)](\frac{S'_{21}-E_X}{E_T})}{[1+(\frac{S'_{11}-E_D}{E_R})E_S][1+(\frac{S'_{22}-E_D}{E_R})E_S] - [(\frac{S'_{21}-E_X}{E_T})(\frac{S'_{12}-E_X}{E_T})E_L^2]} \quad (2.37)$$

with similar results for S_{12} and S_{22}.

So six complex constants (at each frequency of interest) are sufficient to completely characterize the errors of this type of network analyzer. These constants are found by measuring six known standards.

In addition to the assumption of switch-independence, another assumption has been made to arrive at the result above. It is assumed that the only coupling between the reflection and transmission test ports is through the network under test: there are no RF leakage paths (the "leakage path" that gives rise to the D term in (2.29) is in fact just a result of the offset term in the vector voltmeter's response). The assumption of no RF leakage is good in most systems, since coaxial relays, which have very high isolation, are typically used to switch the signal paths. If significant leakage paths do exist, the expressions above are invalid and the closed-form solution impossible.

Finally, for the sake of thoroughness, figure 2.8 shows the architecture of a full S-parameter test set. This is the configuration used in such state-of-the-art network analyzers as the Hewlett-Packard 8510. It consists essentially of two transmission-reflection test sets of the type just discussed placed back to back. Another coaxial switch selects which end of the setup receives the test signal. Thus, there is no need to flip the device under test end for end. This improves measurement speed and accuracy. As long as the detector switch is isolated from the network as described above, an analysis similar to that above can be performed to yield closed-form expressions for the S-parameters. The analysis is essentially performed twice, once for each position of the source switch. The result is two signal flow graphs like that of figure 2.7, and an error model which contains twelve complex constants. This is the "full twelve term error model" which is often mentioned in connection with these analyzers.

So in summary, four-port type network analyzers measure the S-parameters of two-ports by using a single vector voltmeter with an arrangement of switches and directional couplers to route the appropriate signals to the voltmeter. As long as the networks used satisfy requirements of switch independence and isolation, the S-parameters of the unknown device can be found from the measured data.

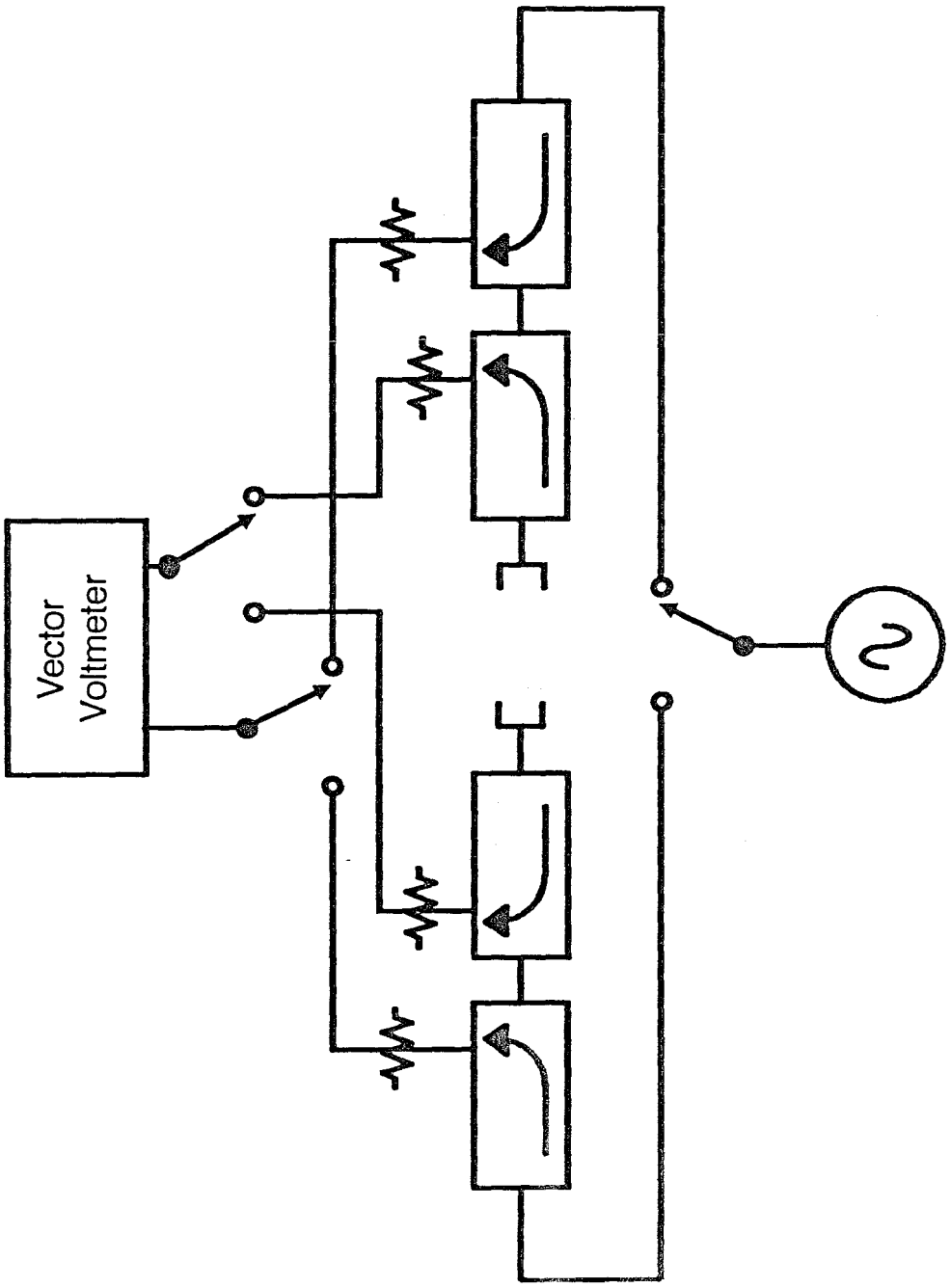

Figure **2.8** A full S-parameter test set using the 4-port network analyzer

As will be seen in the next chapter, things are simplified somewhat if two vector voltmeters are included in the system, and the number of switches reduced. This is the approach taken when six-port network analyzers are used to measure S-parameters.

References

[1] R.D. Middlebrook, *EE 114. Electronic Circuit Design,* Course Notes, California Institute of Technology, 1984–85 academic year

[2] A.A.M. Saleh, "Explicit formulas for error correction in microwave measuring sets with switching-dependent port mismatches," *IEEE Trans. Instrum. Meas.,* vol. IM-28, no. 1, Mar. 1979.

[3] J.G. Evans, "Linear two-port characterization independent of measuring set impedance imperfections," *Proc. IEEE,*(Lett.), vol. 56, no. 4, pp. 754–755, Apr. 1968.

[4] Larry R. D'Addario, "Computer-corrected reflectometer using the HP-8410 and an Apple II," *National Radio Astronomy Observatory Electronics Division Internal Report,* no. 228, May 1982

[5] R.C. Compton and D.B. Rutledge, *Puff: Computer Aided Design for Microwave Integrated Circuits,* Pasadena: Calif. Inst. of Tech., 1987

[6] W.L. Williams, R.C. Compton and D.B. Rutledge, "Elf: computer automation and error correction for a microwave network analyzer," *IEEE Trans. Instrum. Meas.,* vol. 37, no. 1, pp. 95–100, Mar. 1988

[7] W. Kruppa and K.F. Sodomsky, "An explicit solution for the scattering parameters of a linear two-port with an imperfect test set," *IEEE Trans. Microwave Theory Tech.,* vol. MTT-19, no. 1, pp. 122–123, Jan. 1971

[8] S. Rehnmark, "On the calibration process of automatic network analyzer systems," *IEEE Trans. Microwave Theory Tech.,* vol. MTT-22, no. 4, pp. 457–458, Apr. 1974

[9] S.F. Adam, "A new precision automatic microwave measurement system," *IEEE Trans. Instrum. Meas.,* vol. IM-17, no. 4, pp. 308–313, Dec. 1968

[10] D. Woods, "Rigorous derivation of computer-corrected network analyzer calibration equations," *Electron. Lett.,* vol. 11, no. 17, pp. 403–405, Aug. 21, 1975

[11] O.J. Davies, R.B. Doshi, B. Nagenthiram, "Correction of microwave network analyzer measurements of 2-port devices," *Electron. Lett.,* vol. 9, no. 23, pp. 543–544, Nov. 15, 1973

[12] R.A. Hackborn, "An automatic network analyzer," *Microwave J.*, vol. 11, no. 5, pp. 44–52, May 1968

[13] H.V. Shurmer, "Calibration procedure for computer-corrected s-parameter characterization of devices mounted in microstrip," *Electron. Lett.*, vol. 9, no. 14, pp. 323–324, July 12, 1973

[14] E.F. da Silva and M.K. McPhun, "Calibration of microwave network analyzer for computer-corrected s-parameter measurements," *Electron. Lett.*, vol. 9, no. 6, pp. 126–128, March 22, 1973

[15] J.G. Evans, F.W. Kerfoot and R.L. Nichols, "Automated network analyzer for the 0.9 to 12.4 GHz range," *Bell Syst. Tech. J.*, vol. 55, no. 6, pp. 691–721, July–Aug. 1976

[16] D. Woods, "Reappraisal of computer-corrected network analyzer design and calibration," *Proc. Inst. Elec. Eng.*, vol. 124, no. 3, pp. 205–211, Mar. 1977

[17] J.G. Evans, "Measuring frequency characteristics of linear two-port networks automatically," *Bell Syst. Tech. J.*, vol. 48, no. 5, pp. 1313–1338, May–June 1969

[18] H.V. Shurmer, "A new method of calibrating a network analyzer," *Electron. Lett.*, vol. 6, no. 23, pp. 733–734, Nov. 12, 1970

[19] K. Kurokawa, "Power waves and the scattering matrix," *IEEE Trans. Microwave Theory Tech.*, vol. MTT-13, pp. 194–202, March 1965

Chapter 3

Six-Port Network Analyzer Theory

It was shown in chapter 2 that if the complex ratio, b_3/b_4, of two voltage waves emerging from a four-port network can be determined, then the reflection coefficient Γ of the unknown load connected to the four-port's test port can be calculated. The *six-port* network analyzer allows b_3/b_4 to be determined without the use of a vector voltmeter. This reduces the cost and complexity of the system.

Figure 3.1 shows the general six-port network analyzer configuration [1]. Only microwave power detectors are used in this instrument. These are square law detectors; that is $P_i \propto |b_i|^2, i = 3 \cdots 6$. By measuring the magnitudes of the voltage waves emerging from port 3, 4, 5 and 6, and doing some trigonometry, the complex ratio of the wave emerging from port 3 to that at port 4 can be calculated. This reduces the six-port to an equivalent four-port network analyzer, which may be calibrated as described in chapter 2.

The equivalence of the six-port and the four-port analyzers can be seen by noting that the addition of ports 5 and 6 does not change any of the arguments presented in chapter 2. One can think of ports 5 and 6, and their terminating impedances being absorbed into the network, leaving a four-port network.

The six-port network, with power detectors installed, then, is like a four-port network with a built-in vector voltmeter. Since power detectors are relatively inexpensive, it is usually unnecessary to switch-multiplex them between two six-port networks as was done with the vector voltmeter in the four-port

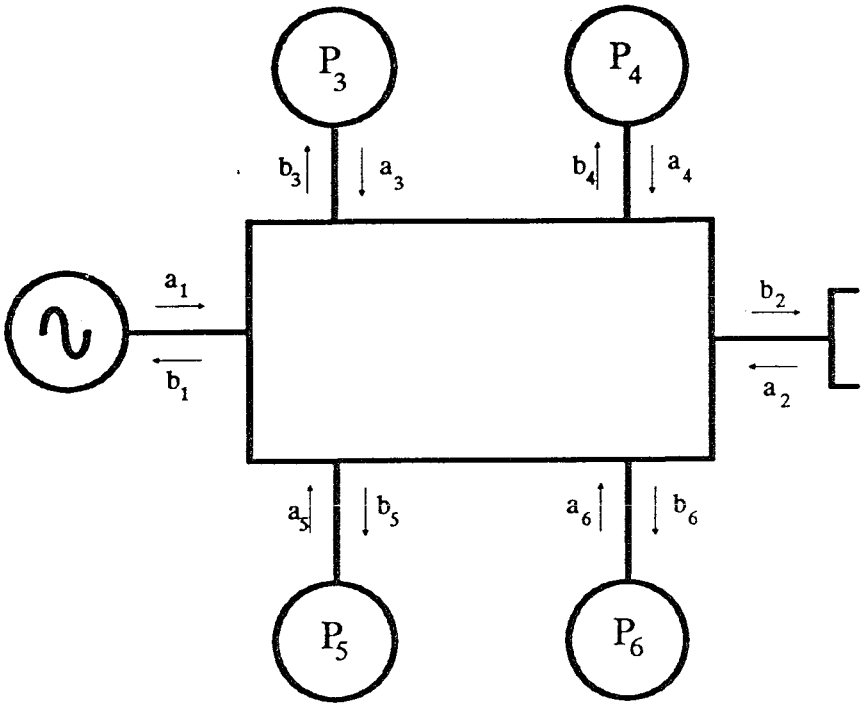

Figure 3.1 The six-port network analyzer uses only power detectors to determine the complex ratio a_2/b_2 at its test port.

measurement systems described above. The self-contained reflectometer module becomes the basic building block of measurement systems using the six-port network analyzer. As will be seen below, this facilitates measurement architectures and procedures different from those used with the four-port system.

As in chapter 2, the theory of the reflectometer will be described first, followed by that of the S-parameter measurement system.

3.1 Reflection Measurements with the 6-Port Network Analyzer

With the reflectometer of figure 3.1, the goal is to find the ratio of b_3/b_4. This quantity is defined as w. Once the complex ratio w is found, the same calibration and measurement procedures as were used for the four-port network analyzer can be applied. For this reason, finding w from the six-port's power detector outputs is termed a six-port to four-port conversion. Although w is a bilinear transform of the desired quantity Γ, the complex w-plane is the most convenient in which to work for many of the calculations related to calibration and measurement with the six-port.

The key observation for making the six-port to four-port conversion is that the voltage waves emerging from ports 5 and 6 of the six-port are related to those from ports 3 and 4 in a simple way [2]:

$$b_5 = Kb_3 + Lb_4 \tag{3.1}$$

$$b_6 = Mb_3 + Nb_4 \tag{3.2}$$

Rearranging and taking magnitudes gives

$$\frac{1}{|K|}\left|\frac{b_5}{b_4}\right| = \left|\frac{b_3}{b_4} + \frac{L}{K}\right| \tag{3.3}$$

$$\frac{1}{|M|}\left|\frac{b_6}{b_4}\right| = \left|\frac{b_3}{b_4} + \frac{N}{M}\right| \tag{3.4}$$

Taking $w \equiv b_3/b_4$, these expressions can be written as

$$|w| = \left|\frac{b_3}{b_4}\right| \tag{3.5}$$

$$|w - w_1| = \frac{1}{|K|}\left|\frac{b_5}{b_4}\right| \tag{3.6}$$

$$|w - w_2| = \frac{1}{|M|}\left|\frac{b_6}{b_4}\right| \tag{3.7}$$

where $w_1 = -L/K$ and $w_2 = -N/M$. In terms of the powers measured at the various ports, this gives

$$|w|^2 = \frac{P_3}{P_4} \tag{3.8}$$

$$|w - w_1|^2 = \zeta \frac{P_5}{P_4} \tag{3.9}$$

$$|w - w_2|^2 = \rho \frac{P_6}{P_4} \tag{3.10}$$

In the complex w plane these are just equations of circles, as shown in figure 3.2. So with the powers at ports 3, 4, 5 and 6 known, the problem of finding the complex quantity b_3/b_4 and reducing the six-port to an equivalent four-port is just one of finding the intersection of three circles.

The more difficult problem is that of finding the calibration constants, w_1, w_2, ζ and ρ. This requires an additional level of calibration for the six-port. First, a six-port-to-four-port calibration determines these constants, and then a four-port calibration procedure which may be similar to that described in chapter 2 completes the system calibration.

Interestingly enough, no precision calibration standards are required for the six-port-to-four-port calibration. A constraining relationship can be found between the calibration constants based solely on the linearity of the six-port network. This relationship allows the calibration constants to be determined by observing measurements of a few roughly-known reflection coefficients. The values of the calibration constants determined are independent of the particular reflection coefficient values used for the calibration.

The procedure for deriving the constraining relationship, as outlined by Engen [3], is to solve (3.9) and (3.10) to give the real and imaginary parts of w in terms of the measured powers and the calibration constants. Then, using (3.8), $(\mathrm{Re}\, w)^2 + (\mathrm{Im}\, w)^2 = P_3/P_4$ eliminates the dependence on w altogether, leaving the desired result.

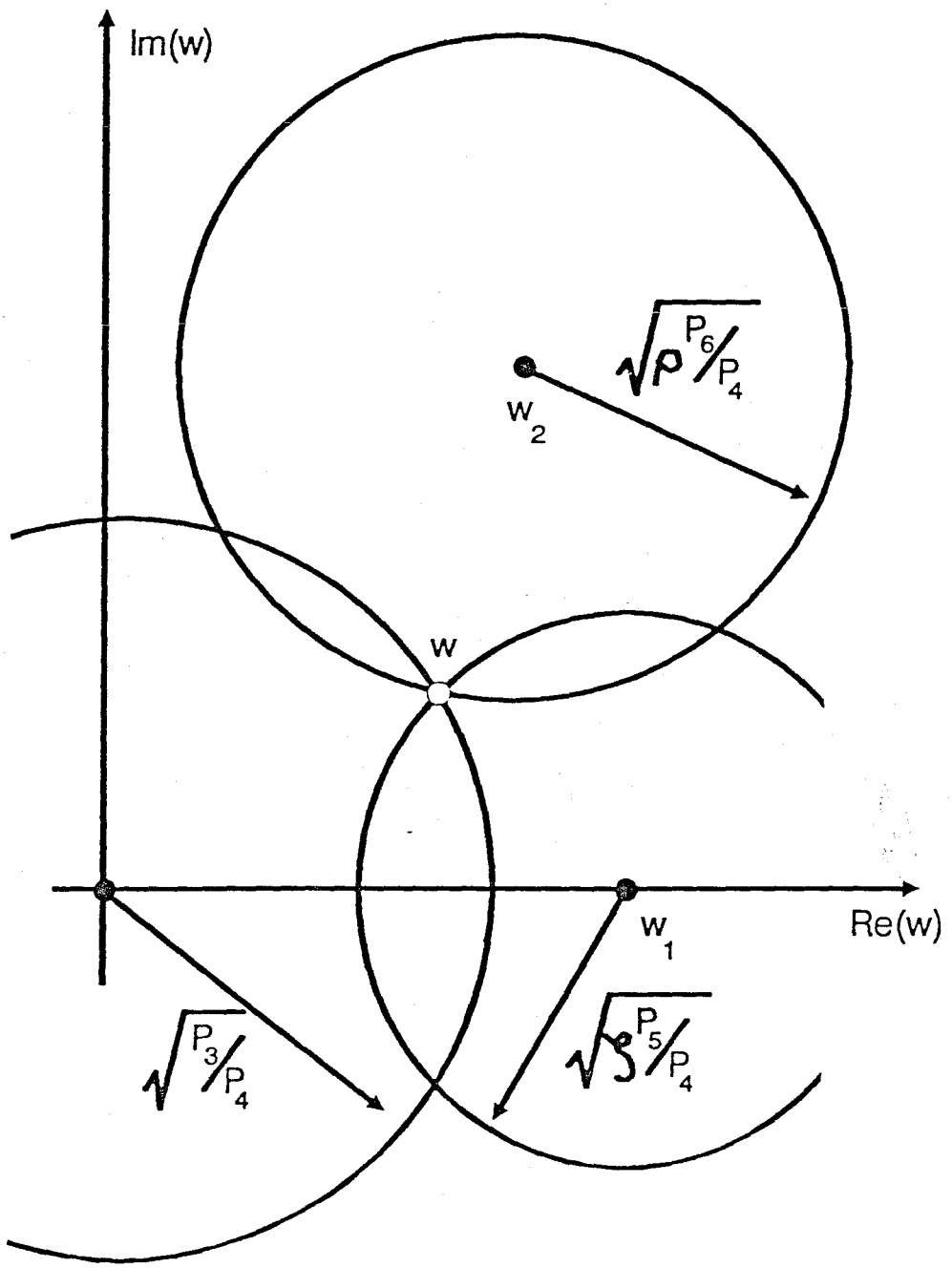

Figure 3.2 Outputs of the six-port's power detectors give a family of circles that can be solved for the complex ratio of the signals at two of the detectors.

Expanding (3.9) gives

$$(w - w_1)(w^* - w_1^*) = \zeta \frac{P_5}{P_4} \tag{3.11}$$

$$|w|^2 - ww_1^* - w_1 w^* + |w_1|^2 = \zeta \frac{P_5}{P_4} \tag{3.12}$$

$$|w|^2 - 2\mathrm{Re}\,(ww_1^*) + |w_1|^2 = \zeta \frac{P_5}{P_4} \tag{3.13}$$

Substituting (3.8) into (3.13) and expanding $\mathrm{Re}\,(ww_1^*)$ gives

$$\frac{P_3}{P_4} - 2[(\mathrm{Re}\,w)(\mathrm{Re}\,w_1) + (\mathrm{Im}\,w)(\mathrm{Im}\,w_1)] + |w_1|^2 = \zeta \frac{P_5}{P_4} \tag{3.14}$$

which is a linear equation in $\mathrm{Re}\,w$ and $\mathrm{Im}\,w$. Performing the same operations on (3.10) gives

$$\frac{P_3}{P_4} - 2[(\mathrm{Re}\,w)(\mathrm{Re}\,w_2) + (\mathrm{Im}\,w)(\mathrm{Im}\,w_2)] + |w_2|^2 = \rho \frac{P_6}{P_4} \tag{3.15}$$

These two equations can be solved for $\mathrm{Re}\,w$ and $\mathrm{Im}\,w$ to give

$$\mathrm{Re}\,w = \frac{1}{2} \frac{(\mathrm{Im}\,w_1)(|w_2|^2 + P_3/P_4 - \rho P_6/P_4) + (\mathrm{Im}\,w_2)(\zeta P_5/P_4 - P_3/P_4 - |w_1|^2)}{(\mathrm{Re}\,w_2)(\mathrm{Im}\,w_1) - (\mathrm{Re}\,w_1)(\mathrm{Im}\,w_2)} \tag{3.16}$$

$$\mathrm{Im}\,w = -\frac{1}{2} \frac{(\mathrm{Re}\,w_1)(|w_2|^2 + P_3/P_4 - \rho P_6/P_4) + (\mathrm{Re}\,w_2)(\zeta P_5/P_4 - P_3/P_4 - |w_1|^2)}{(\mathrm{Re}\,w_2)(\mathrm{Im}\,w_1) - (\mathrm{Re}\,w_1)(\mathrm{Im}\,w_2)} \tag{3.17}$$

Squaring these and adding them gives, after some lengthy algebra,

$$\begin{aligned} &a\left(\frac{P_3}{P_4}\right)^2 + b\zeta^2\left(\frac{P_5}{P_4}\right)^2 + c\rho^2\left(\frac{P_6}{P_4}\right)^2 + (c-a-b)\zeta\left(\frac{P_3P_5}{P_4^2}\right) \\ &\quad + (b-a-c)\rho\left(\frac{P_3P_6}{P_4^2}\right) + (a-b-c)\zeta\rho\left(\frac{P_5P_6}{P_4^2}\right) \\ &\quad + a(a-b-c)\frac{P_3}{P_4} + b(b-a-c)\zeta\frac{P_5}{P_4} + c(c-a-b)\rho\frac{P_6}{P_4} + abc = 0 \end{aligned} \tag{3.18}$$

where

$$a = |w_1 - w_2|^2 \tag{3.19}$$

$$b = |w_2|^2 \tag{3.20}$$

$$c = |w_1|^2 \tag{3.21}$$

Equation (3.18) gives the relationship between w_1, w_2, ζ and ρ and the power readings observed for any measured reflection coefficient. From here, the calibration can proceed in one of two ways. Observing nine different values of reflection coefficient, and inserting the observed values of power into (3.18) generates a 9×9 matrix, which can be solved to give the values of $a/(abc), b\zeta^2/(abc), \ldots, c(c-a-b)\rho/(abc)$. In order to find $a, \ldots, \rho$, however, this third-order set of equations must be solved simultaneously, an iterative process which does not always converge to the proper values.

There is an alternative approach, pointed out by Engen [3], which yields the values of $a, \ldots, \rho$ in closed form with as few as five observations of reflection coefficients. The assumption that results in this simplification is that all of the values used in the calibration lie along a single circle in the w-plane. This can be achieved experimentally to a good precision through the use of a sliding short circuit. Sliding short circuits are readily available in coaxial transmission lines and rectangular waveguides. As the short circuit moves from point to point in the transmission line, it traces out a circle in the reflection coefficient plane ($|\Gamma| = 1$). A bilinear transform always carries a circle into a circle, so in the w-plane, another circle is traced out, $|w - R_c|^2 = R^2$.

The situation is shown in figure 3.3. Only one measurement center, w_1, is considered in the first stage of the calibration. It can be assumed that this first center lies on the w-plane's real axis. This simply amounts to an arbitrary choice of the phase of b_3. Since the phase quantity to be found is the phase difference

between b_3 and b_4, this does not affect the problem. Choosing the phase of w_1 sets the value of the phase of w_2, which must be found later in the procedure.

A relationship similar to (3.18) between the observed powers and the calibration constants must be found. This can be done most easily by observing that the equations that define the present case, $|w|^2 = P_3/P_4$, $|w - w_1|^2 = \zeta P_5/P_4$ and $|w - R_c|^2 = R^2$ differ from (3.8–3.10) only in the last equation. Thus, the result of eliminating w from these equations can be found by substituting R_c for w_2 and R^2 for $\rho P_6/P_4$ in equation (3.18). This gives

$$A\left(\frac{P_3}{P_4}\right)^2 + 2B\left(\frac{P_3P_5}{P_4^2}\right) + C\left(\frac{P_5}{P_4}\right)^2 + 2D\left(\frac{P_3}{P_4}\right) + 2E\left(\frac{P_5}{P_4}\right) + F = 0 \quad (3.22)$$

where

$$A = a' \quad (3.23)$$

$$B = \zeta(c - a' - b')/2 \quad (3.24)$$

$$C = \zeta^2 b' \quad (3.25)$$

$$D = \left[R^2(b' - a' - c) + a'(a' - b' - c)\right]/2 \quad (3.26)$$

$$E = \zeta\left[R^2(a' - b' - c) + b'(b' - a' - c)\right]/2 \quad (3.27)$$

$$F = \left[R^4 + R^2(c - a' - b') + a'b'\right]c \quad (3.28)$$

and where

$$a' = |w_1 - R_c|^2 \quad (3.29)$$

$$b' = |R_c|^2 \quad (3.30)$$

$$c = |w_1|^2 \quad (3.31)$$

$$\zeta = \frac{1}{|K|^2} \quad (3.32)$$

Surprisingly, as will be seen below, (3.23–3.28) can be solved in closed form to give a', b', c, ζ and R^2. First, however, values of $A, \ldots, F$ must be determined experimentally.

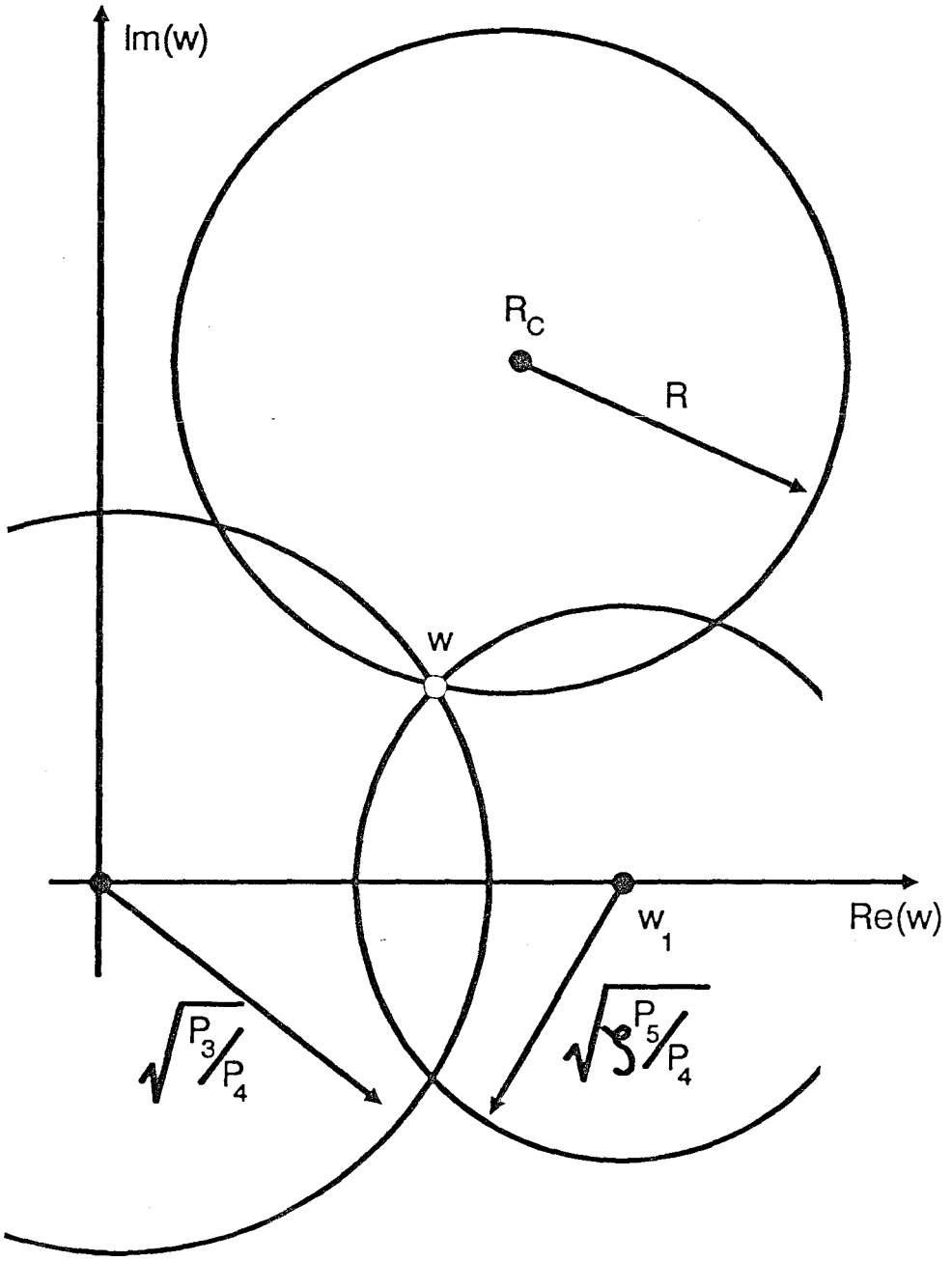

Figure 3.3 The sliding short circuit, used in the first stage of the six-port calibration, traces out a circle in the complex w-plane.

Application of a standard test [4] to (3.22) shows that it is the equation of an ellipse in the P_3/P_4, P_5/P_4 plane. This ellipse is constrained to the first quadrant of the plane. Thus, $A, \ldots, F$ can be determined by least-squares fitting a conic section to the observed pairs $(P_3/P_4, P_5/P_4)$, and then testing to assure that the resulting coefficients give an ellipse in the first quadrant. A six-port network with the center w_1 badly placed (e.g., w_1 very close to zero relative to the radius R) can fail these tests. In this case, the observed pairs will lie along an ellipse that is so eccentric that small measurement errors in the values of $(P_3/P_4,\ P_5/P_4)$ can cause the best-fit conic section to be a hyperbola, or an ellipse crossing out of the first quadrant. A failure of this type indicates that measurement accuracy of the six-port at the frequency of the failure would be intolerably bad.

For a properly designed six-port network analyzer, failures due to a bad ellipse fit will not be observed. For the sampled-line network analyzer, as will be seen in the next chapter, however, testing for this type of failure is important. At a given frequency, the sampled-line analyzer has a certain number of primary detectors that determine the value of w to good accuracy, and then a number of secondary detectors that provide additional accuracy enhancement. The network is designed so that ellipse fit errors do not occur with any of the primary detectors, but can occur with the secondary detectors. Thus, these must be tested and marked as bad outputs, not to be used in the accuracy enhancement procedure of the measurement.

The best fit conic section can be found in a straightforward way. Substituting $x = P_3/P_4$ and $y = P_5/P_4$ into (3.22) and dividing through by F gives

$$\frac{A}{F}x^2 + 2\frac{B}{F}xy + \frac{C}{F}y^2 + +2\frac{D}{F}x + 2\frac{E}{F}y + 1 = 0 \tag{3.33}$$

The error to be minimized can then be written as

$$\xi = \sum_i \left(\frac{A}{F}x_i^2 + 2\frac{B}{F}x_i y_i + \frac{C}{F}y_i^2 + +2\frac{D}{F}x_i + 2\frac{E}{F}y_i + 1 \right)^2 \tag{3.34}$$

To minimize this error, the partial derivatives $\partial\xi/\partial(A/F),\ldots,\partial\xi/\partial(E/F)$ are taken and set equal to zero. This yields five linear equations in the five unknowns $A/F,\ldots,E/F$. Observing at least five different values of reflection coefficient, and solving a 5×5 matrix, then, yields values of $A/F,\ldots,E/F$. Given these values, the task remaining is to solve (3.23–3.28) for $a',\ldots,\zeta$.

This is achieved by first making the following definitions:

$$\alpha = (R^2 + a')/\zeta \tag{3.35}$$

$$\beta = \left[(R^2 - a')(R^2 - b') + 2R^2 c\right]/\zeta \tag{3.36}$$

$$\gamma = R^2 + b' \tag{3.37}$$

$$\delta = (R^2 - a')/\zeta \tag{3.38}$$

$$\epsilon = R^2 - b' \tag{3.39}$$

Substitution shows that the quantities $\alpha,\ldots,\epsilon$ can be expressed directly in terms of $A,\ldots,F$:

$$\frac{BD - AE}{AC - B^2} = \alpha \tag{3.40}$$

$$\frac{DE - BF}{AC - B^2} = \beta \tag{3.41}$$

$$\frac{BE - DC}{AC - B^2} = \gamma \tag{3.42}$$

$$\frac{AF - D^2}{AC - B^2} = \delta^2 \tag{3.43}$$

$$\frac{CF - E^2}{AC - B^2} = \epsilon^2 \tag{3.44}$$

It is observed that the numerators and denominators of the left sides of (3.40–3.44) can be divided through by F^2 to yield expressions only in terms of

$A/F, \ldots, E/F$. Thus the values of $\alpha, \ldots, \epsilon^2$ can be found directly from the sliding short calibration data. The expressions for $\alpha, \ldots, \epsilon^2$, (3.35–3.39) can in turn be solved for $a', \ldots, R^2$:

$$a' = |w_1 - R_c|^2 = \frac{(\alpha - \delta)(\gamma + \epsilon)}{2(\alpha + \delta)} \tag{3.45}$$

$$b' = |R_c|^2 = \frac{\gamma - \epsilon}{2} \tag{3.46}$$

$$c = |w_1|^2 = \frac{\beta - \delta\epsilon}{\alpha + \delta} \tag{3.47}$$

$$\zeta = \frac{\gamma + \epsilon}{\alpha + \delta} \tag{3.48}$$

$$R^2 = \frac{\gamma + \epsilon}{2} \tag{3.49}$$

So the total six-port-to-four-port reduction is a three-step process. First, the sliding short calibration data are summed into the 5×5 matrix derived from (3.34). Solving this gives $A/F, \ldots, E/F$. Next, these values are used in (3.40–3.44) to give values of $\alpha, \ldots, \epsilon^2$. Finally, these quantities are used in (3.45–3.49) to give values of $a', \ldots, R^2$, which contain the calibration constants wanted.

There are still problems, however. Since (3.43) and (3.44) only give expressions for δ^2 and ϵ^2, there is a sign ambiguity in the determinations of δ and ϵ. Sign ambiguity problems are inherent in the six-port network analyzer, since only magnitudes squared are measured by the instrument. Such ambiguities are encountered at several steps of calibration and measurement, and must be carefully resolved at each step to assure the validity of subsequent results.

In the present case, it is seen from the definition (3.39) that ϵ is negative if $|R_c|^2 > R^2$, that is, if the circle drawn in the w-plane does not enclose the origin. Similarly from (3.38), δ is negative if the measurement center w_1 is outside the circle drawn by the sliding short. This provides one method of resolving this sign ambiguity using knowledge of the network used. Assume first that the interior of

the $|\Gamma| = 1$ circle maps to the interior of the corresponding circle in the w-plane. This is the case for most practical six-ports and can be verified by checking the values of P_3/P_4 and P_5/P_4 for some Γ, $|\Gamma| < 1$ and verifying that the resulting point falls inside the sliding short's ellipse. Given this, if it is known that $|b_3| \to 0$ for some value of Γ with $|\Gamma| \leq 1$, then the $|\Gamma| = 1$ circle encloses the origin of the w-plane and $\epsilon > 0$. A similar argument using b_5 can be used for δ.

This is the approach taken with the sampled-line network analyzer. The system is engineered so that none of the $|b_i|$'s can go to zero for any Γ, $|\Gamma| \leq 1$, ensuring that $\epsilon < 0$ and $\delta < 0$.

If the properties of the six-port network are not known, this sign ambiguity can still be resolved, through a clever technique outlined by Engen. One takes all four possible choices of sign for ϵ and δ. Using the resulting values of the calibration constants and the calibration data from the sliding short and a matched termination, four parallel calculations of the value of w_2 can be performed. All the calculations with incorrect sign assumptions yield self-contradictory results. The one with the correct δ and ϵ will yield the correct value of w_2.

Given that ϵ and δ are found correctly, there is still a sign ambiguity that can not be resolved through the equations above. This ambiguity is in the sign of $\operatorname{Im} R_c$. If it is chosen incorrectly, the value found by the six-port will be w^* instead of w.

Knowledge of the properties of the six-port used provides the best way to find the sign of $\operatorname{Im} R_c$. This is the approach used with sampled-line network analyzer. Otherwise, some completely independent scheme must be devised, perhaps using the reflection coefficient of an additional known standard.

With these sign ambiguities in the determination of $a, \ldots, R^2$ and $\operatorname{Im} R_c$ resolved, there is still the problem of finding w_2 and ρ. Engen's method described above is an option here. Another option is to substitute w_2 for w_1 and ρ for ζ, in the above and redo the procedure used to find w_1.

This yields w_2 on the real axis, but the value of R_c found has a different angle from that found in the determination of w_1. Rotating the second result for R_c so that it matches the first rotates w_2 to its proper angle in the plane of the first solution as well. This is the approach used in the sampled-line network analyzer. It is fairly simple and allows the results from the various detector outputs to be compared with uniform criteria in the calibration procedure.

It is interesting to note at this point that, without any knowledge of w_2 or ρ, it is possible to determine w to within a sign. As can be seen by returning to figure 3.2, the value of w must be at one of the two intersections of the b_3/b_4 circle and the b_5/b_4 circle. The b_6/b_4 circle simply resolves this ambiguity. If, however, there is another constraint imposed by the network used, which rules out one of these intersections, then the third circle is unnecessary. Then only three detector outputs are required to determine w, and the resulting instrument is known as a five-port network analyzer. The sampled-line network analyzer has this property and is in many ways an extension of the five-port network analyzer concept.

If additional accuracy is sought in determination of the calibration constants, the values found through the closed-form approach outlined above can be used as first estimates of the coefficients of (3.18). An optimizer can then be used to minimize the sum of the squares of the values found in evaluating the left side of (3.18) for all the reflection coefficients observed in the calibration procedure.

An important determinant of system accuracy is the geometric placement of the measurement centers around the $|\Gamma| = 1$ circle in the w-plane. This placement is set by the particular six-port network used in the implementation of the network analyzer. Clearly, if all the measurement centers are close together compared to the unit circle, then triangulating from them to find Γ will yield

poor accuracy. Figure 3.4 shows an implementation used at NBS [5], and the resulting placement of the measurement centers.

This implementation has the advantage that b_4 depends only on b_2, to the limit of the directivity of the hybrids used. This makes b_3/b_4 approximately a *linear* transform of Γ instead of a bilinear transform, which can simplify some of the preliminary calculations. The regular spacing of the measurement centers around the unit circle results in good accuracy for this instrument.

As has been seen, the six-port network can be calibrated to measure the complex ratio of b_3/b_4. This ratio must then be calibrated to yield the value of $\Gamma = a_2/b_2$. As noted above, this requires determination of the three complex constants of the bilinear transform relating Γ and b_3/b_4.

If a single six-port reflectometer is used, then the same calibration options are available as with the four-port reflectometer. Three known standards are measured, and the results can be inverted to give the complex constants of the bilinear transform. If two six-ports are used, as in an S-parameter measurement system, however, other options are available, as will be seen below.

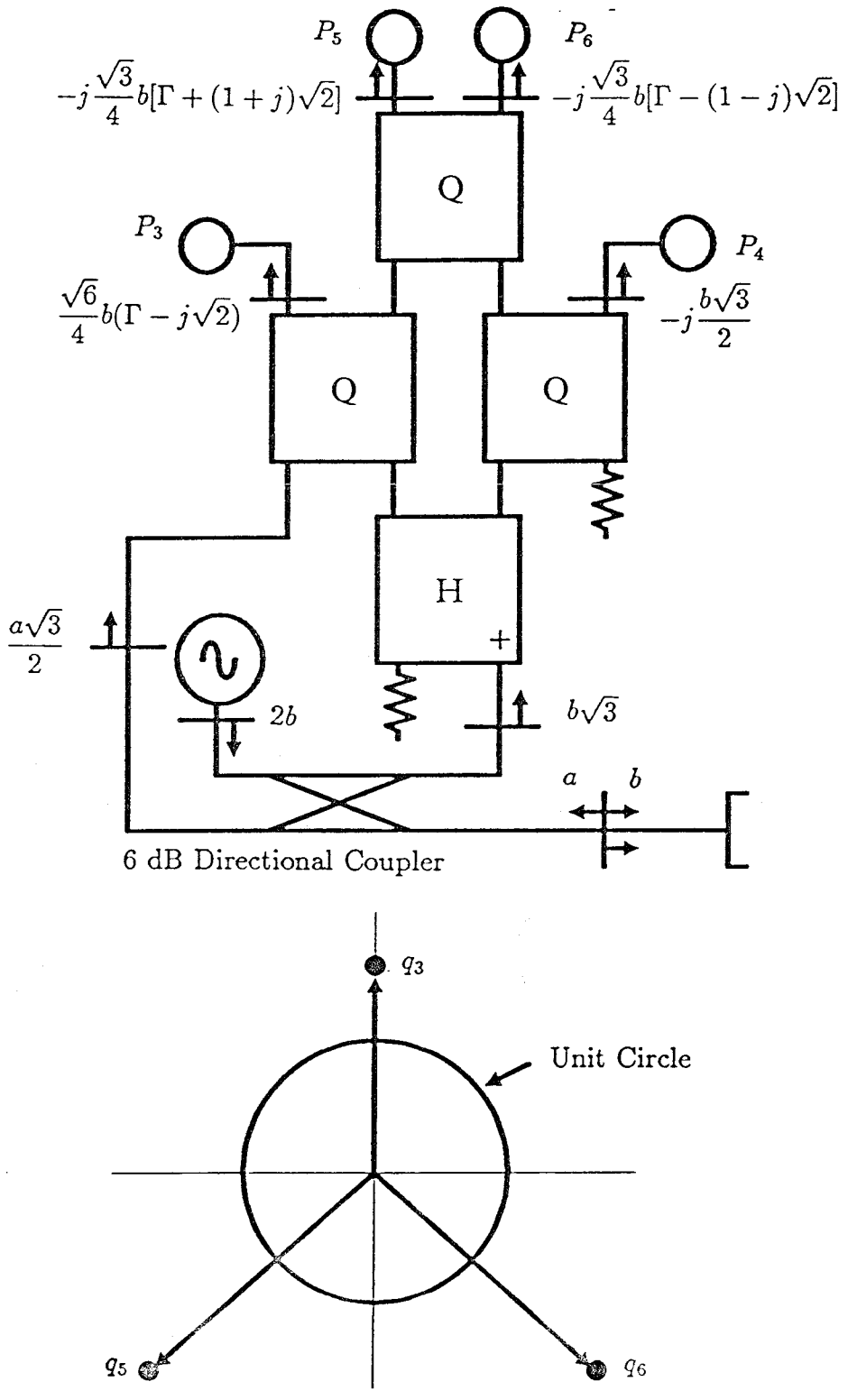

Figure 3.4 The six-port network analyzer as implemented at NBS. The boxes marked 'H' are 180° hybrid networks and those marked with 'Q' are quadrature hybrids.

3.2 Dual Reflectometer Calibration – the TRL Scheme

With a single reflectometer, the final accuracy of a calibration depends on how accurately the reflection coefficients of a set of precision terminations are known. To set the reference plane, the reflection coefficient of at least one of the standards must be known to a precision greater than that of the network analyzer over the entire frequency range of operation. Even with the simplest of calibration standards, the short circuit, this is often impractical.

A set of two reflectometers, however, can "calibrate each other" through a procedure developed at the National Bureau of Standards [6] known as the "thru-reflect-line" or TRL calibration procedure. In this procedure, the precise properties of the calibration standards need not be known, and are in fact derived as a by-product of the calibration. Two standards are used for this procedure. One is a precision coaxial line of approximately known length and the other is a termination with a reflection coefficient different from zero, the exact value of which is only approximately known.

As it turns out, the requirement of having two reflectometers for the TRL procedure is not a drawback. It will be seen below that two reflectometers are used to construct an S-parameter measurement system using six-ports. With two six-ports present in the system in any case, the fact that they can calibrate each other is a bonus.

The TRL calibration procedure is implemented on the sampled-line network analyzer, and will be described briefly here.

The TRL calibration procedure is only a reflectometer calibration procedure. Given two reflectometers that can measure b_3/b_4, TRL provides the coefficients of the bilinear transforms to give the Γ's connected to each reflectometer. Additional calibration is required to allow the two reflectometers to measure the S-parameters of a general two-port network.

The three measurements used for TRL are shown in figure 3.5. As described in chapter 2, an uncalibrated reflectometer can be represented as an ideal reflectometer with an error two-port between its port and the measurement port. This representation is used in figure 3.5. The six-port to four-port conversion described above allows the two reflectometers to measure their respective b_3/b_4's. The goal of the TRL calibration procedure is to determine the parameters of the error boxes A and B.

In the first measurement, the two reflectometers are connected port to port. This measurement yields the cascade of the two error two-ports. In the second measurement, the two reflectometers look at each other through a length of precision transmission line, which by hypothesis contains no internal reflections or reflections from its ports. The length of this line does not need to be known exactly, but for numerical stability, a value near a quarter wavelength at the measurement frequency is desirable. In the final measurement, a nominal short circuit is connected to the two reflectometer ports.

When the two reflectometers look at each other through a given two-port, their responses in terms of that network's S-parameters can be written as follows:

$$b_1 = S_{11}a_1 + S_{12}a_2 \tag{3.50}$$

$$b_2 = S_{21}a_1 + S_{22}a_2 \tag{3.51}$$

where, for the present case $(a_1 \quad a_2)^T = (b_4 \quad b_4')^T$ and $(b_1 \quad b_2)^T = (b_3 \quad b_3')^T$. Dividing (3.50) by a_1 and (3.51) by a_2 and eliminating a_2/a_1 gives

$$w_2 S_{11} + w_1 S_{22} - \Delta = w_1 w_2 \tag{3.52}$$

where

$$\Delta \equiv S_{11}S_{22} - S_{12}S_{21} \tag{3.53}$$

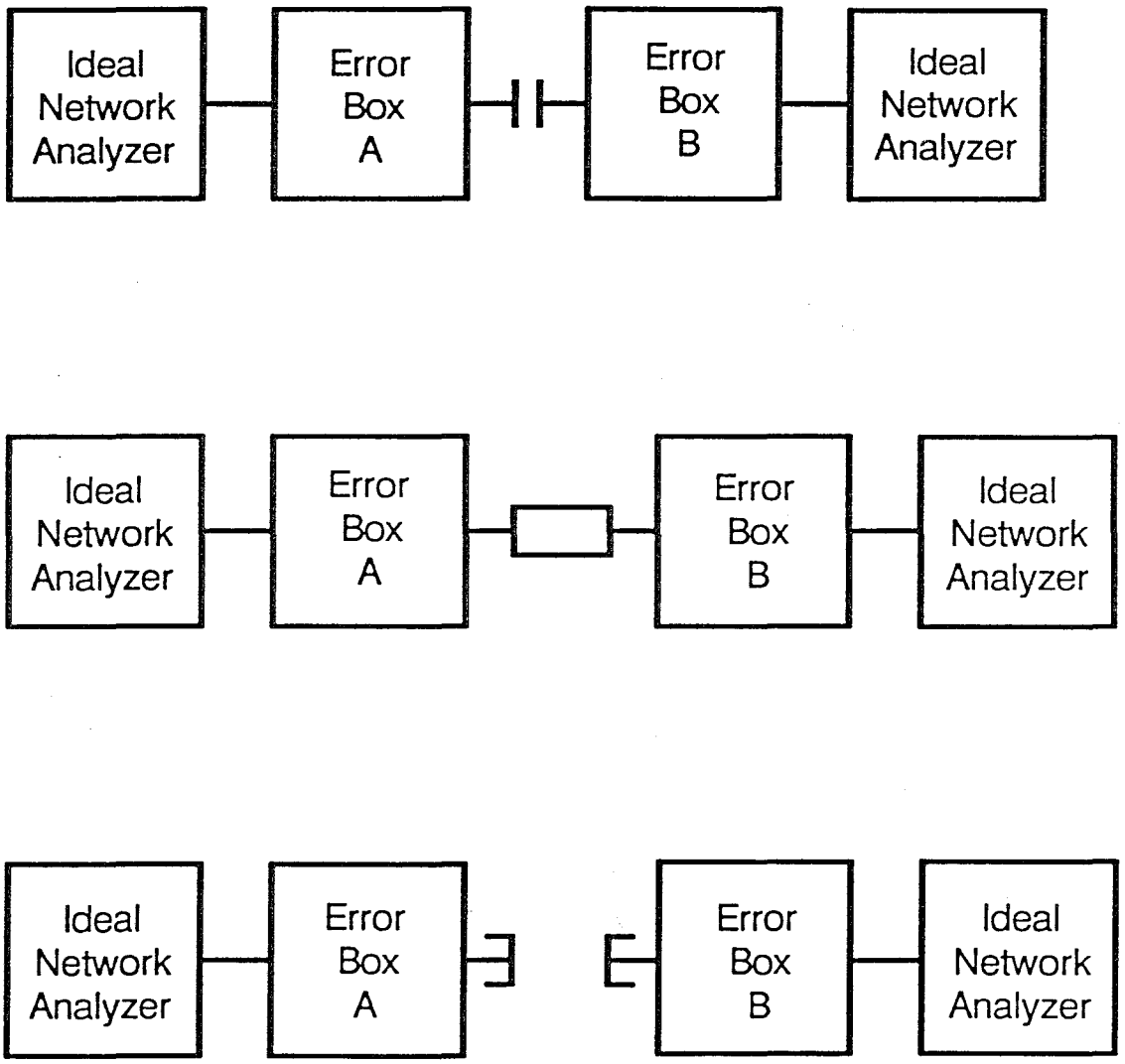

Figure 3.5 In the TRL calibration procedure, the coefficients of the error boxes A and B of two reflectometers are determined by making the three measurements shown here. A straight through, a length of line and a high-reflection load of approximately known value are used.

and

$$w_1 = b_1/a_1 = b_3/b_4 \tag{3.54}$$

$$w_2 = b_2/a_2 = b_3'/b_4' \tag{3.55}$$

By observing values of w_1 and w_2 for three values of a_2/a_1, a set of three linear equations in three unknowns can be generated, and solving these gives the values of S_{11}, S_{22} and Δ. In the laboratory, the value of a_2/a_1 is changed by placing a variable phase shifter or variable attenuator between one of the reflectometer heads and the signal generator. In practice, more than three values of a_2/a_1 are used and a least-squares solution is found.

Since the TRL procedure involves cascaded two-port networks, it is convenient to work in terms of the wave cascading parameters or T-parameters. The T-parameters are defined by

$$\begin{pmatrix} b_1 \\ a_1 \end{pmatrix} = \begin{pmatrix} T_{11} & T_{12} \\ T_{21} & T_{22} \end{pmatrix} \begin{pmatrix} a_2 \\ b_2 \end{pmatrix} \tag{3.56}$$

$$= \mathbf{T} \begin{pmatrix} a_2 \\ b_2 \end{pmatrix} \tag{3.57}$$

The T-matrix for the cascade of two networks is just the product of the T-matrices of the two networks.

The T-matrix can be written in terms of the S-matrix as

$$\begin{pmatrix} T_{11} & T_{12} \\ T_{21} & T_{22} \end{pmatrix} = \frac{1}{S_{21}} \begin{pmatrix} -\Delta & S_{11} \\ -S_{22} & 1 \end{pmatrix} \tag{3.58}$$

This result is interesting in that it shows that by solving a set of equations like (3.52) all the T-parameters of an unknown network can be found to within a multiplicative factor, $1/S_{21}$. As will be seen below, the TRL method deals only with *ratios* of T-parameters, so all the required information can be found in this way. With this recognized, the description of the TRL procedure may continue.

If **A** and **B** represent the T-matrices of the two error boxes, A and B, respectively, then for the "thru" connection, the fictional two-port **U** that is observed is given by

$$\mathbf{U} = \mathbf{AB} \tag{3.59}$$

For the "line" connection, the observed two-port **D** is

$$\mathbf{D} = \mathbf{ALB} \tag{3.60}$$

where **L** represents the T-parameters of the line inserted between the two reflectometers.

Equation (3.60) can be solved for **B** to give

$$\mathbf{B} = \mathbf{A}^{-1}\mathbf{U} \tag{3.61}$$

Inverting both sides of (3.61) and post-multiplying (3.59) by the result gives

$$\mathbf{DU}^{-1}\mathbf{A} = \mathbf{ALBB}^{-1} \tag{3.62}$$

$$\mathbf{XA} = \mathbf{AL} \tag{3.63}$$

where

$$\mathbf{X} = \mathbf{DU}^{-1} \tag{3.64}$$

An assumption must be made about the value of **L**, the T-parameters of the length of line used as a calibration standard. It is taken to be

$$\mathbf{L} = \begin{pmatrix} e^{-\gamma l} & 0 \\ 0 & e^{\gamma l} \end{pmatrix} \tag{3.65}$$

This assumes that the line is uniform, not necessarily lossless, and that there are no reflections from it ($S_{11} = S_{22} = 0$).

Given this assumption, equation (3.63) can be expanded to give

$$X_{11}A_{11} + X_{12}A_{21} = A_{11}e^{-\gamma l} \tag{3.66}$$

$$X_{21}A_{11} + X_{22}A_{21} = A_{21}e^{-\gamma l} \tag{3.67}$$

$$X_{11}A_{12} + X_{12}A_{22} = A_{12}e^{\gamma l} \tag{3.68}$$

$$X_{21}A_{12} + X_{22}A_{22} = A_{22}e^{\gamma l} \tag{3.69}$$

Dividing (3.66) by (3.67) and (3.68) by (3.69) gives

$$\frac{X_{21}}{X_{12}}\left(\frac{A_{11}}{A_{21}}\right)^2 + \frac{X_{22} - X_{11}}{X_{12}}\left(\frac{A_{11}}{A_{21}}\right) - 1 = 0 \tag{3.70}$$

$$\frac{X_{21}}{X_{12}}\left(\frac{A_{12}}{A_{22}}\right)^2 + \frac{X_{22} - X_{11}}{X_{12}}\left(\frac{A_{12}}{A_{22}}\right) - 1 = 0 \tag{3.71}$$

So it is seen that the values A_{11}/A_{21} and A_{12}/A_{22} are solutions of the same quadratic equation. The coefficients of this equation can be determined from the measured b_3/b_4's for the thru and line measurements via (3.52) and (3.64).

It is easy to see that $(A_{11}/A_{21}) \neq (A_{12}/A_{22})$. From (3.58) this would require that the error box A have $S_{12}S_{21} = 0$ so there would be no transmission through the box.

Thus (A_{11}/A_{21}) and (A_{12}/A_{22}) are the two distinct roots of the quadratic equation. The question of root choice then arises again: which root represents which ratio? Approximate knowledge of the properties of the line calibration standard can be used to answer this question.

Dividing (3.69) by (3.67) gives

$$e^{2\gamma l} = \frac{X_{21}(A_{12}/A_{22}) + X_{22}}{X_{12}(A_{21}/A_{11}) + X_{11}} \tag{3.72}$$

so if the length of the transmission line used as the line standard is known fairly accurately, the value of $e^{2\gamma l}$ can be calculated, and this can be used to resolve the root ambiguity. This method has the advantage that it depends

only on quantities found in the course of the TRL calibration procedure, but unfortunately it is not foolproof. As stated above, the transmission line standard is chosen to have a phase delay near $\pm 90°$. It is a low-loss line, so $|e^{\gamma l}| \approx 1$. This places $e^{2\gamma l}$ near ± 1. The two possible root choices, when inserted in the right side of (3.72), yield values that are reciprocals of each other. If the phase delay of the line is too near $\pm 90°$, then $e^{2\gamma l}$ and its reciprocal cannot be easily distinguished, and measurement errors may lead to an improper root choice.

An alternative approach uses the result found in chapter 2, that for the reflectometer with error box A,

$$w_1 = \frac{a\Gamma + b}{c\Gamma + 1} \tag{3.73}$$

where Γ is the reflection coefficient measured by the reflectometer and

$$a = A_{11}/A_{22} \tag{3.74}$$

$$b = A_{12}/A_{22} \tag{3.75}$$

$$c = A_{21}/A_{22} \tag{3.76}$$

A rough calibration using three impedance standards, such as a short circuit, an open circuit and a matched load, can be performed to find approximate values of a, b, and c. Only one of the roots of (3.70) and (3.71) will be close to b, and this serves to resolve the root ambiguity. This method does not suffer the problems of the previous one, but does require additional known, independent calibration standards, which are not easy to come by in all types of transmission line.

Inspecting (3.73–3.76), it is seen that b and a/c have been determined from the roots of the quadratic equation (3.70). All that remains to characterize error box A is to determine the value of a. Rearranging (3.73) gives

$$a = \frac{w_1 - b}{\Gamma(1 - w_1 c/a)} \tag{3.77}$$

So, if one uses one precision standard, say a short circuit, then (3.77) can be solved for a and the calibration of error box A is complete. This approach is known as the "thru-short-delay," or TSD calibration procedure. Error box B can then be determined from (3.59).

For the TRL procedure it is assumed that Γ is not known precisely. More manipulation shows that this knowledge is not required for the determination of a. Equation (3.59) can be rewritten as

$$A_{22}B_{22}\begin{pmatrix} a & b \\ c & 1 \end{pmatrix}\begin{pmatrix} \alpha & \beta \\ \gamma & 1 \end{pmatrix} = U_{22}\begin{pmatrix} d & e \\ f & 1 \end{pmatrix} \tag{3.78}$$

where

$$a = A_{11}/A_{22} \tag{3.79}$$

$$b = A_{12}/A_{22} \tag{3.80}$$

$$c = A_{21}/A_{22} \tag{3.81}$$

$$\alpha = B_{11}/B_{22} \tag{3.82}$$

$$\beta = B_{12}/B_{22} \tag{3.83}$$

$$\gamma = B_{21}/B_{22} \tag{3.84}$$

$$d = U_{11}/U_{22} \tag{3.85}$$

$$e = U_{12}/U_{22} \tag{3.86}$$

$$f = U_{21}/U_{22} \tag{3.87}$$

By premultiplying both sides of (3.78) by $\mathbf{A}^{-1}$ and expanding, it can be shown that

$$\gamma = \frac{f - dc/a}{1 - ec/a} \tag{3.88}$$

$$\beta/\alpha = \frac{e - b}{d - bf} \tag{3.89}$$

$$a\alpha = \frac{d - bf}{1 - ec/a} \tag{3.90}$$

All the quantities on the right side of (3.88–3.90) are known, so γ, β/α and $a\alpha$ can be determined. A relationship like (3.77) holds for error box B. It is

$$\alpha = \frac{w_2 + \gamma}{\Gamma(1 + w_2\beta/\alpha)} \tag{3.91}$$

Assuming that the same Γ is connected to both reflectometers during the calibration procedure, Γ can be eliminated from (3.77) and (3.91) to give

$$a/\alpha = \frac{(w_1 - b)(1 + w_2\beta/\alpha)}{(w_2 + \gamma)(1 - w_1 c/a)} \tag{3.92}$$

and finally, (3.92) can be combined with (3.90):

$$a = \pm\sqrt{\frac{(w_1 - b)(1 + w_2\beta/\alpha)(d - bf)}{(w_2 + \gamma)(1 - w_1 c/a)(1 - ec/a)}} \tag{3.93}$$

and

$$\alpha = \frac{(d - bf)}{a(1 - ec/a)} \tag{3.94}$$

The sign ambiguity in (3.92) can be resolved by approximate knowledge of Γ. Use of a short circuit for Γ is convenient here. Good short circuit standards are readily available in coaxial lines and waveguides, and can be constructed without great difficulty in many of the transmission lines used in microwave ICs.

So the final result of the above is that two reflectometers can calibrate each other without the use of high-precision calibration standards. The one big assumption made in the preceding development is that the transmission line standard used is reflectionless. The effects of reflections in this standard have not been fully evaluated, but experimental results at the National Bureau of Standards indicate that the TRL procedure yields a very accurate calibration. Typical errors estimated at ± 0.001 dB in measuring a 20 dB attenuator have been reported [7].

3.3 S-Parameter Measurements with the 6-Port Network Analyzer

Figure 3.6 shows how two six-port network analyzers are used to construct an S-parameter measurement system. It is assumed here that both six-ports have been calibrated to read the true ratios, Γ_1 $(= b_1/a_1)$ and Γ_2 $(= b_2/a_2)$ at the reference planes 1 and 2. This calibration may proceed through any of the methods outlined in the previous sections.

Through a procedure identical to that given in equations (3.50–3.55) above, then, the values of S_{11}, S_{22} and Δ for the unknown two-port can be determined by observing the values of Γ_1 and Γ_2 for at least three different excitations (positions of the phase shifter or attenuators).

In order to find the complete S-parameters, some way of separating Δ to give S_{12} and S_{21} must be found. Rewriting (3.50–3.51) gives

$$S_{12} = (\Gamma_1 - S_{11})\frac{a_1}{a_2} \tag{3.95}$$

$$S_{21} = (\Gamma_2 - S_{22})\frac{a_2}{a_1} \tag{3.96}$$

so if the value of a_2/a_1 can be found for each measurement, then S_{12} and S_{21} can be found. Some additional calibration is necessary for this determination.

Consider the measurement system of figure 3.6 as a three-port network with its port 3 near the generator and ports 1 and 2 being the measurement reference planes as numbered. Then it can be shown [7] that

$$\frac{a_2}{a_1} = \left(s_{21} - s_{11}\frac{s_{23}}{s_{13}}\right)\Gamma_1 - \left(s_{12}\frac{s_{23}}{s_{13}} - s_{22}\right)\Gamma_2\frac{a_2}{a_1} + \frac{s_{23}}{s_{13}} \tag{3.97}$$

where the s_{ij}'s are the S-parameters of the measurement system three-port. This can be rewritten as

$$\frac{a_2}{a_1} = C_1\Gamma_1 - C_2\Gamma_2\frac{a_2}{a_1} + C_3 \tag{3.98}$$

which can be rearranged to give

$$\frac{a_2}{a_1} = \frac{C_3 + C_1\Gamma_1}{1 + C_2\Gamma_2} \tag{3.99}$$

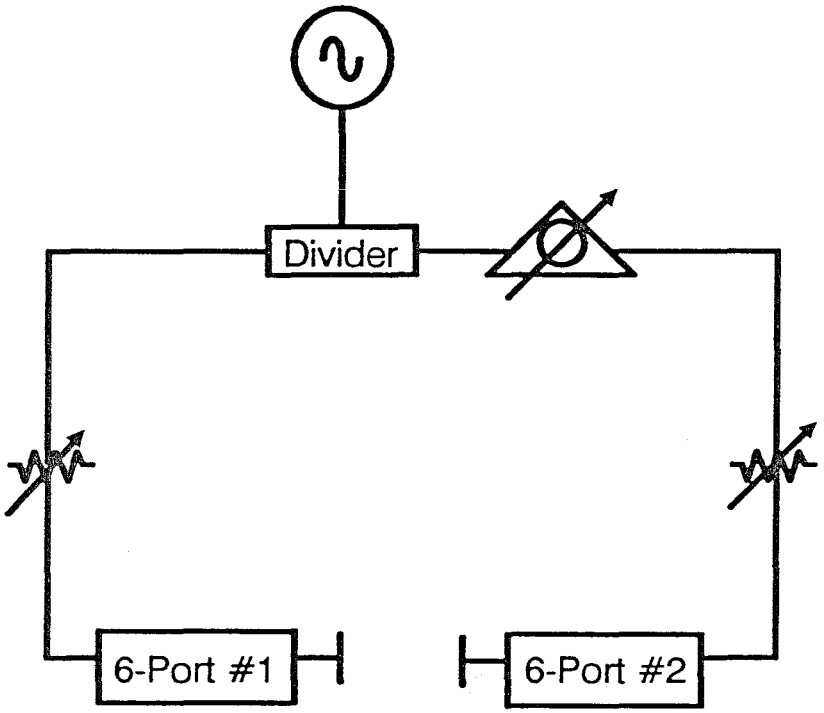

Figure 3.6 A full S-parameter measurement system using six-port network analyzers.

With equation (3.99), then, a_2/a_1 can be determined from the observed Γ's for any measurement. The remaining difficulty is to find the values of the C's. This can be done by noting that equation (3.98) is linear in the C's. Using at least three known values of Γ_1, Γ_2 and a_2/a_1, a system of linear equations is formed which can be solved for the C's.

The values of the Γ's to plug into this set of equations are, of course, directly available from the measurements. The values of a_2/a_1 must be derived somewhat indirectly. This is done by measuring a set of calibration standards for which the S-parameters are approximately known. A set of precision transmission lines of approximately known length is a common choice. These lines are reciprocal, and so their complete S-parameters can be found from the knowledge of S_{11}, S_{22} and Δ which is found as noted above.

$$|S_{12}| = |S_{21}| = \sqrt{|\Delta - S_{11}S_{22}|} \tag{3.100}$$

$$\arg(S_{12}) = \arg(S_{12}) = \frac{\arg(\Delta - S_{11}S_{22})}{2} + n\pi \tag{3.101}$$

The $n\pi$ in equation (3.101) results from the sign ambiguity of the square root. Since in this case, the length of each of the calibration standards is approximately known, this sign ambiguity can be resolved by calculating the expected value of $\arg(S_{12})$ and choosing the sign that gives the value closest to this.

With all the S-parameters for the calibration standards thus measured, equations (3.95) or (3.96) can be used to find a_2/a_1 for each measurement, and determination of the values of the C's can proceed.

The values of the C's change when the phase shifter or variable attenuators are switched. Thus C's must be calculated and stored for all possible configurations of the measurement system.

After all calibration has been completed, measurement of the S-parameters of an unknown two-port proceeds as follows: the measurement system is stepped through all combinations of the phase shifter and attenuator positions and the

values of the Γ's resulting are stored. These are then summed into a matrix and least-squares estimates of S_{11}, S_{22} and Δ for the unknown network are determined through a set of equations like (3.52). Then the C's are used to find a_2/a_1 for each of the measurement configurations, and calculate S_{12} and S_{21} by solving equations (3.95) and (3.96), respectively. The resulting values of S_{12} and S_{21}, respectively, are averaged to yield the final estimates of these quantities.

This is the general procedure. If it is known that the two-port being measured is reciprocal, then greater accuracy can be achieved by using (3.100–3.101) to find $S_{12} \equiv S_{21}$. Then the results from (3.95–3.96) and (3.99) can be used only to resolve the sign ambiguity in (3.101).

By changing the positions of the variable attenuators, the value of a_2/a_1 can be made arbitrarily large or small. This can be used to advantage in some measurement situations. In measuring an amplifier, for example, the signal on the output side of the amplifier is at a much higher level than that on the input side. Most six-port reflectometers have their best accuracy when measuring values of Γ for which $|\Gamma| \leq 1$. By making $|a_2/a_1|$ approximately equal to the gain of the amplifier, ratios near unity will be measured by both the input and output reflectometers.

In summary, two six-port reflectometers can be combined in a system that can measure the full S-parameters of unknown two-ports. This system has none of the switch-dependency problems that can occur with the four-port-based systems. As long as the various switches (attenuators and phase shifters) in the six-port system are repeatable, their effects are calibrated out.

References

[1] G.F. Engen, "Calibration of an arbitrary six-port junction for measurement of active and passive circuit parameters," *IEEE Trans. Inst. Meas.*, vol. IM-22, no. 4, pp. 295–299, Dec. 1973

[2] G.F. Engen, "The six-port reflectometer: An alternative network analyzer," in *1977 IEEE Mtt-S Int. Microwave Symp. Dig.*, June 1977, pp. 44–45, 53–55

[3] G.F. Engen, "Calibrating the six-port reflectometer by means of sliding terminations," *IEEE Trans. Microwave Theory Tech.*, vol. MTT-26, no. 12, pp. 951–957, Dec. 1978

[4] *CRC Standard Math Tables,* Boca Raton, FL: CRC Press, Inc.

[5] G.F. Engen, "An improved circuit for implementing the six-port technique of microwave measurements," *IEEE Trans. Microwave Theory Tech.*, vol. MTT-25, no. 12, pp. 1080–1083, Dec. 1977

[6] G.F. Engen and C.A. Hoer, "'Thru-reflect-line': An improved technique for calibrating the dual six-port automatic network analyzer," *IEEE Trans. Microwave Theory Tech.*, vol. MTT-27, no. 12, pp. 987–993, Dec. 1979

[7] C.A. Hoer, "A network analyzer incorporating two six-port reflectometers," *IEEE Trans. Microwave Theory Tech.*, vol. MTT-25, no. 12, pp. 1070–1074, Dec. 1977

[8] C.A. Hoer, "Performance of a dual six-port automatic network analyzer," *IEEE Trans. Microwave Theory Tech.*, vol. MTT-27, no. 12, pp. 993–998, Dec. 1979

[9] C.A. Hoer, "Using six-port and eight-port junctions to measure active and passive circuit parameters," *Nat. Bur. Stand. Tech. Note* 673, Sept. 1975

[10] G.F. Engen, "A least squares solution for use in the six-port measurement technique," *IEEE Trans. Microwave Theory Tech.*, vol. MTT-28, no. 12, pp. 1473–1477, Dec. 1980

[11 C.A. Hoer and K.C. Roe, "Using an arbitrary six-port junction to measure complex voltage ratios," *IEEE Trans. Microwave Theory Tech.*, vol. MTT-23, pp. 978–984, Dec. 1975

[12] I. Kasa, "Closed-form mathematical solutions to some network analyzer calibration equations," *IEEE Trans. Instrum. Meas.*, vol. IM-23, no. 4, pp. 399–402, Dec. 1974

[13] H.M. Cronson and L. Susman, "A six-port automatic network analyzer," *IEEE Trans. Microwave Theory Tech.*, vol. MTT-25, no. 12, pp. 1086–1091, Dec. 1977

[14] M.P. Weidman, "A semiautomated six-port for measuring millimeter-wave power and complex reflection coefficient," *IEEE Trans. Microwave Theory Tech.*, vol. MTT-25, no. 12, pp. 1083–1085, Dec. 1977

[15] G.F. Engen and C.A. Hoer, "Application of arbitrary six-port junction to power measurement problems," *IEEE Trans. Instrum. Meas.*, vol. IM-21, pp. 470–474, Nov. 1972

[16] G.F. Engen, "Determination of microwave phase and amplitude from power measurements," *IEEE Trans. Instrum. Meas.*, vol. IM-25, no. 4, pp. 414–418, Dec. 1976

[17] H.M. Altschuler, "The measurement of arbitrary linear microwave two-ports," *Proc. Inst. Elec. Eng.*, vol. 109, pt. B. suppl., no. 23, pp. 704–712, May 1962

[18] C.A. Hoer, K.C. Roe and C.M. Allred, "Measuring and minimizing diode detector nonlinearity," *IEEE Trans. Instrum. Meas.*, vol. IM-25, no. 4, pp. 324–329

[19] C.M. Allred and C.H. Manney, "The calibration and use of directional couplers without standards," *IEEE Trans. Instrum. Meas.*, vol. IM-25, no. 1, pp. 84–89, Mar. 1976

[20] G.F. Engen, "An overview of the six-port measurement technique," in *1978 IEEE MTT-S Int. Symp. Dig.*, pp. 174–175

[21] C.A. Hoer, "Calibrating two six-port reflectometers with an unknown length of precision transmission line," in *1978 IEEE MTT-S Int. Symp. Dig.*, pp. 176–178

[22] L. Susman, "A new technique for calibrating dual six-port networks with application to s-parameter measurements," in *1978 IEEE MTT-S Int. Symp. Dig.*, pp. 179–181

[23] G.F. Engen, "Calibrating the six-port reflectometer," in *1978 IEEE MTT-S Int. Symp. Dig.*, pp. 182–183

[24] G.F. Engen, C.A. Hoer and R.A. Speciale, "The application of 'thru-short-delay' to the calibration of the dual six-port," in *1978 IEEE MTT-S Int. Symp. Dig.*, pp. 184–185

Chapter 4

Sampled-Line Network Analyzer Theory

The sampled-line network analyzer is a particularly simple implementation of the six-port type of network analyzer. It removes the need for the broad band directional couplers used in the NBS implementations. Also, the sampled-line analyzer uses more detector diodes than previous implementations and the additional data from these detectors can be used to advantage.

Figure 4.1 shows the sampled-line network analyzer schematically. It consists of a uniform transmission line with several power detector diodes connected in shunt across it. The diodes are resistively isolated from the line to minimize loading effects. An attenuator placed between the line and the device under test prevents deep voltage nulls from occurring on the line. Removal of such nulls is important for the instrument's accuracy, as will be shown below.

The diodes sample the magnitude of the microwave voltage at their points of connection. The incident and reflected waves, travelling in opposite directions on the line, are sampled with different relative phases at different points on the line. A six-port type analysis can be applied to the resulting diode voltages: one diode voltage is chosen as the denominator of the complex ratio w, and all the others are divided by that voltage. The resulting ratios give the radii of circles as in figure 3.2. For n diodes, however, there are $(n-1)$ circles, all ideally intersecting

at a single point in the w-plane. A least-squares estimate of the value of w can be found from this overdetermined system, giving an accurate measurement.

The diode spacing scheme shown in figure 4.1 allows extension of the network analyzer's operation over a broad frequency range. As discussed in chapter 3, a set of three detectors provides two circles that can be used to determine w to within a sign. One circle has its center at zero in the w-plane, and the other has center w_1. Assuming that some way can be found to resolve the sign ambiguity, then the requirement for an accurate measurement is that w_1 be placed in such a way that for any measured Γ, the resulting circles, centered on zero and w_1, do not intersect at too oblique an angle.

Placement of w_1 in the sampled-line analyzer is determined by the spacing of the sampling diodes. A convenient measure of the "goodness" of a particular configuration is the sensitivity of the calculated value of Γ for a given measurement to noise on the detector voltages. The average noise sensitivity in the determination of Γ, over all $|\Gamma| \leq 1$ was calculated for a wide range of diode spacings. The results showed that for a given frequency, the minimum average noise sensitivity is achieved when the three diodes are uniformly spaced along the line with one sixth of a wavelength between each pair of diodes.

It turns out that one such diode triple provides good accuracy (noise sensitivity within a factor of two of the minimum) over about an octave of frequency. When one triple's useful frequency is exceeded, another triple can be formed by placing a fourth diode halfway between one pair of diodes in the original triple. This second triple has a frequency range twice as high as the first, and this method can be continued, to extend the analyzer's operating range to the upper working frequency of the diode detectors.

This is the fundamental difference between the sampled-line analyzer and previous six-port analyzer configurations. Previous analyzers used a fixed number of diodes. To extend their operating bandwidth a broader-band coupling

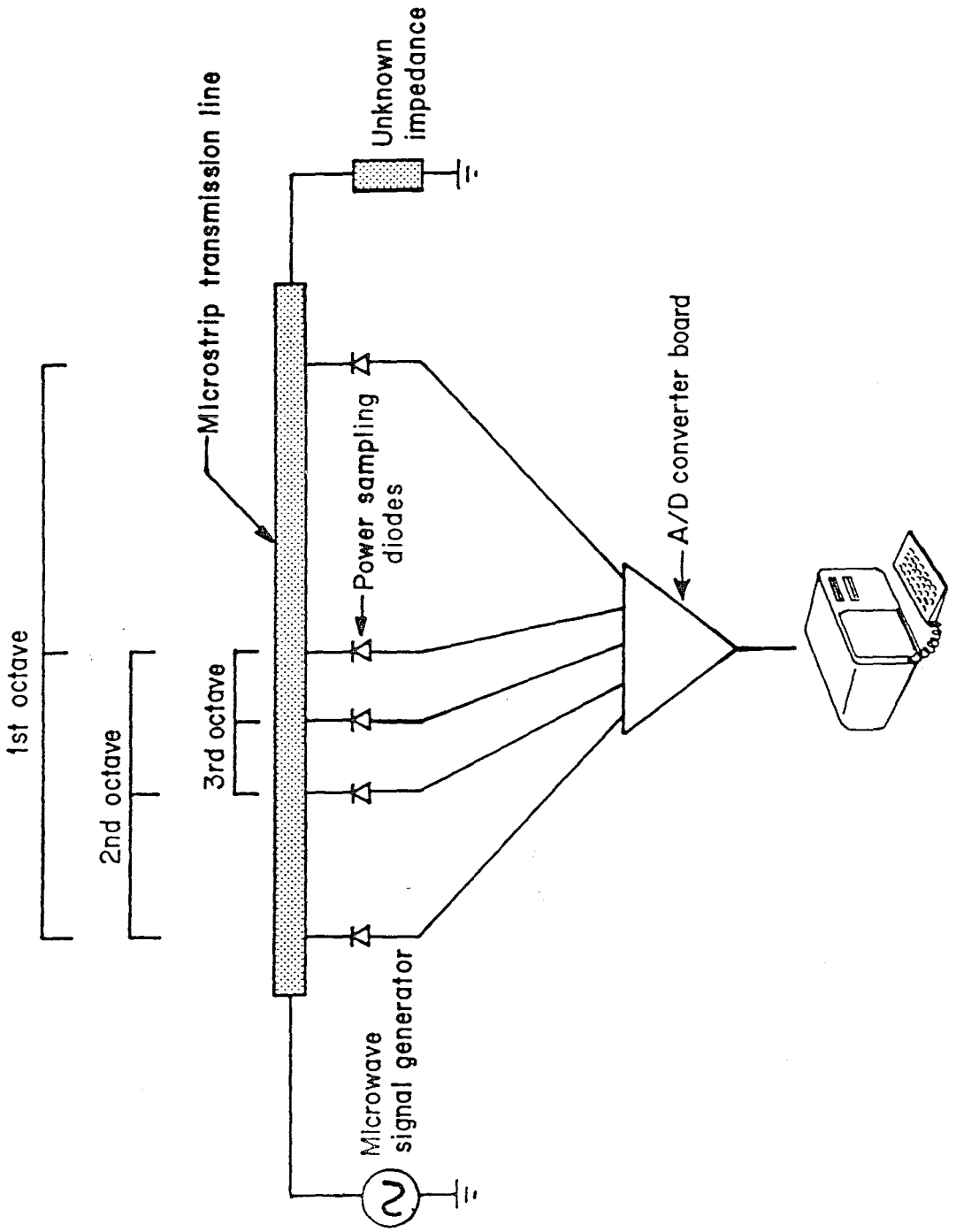

Figure 4.1 The sampled-line analyzer consists of a number of power detectors distributed along a transmission line. The spacing scheme shown allows extension of the operation of the analyzer over a wide frequency range.

structure was required to provide signals to the diodes. In the sampled-line analyzer, a simple resistive coupling structure is used. To extend the analyzer's frequency of operation, additional diodes are added to the system. The larger number of diodes in the system has other advantages. By using information from all the diodes in the system at each measurement frequency to form a least squares estimate of the measured quantity, measurement accuracy is enhanced and the system becomes more robust.

Sampled lines have, of course, been used for impedance measurements for many years [1–4]. These instruments used sums and differences of powers measured at points along the line to determine the reflection coefficient of the device under test. A six-port type analysis could not be applied to the sum and difference data and the loading effects of the samplers were not calibrated out. Also, since ratios of the measured powers were not used, the measurements were affected by fluctuations in the signal source's output power.

4.1 Placement of the Measurement Centers

Given that the sampled-line analyzer is a type of six-port, the best way to examine its operation is to consider the placement in the w-plane of the measurement centers $w_1, w_2, \ldots, w_{(n-2)}$ where n is the number of detectors used.

Figure 4.2 shows the theoretical model of the sampled-line analyzer used to calculate the positions of the measurement centers and scale factors. It is assumed that the detectors do not load the transmission line at all. The θ's are the electrical lengths of the various sections of transmission line, and the detectors are numbered as shown. Only four detectors are shown here, though there may in general be many more. Detectors 3, 4, and 5 are assumed to have the uniform $\lambda/6$-spacing, and detector i has some arbitrary placement on the line. No attenuator is placed between the line and the device under test for this analysis.

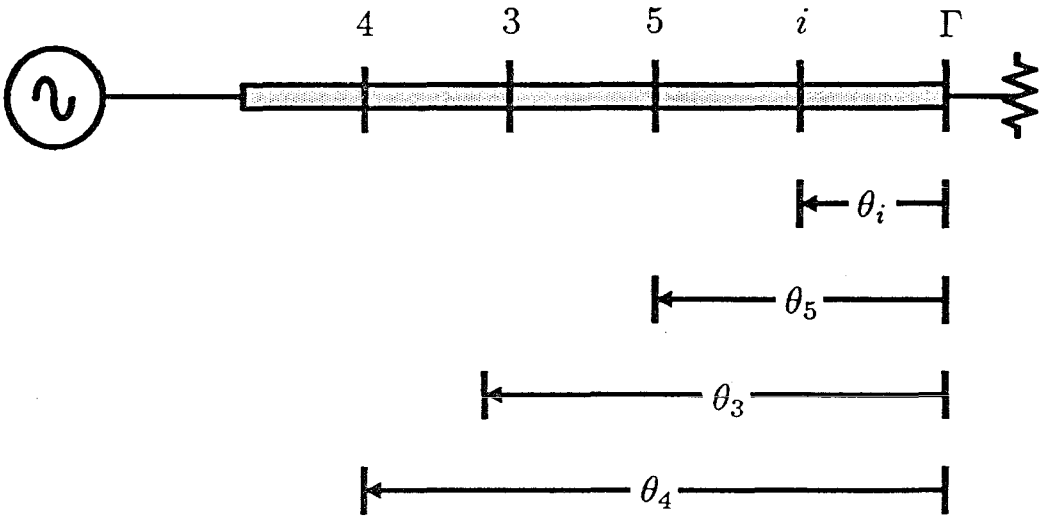

Figure 4.2 Model of the ideal sampled-line at a single frequency. The detectors have infinite impedance. Their response is the square of the magnitude of the voltage at the point of connection on the line.

As in chapter 3,

$$b_5 = Kb_3 + Lb_4 \tag{4.1}$$

$$\frac{1}{|K|^2}\left|\frac{b_5}{b_4}\right|^2 = \left|\frac{b_3}{b_4} + \frac{L}{K}\right|^2 \tag{4.2}$$

$$\zeta_1 \frac{P_5}{P_4} = |w - w_1|^2 \tag{4.3}$$

The values of $\zeta_1 = 1/|K|^2$ and $w_1 = -L/K$ are to be found.

The voltage measured by a given sampler is the sum of the left and right travelling voltage waves on the line at the point where the sampler is connected. Associating this complex voltage with a single travelling wave value, b_i, may seem odd, but it is easy to see that such an assignment is valid. The sampler could be replaced with an ideal voltage amplifier which would sample the voltage on

the line and produce a travelling wave at its output with an amplitude equal to the sampled voltage. Keeping this in mind, then, expressions for $b_3, \ldots, b_6$ can be written:

$$b_4 = b_2(1 + \Gamma e^{-j2\theta_4}) \tag{4.4}$$

$$b_3 = b_2(1 + \Gamma e^{-j2\theta_3})e^{-j(\theta_4-\theta_3)} \tag{4.5}$$

$$b_5 = b_2(1 + \Gamma e^{-j2\theta_5})e^{-j(\theta_4-\theta_5)} \tag{4.6}$$

$$b_6 = b_2(1 + \Gamma e^{-j2\theta_6})e^{-j(\theta_4-\theta_6)} \tag{4.7}$$

Substituting (4.4–4.6) in (4.1) gives

$$(1 + \Gamma e^{-j2\theta_5})e^{-j(\theta_4-\theta_5)} = K(1 + \Gamma e^{-j2\theta_3})e^{-j(\theta_4-\theta_3)} + L(1 + \Gamma e^{-j2\theta_4}) \tag{4.8}$$

$$e^{-j(\theta_4-\theta_5)} + \Gamma e^{-j(\theta_4+\theta_5)} = Ke^{-j(\theta_4-\theta_3)} + K\Gamma e^{-j(\theta_4+\theta_3)} + L + L\Gamma e^{-j2\theta_4} \tag{4.9}$$

Since (4.9) must be true for all values of Γ, it can be rewritten as two equations:

$$e^{-j(\theta_4-\theta_5)} = Ke^{-j(\theta_4-\theta_3)} + L \tag{4.10}$$

$$e^{-j(\theta_4+\theta_5)} = Ke^{-j(\theta_4+\theta_3)} + Le^{-j2\theta_4} \tag{4.11}$$

When these two equations are solved for K and L they give

$$K = \frac{\sin(\theta_4 - \theta_5)}{\sin(\theta_4 - \theta_3)} \tag{4.12}$$

$$L = \frac{\sin(\theta_3 - \theta_5)}{\sin(\theta_3 - \theta_4)} \tag{4.13}$$

and thus

$$w_1 = -\frac{L}{K} = \frac{\sin(\theta_3 - \theta_5)}{\sin(\theta_4 - \theta_5)} \tag{4.14}$$

$$\zeta_1 = \frac{1}{|K|^2} = \frac{\sin^2(\theta_4 - \theta_3)}{\sin^2(\theta_4 - \theta_5)} \tag{4.15}$$

An identical analysis for detector i, placed an electrical distance of θ_i from the load gives

$$w_{(i-4)} = \frac{\sin(\theta_3 - \theta_i)}{\sin(\theta_4 - \theta_i)} \tag{4.16}$$

$$\zeta_{(i-4)} = \frac{\sin^2(\theta_4 - \theta_3)}{\sin^2(\theta_4 - \theta_i)} \tag{4.17}$$

Finally, from (4.4–4.6), the expression for $w = b_3/b_4$ can be written:

$$\frac{b_3}{b_4} = \frac{1 + \Gamma e^{-j2\theta_3}}{1 + \Gamma e^{-j2\theta_4}} e^{-j(\theta_4 - \theta_3)} \tag{4.18}$$

Figure 4.3 shows these results graphically. The circles of constant $|\Gamma|$ show how the bilinear transform maps the Γ-plane to the w-plane. First, $\Gamma = 0$ is mapped to $w = e^{-j(\theta_4 - \theta_3)}$. Since detectors 3 and 4 are assumed to be $\lambda/6$ apart, the zero reflection coefficient point maps to $e^{-j\pi/3}$.

The $\Gamma = 0$ point maps to a unity-magnitude w for any diode spacing. The spacing determines the angle of the resulting w. This must be the case since, when $\Gamma = 0$, there is no standing wave on the sampled-line, and all detectors observe signals of the same magnitude. The ratio of samples at any two points on the line then has unity magnitude.

The $|\Gamma| = 1$ circle is mapped to the real axis of the w-plane. This can be seen by substituting $\Gamma = e^{j\phi}$ into (4.18). The result is

$$w = \frac{\cos(\theta_3 - \phi/2)}{\cos(\theta_4 - \phi/2)} \tag{4.19}$$

This equation shows that $w \to 0$ when there is a standing wave null at sampler 3, and $w \to \infty$ when there is a null at sampler 4, as must be the case for the sampled-line.

Completing the picture, it is observed from equations (4.14) and (4.16) that all the measurement centers, $w_1, \ldots, w_{(n-2)}$, lie along the real axis as well. This

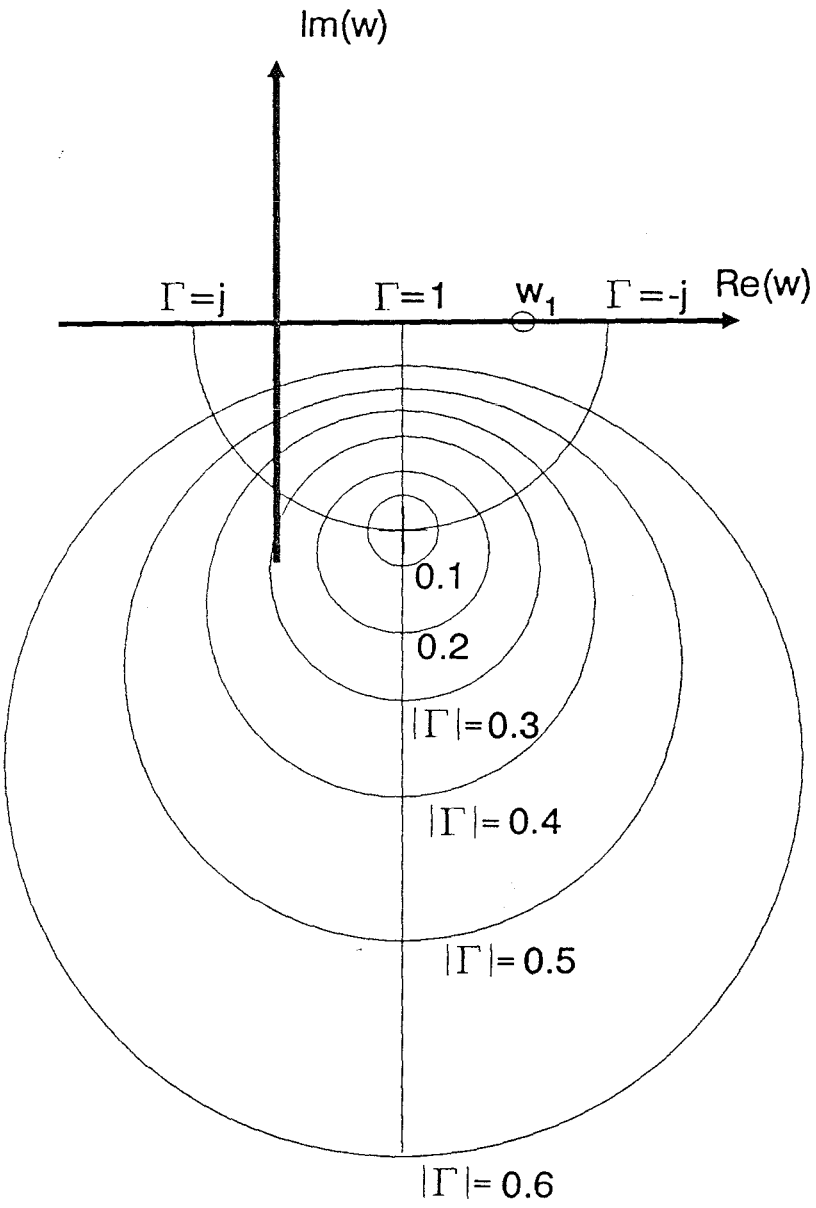

Figure 4.3 The sampled-line analyzer maps the Γ-plane to the w-plane as shown here.

can also be seen by examination of the physical configuration. From equation (4.3) it is seen that $w = w_1$ is the point at which P_5 goes to zero. On the sampled-line, a zero detector output indicates a standing wave null. Only unity-magnitude Γ's produce nulls, and the corresponding w lies on the real w-axis, as noted above.

So the ideal sampled-line network analyzer transforms the Γ plane such that the region of $|\Gamma| > 1$ is mapped into the upper half of the w-plane ($\mathrm{Im}\, w > 0$), and $|\Gamma| < 1$ is mapped to the ($\mathrm{Im}\, w < 0$) region. This has the advantage that when measuring passive circuits, only the data from three detectors need be used to find the value of Γ. These data give two circles, which will intersect at two points. The ambiguity in the value of w is resolved immediately, however, since only one of these intersections, the one with $\mathrm{Im}\, w \leq 0$, corresponds to a realizable Γ. As noted in chapter 3, this makes the sampled-line network analyzer a "five-port" network analyzer.

Having the measurement centers lie along a line in the w-plane is a disadvantage. If it is not known whether the measured Γ has a magnitude greater than or less than one, then the ambiguity cannot be resolved from the diode data directly. Losses in the line and reflections from the diodes do cause the centers not to lie exactly along a line, but the scatter is usually small and cannot be used reliably to resolve the ambiguity. In future versions, a method of resolving the ambiguity will need to be incorporated. Having one diode upstream of the others (toward the generator) with an attenuator between it and the others would be one possibility. This diode would give a center above the real axis of the w-plane.

There is another problem, with the sampled-line analyzer as shown in figure 4.2. Its measurement accuracy for $|\Gamma| \approx 1$ is bad. Reexamining Figure 4.3, for a value of w near the real axis, all the circles resulting from the measured data intersect at very oblique angles. Thus, a small error due to circuit noise in

one of the circles' radii results in a large error in the determination of the point of intersection.

This problem is reduced by placing an attenuator between the device under test and the sampled-line as noted above. The results are shown in figures 4.4 and 4.5. These show contour plots of error sensitivity in the Γ-plane. For three $\lambda/6$-spaced diodes, define $\mathrm{Re}\,\Gamma = f(v_1, v_2, v_3)$ and $\mathrm{Im}\,\Gamma = g(v_1, v_2, v_3)$ where v_1, v_2, and v_3 are the observed detected voltages. Then the quantity plotted in the following figures is

$$E = \left(\frac{\partial f}{\partial v_1}\right)^2 + \left(\frac{\partial f}{\partial v_2}\right)^2 + \left(\frac{\partial f}{\partial v_3}\right)^2 + \left(\frac{\partial g}{\partial v_1}\right)^2 + \left(\frac{\partial g}{\partial v_2}\right)^2 + \left(\frac{\partial g}{\partial v_3}\right)^2 \tag{4.20}$$

These plots are in the Γ-plane. The value of w, with noise added, is found and then transformed into the Γ-plane. It is interesting to note how the transformation process symmetrizes the error around the origin of the Γ-plane. The effect of the attenuator is interesting, as well. The error function is bowl-shaped, rising steeply at the edges. Adding attenuation between the analyzer and the device under test degrades measurement accuracy slightly at the minimum of the bowl, but it flattens out the bowl, improving the accuracy near the edge.

An optimum value for the attenuator attached to the sampled-line has not been found. Other considerations come into play, such as A/D quantization error when the transformed circle becomes too small. Experimentally, values ranging from 3 to 6 dB have been found satisfactory with various versions of the sampled-line analyzer.

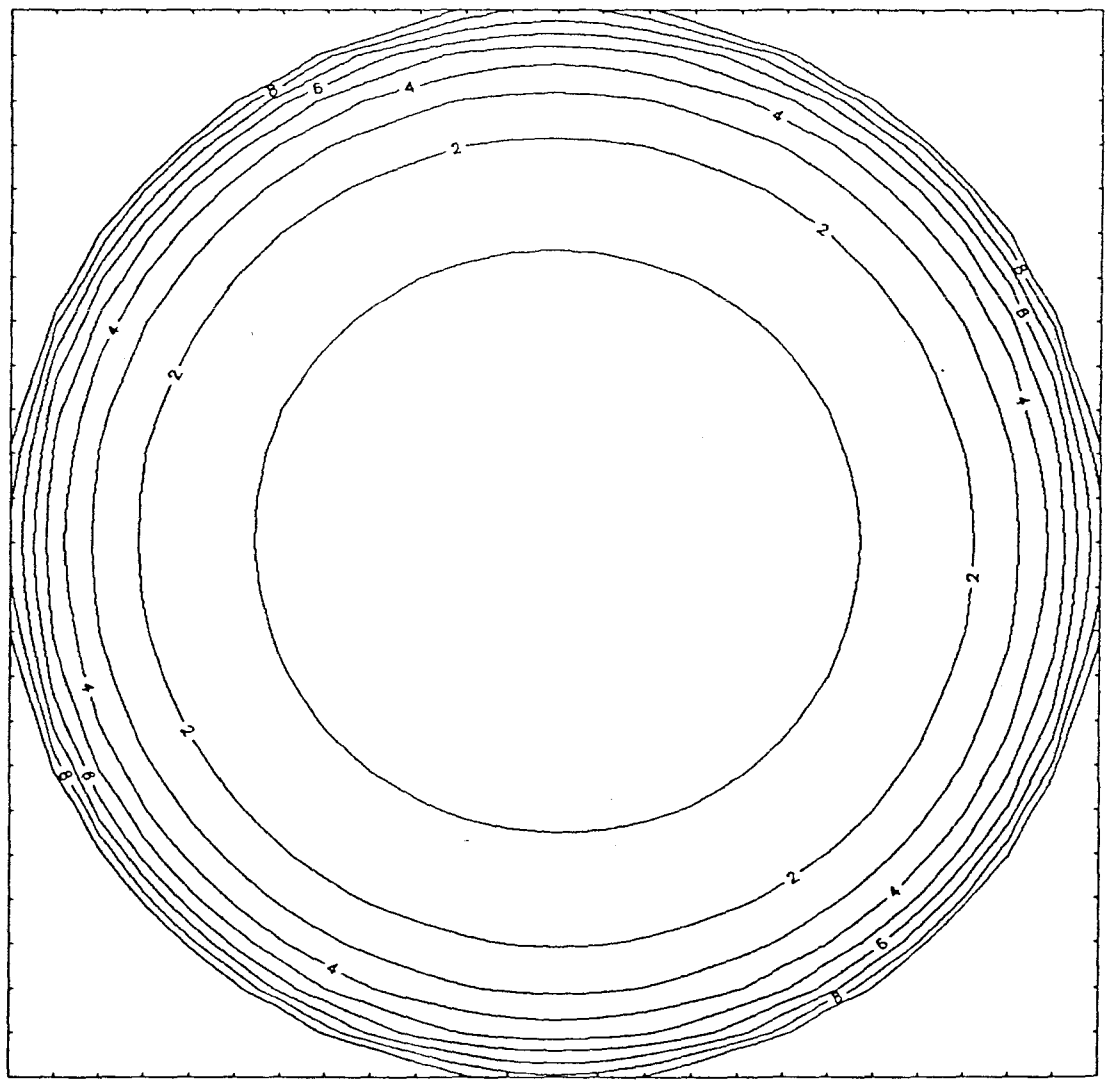

Figure 4.4 Sensitivity of the calculated Γ to noise in the power detectors over the $\Gamma \leq 1$ region with a 0.5 dB attenuator between the sampled-line and the device under test.

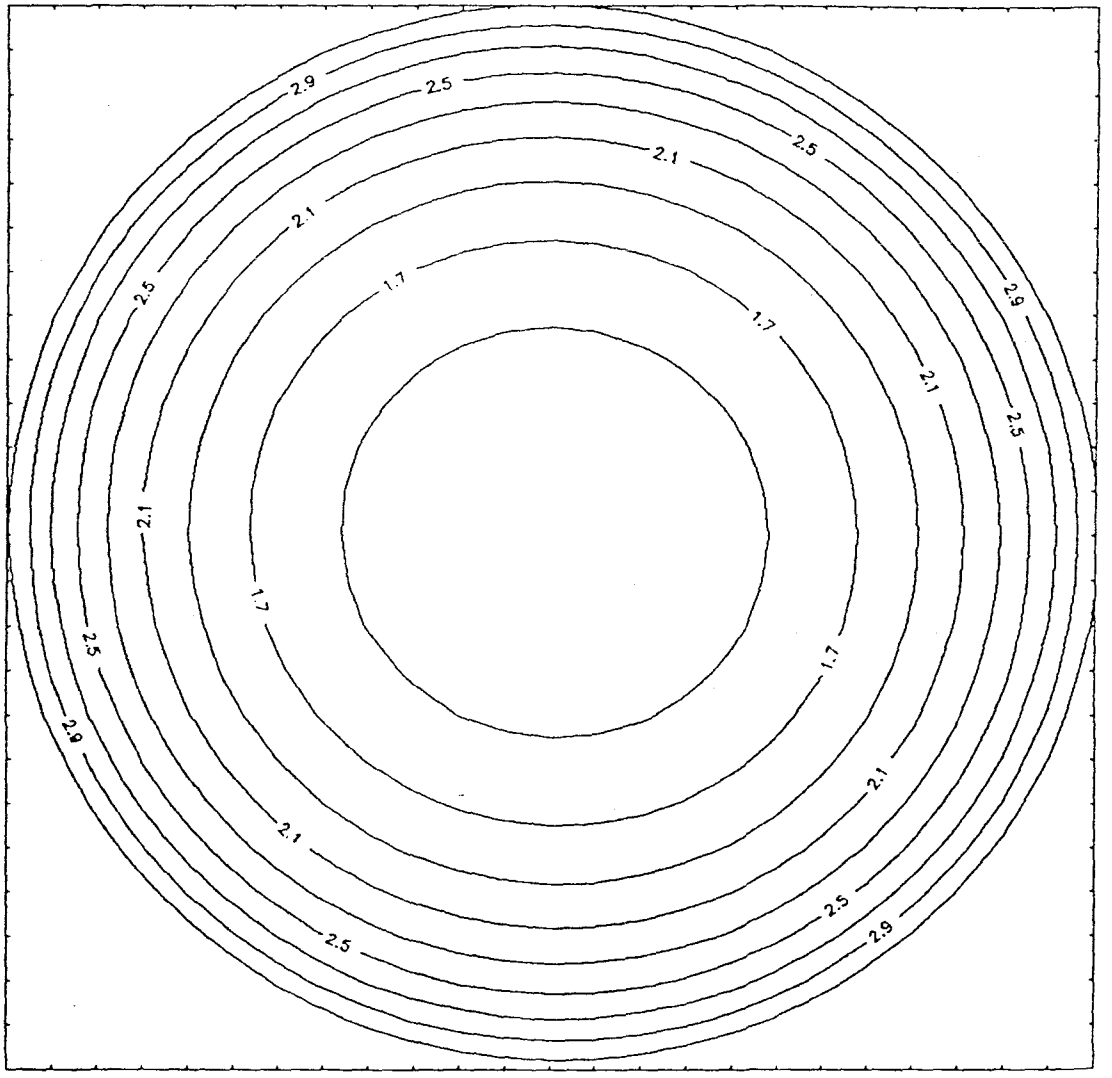

Figure 4.5 Sensitivity of the calculated Γ to noise in the power detectors over the $\Gamma \leq 1$ region with a 3 dB attenuator between the sampled-line and the device under test.

4.2 Calibration and Measurement Options

Having several sampling diodes on the line allows the sampled-line analyzer to present options not available with conventional six-ports.

From a practical point of view, the sampled-line analyzer can fail soft. Should one diode on the line fail, it will seriously affect only measurement accuracy over a fraction of the analyzer's total operating frequency range. With judicious placement of a few additional backup diodes, even this might be avoided, and the analyzer could continue to operate through the failure.

In calibration and measurement, the data supplied by the additional diodes add redundancy and improve accuracy. As noted in chapter 3, calibration of a six-port type network analyzer proceeds in two steps. In the first step, which typically uses a sliding short circuit, the w_i's or measurement centers for the network are found. This reduces the analyzer to an equivalent four-port network analyzer, which is then calibrated to read the true Γ. It has been found that the additional diodes do not help particularly in the first step of the calibration. A center and a scale factor must be found for each diode, so the number of unknowns tends to keep pace with the data available. The cross terms between the constraining relations on the diodes can be used in a optimization. $\binom{n-2}{2}$ equations like (3.18) can be written which must be satisfied simultaneously for every measurement, where n is the number of diodes on the line. Finding the least squares best solution to this set of equations iteratively has not been found to materially improve on the initial estimates of the centers and scale factors for the diodes. The best way found to improve this first step of calibration is to use more sliding short positions.

The additional diodes in the sampled-line analyzer yield improvements, however, in the second stage of the calibration and in the measurement routines. Here, instead of using the data from three detectors to find the complex ratio w trigonometrically, the data from all the detectors are used to find the value

of w which minimizes $\sum c_i[|w - w_i|^2 - R_i^2]^2$. Here w_i is the position of the ith measurement center, R_i is the distance from w to w_i predicted by the measurement ($R_i^2 = \zeta_i P_i / P_4$), and c_i is a weighting factor. The sum is over all the measurement centers.

4.3 Effects of Detector Loading

Up to this point, analysis of the sampled-line analyzer has been concerned only with the ideal case in which the detectors do not affect the sampled-line at all. A computer simulation was used to investigate the effects of detectors that present a nonzero shunt admittance to the sampled-line.

Figure 4.6 shows the sampled-line analyzer as it was simulated. This model coincides with the layout of the present version of the analyzer, designed for operation over the range of 0.6 to 20 GHz. It consists of seven diodes spaced as described above, with spacings ranging from $16l_0$ to l_0, where l_0 is $\lambda/6$ at 14 GHz. The admittance Y of the sampling diodes is variable. A 6 dB attenuator is assumed between the sampled-line and the device under test.

The analysis is done using T-matrices. The program steps along the line calculating at each point the T-matrices of everything to the left and everything to the right of that point on the line. The magnitude of the voltage at that point on the line is calculated from these matrices.

Figure 4.7 shows the ideal case, with zero diode admittance. Three standing wave patterns are shown, for the cases where a short circuit, an open circuit and a matched load ($Z = Z_0$) are connected to the sampled-line analyzer. In this and the three following plots, the generator is on the left side of the plot, and the devices under test are connected on the right side. The $\times$'s on the plot indicate the positions of the samplers. The vertical scale is normalized to the magnitude of the voltage incident on the sampled-line from the generator. In figure 4.7, the samplers do not affect the line at all: the matched load has no standing wave, and the short and open give patterns that are 180° out of phase.

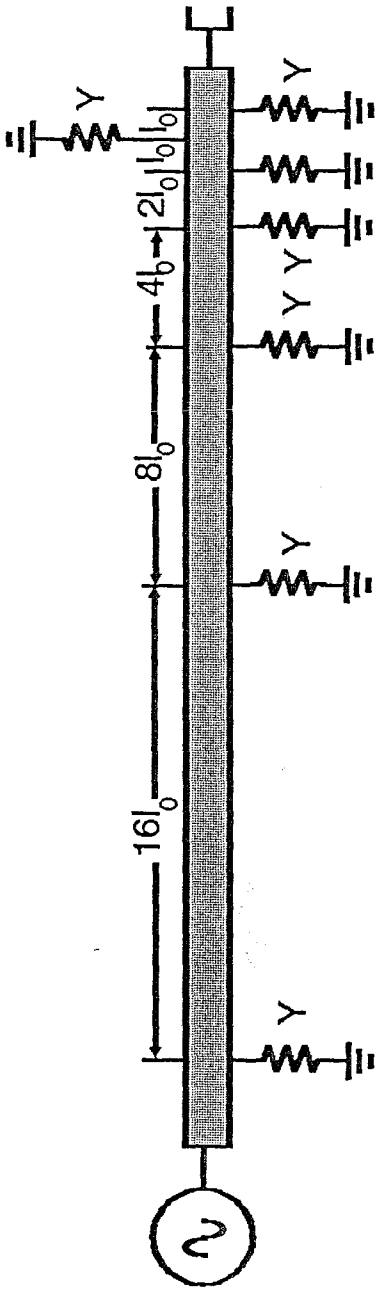

Figure 4.6 The sampled-line analyzer as it was modelled for calculation of the effects of diode loading. The length l_0 is $\lambda/6$ at 14 GHz.

In figure 4.8, the detector admittance has been increased to $0.1Y_0$. On a $50\,\Omega$ line, as is used in all versions of the sampled-line analyzer built to date, this corresponds to a shunt $500\,\Omega$ resistor connected at each sample point. The standing wave pattern for the matched load case now has a magnitude comparable to that of the short circuit. The short and open circuit patterns are still quite distinct, however, and maintain their 180° relative phase.

The alarming trend continues in figure 4.9. Here the detector admittance has been increased to $0.2Y_0$. The patterns for the open circuit and matched load are beginning to look similar and the phases of the open circuit and short circuit are drifting together.

Finally in figure 4.10, the detector admittance is $0.5Y_0$, and here the standing wave pattern is almost completely determined by the samplers.

Figure 4.11 shows the same analyzer at a lower frequency. At this frequency, the entire analyzer is a third of a wavelength long. The plot shows the standing wave pattern on the line when a matched load is connected to it. The plots are for four different values of detector admittance, 0, $0.1Y_0$, $0.2Y_0$ and $0.5Y_0$. This shows more clearly an effect that is evident in the previous plots as well: as the diode admittance increases, diodes downstream from the generator are increasingly starved for signal. At each detector, power is reflected back up the line toward the generator, and some is dissipated. Thus, the amount of power reaching the device under test, and producing a standing wave pattern which can be measured, decreases steadily as detector admittance increases.

The effect of detector admittance on the calibration procedures is shown in table 4.1. Here, the values of the measurement centers, and the position and size of the transformed $|\Gamma| = 1$ circle in the w-plane are calculated for several values of detector admittance.

The most profound effect is upon the radius of the transformed $|\Gamma| = 1$ circle. As the detector admittance increases, this circle shrinks to a point. This again

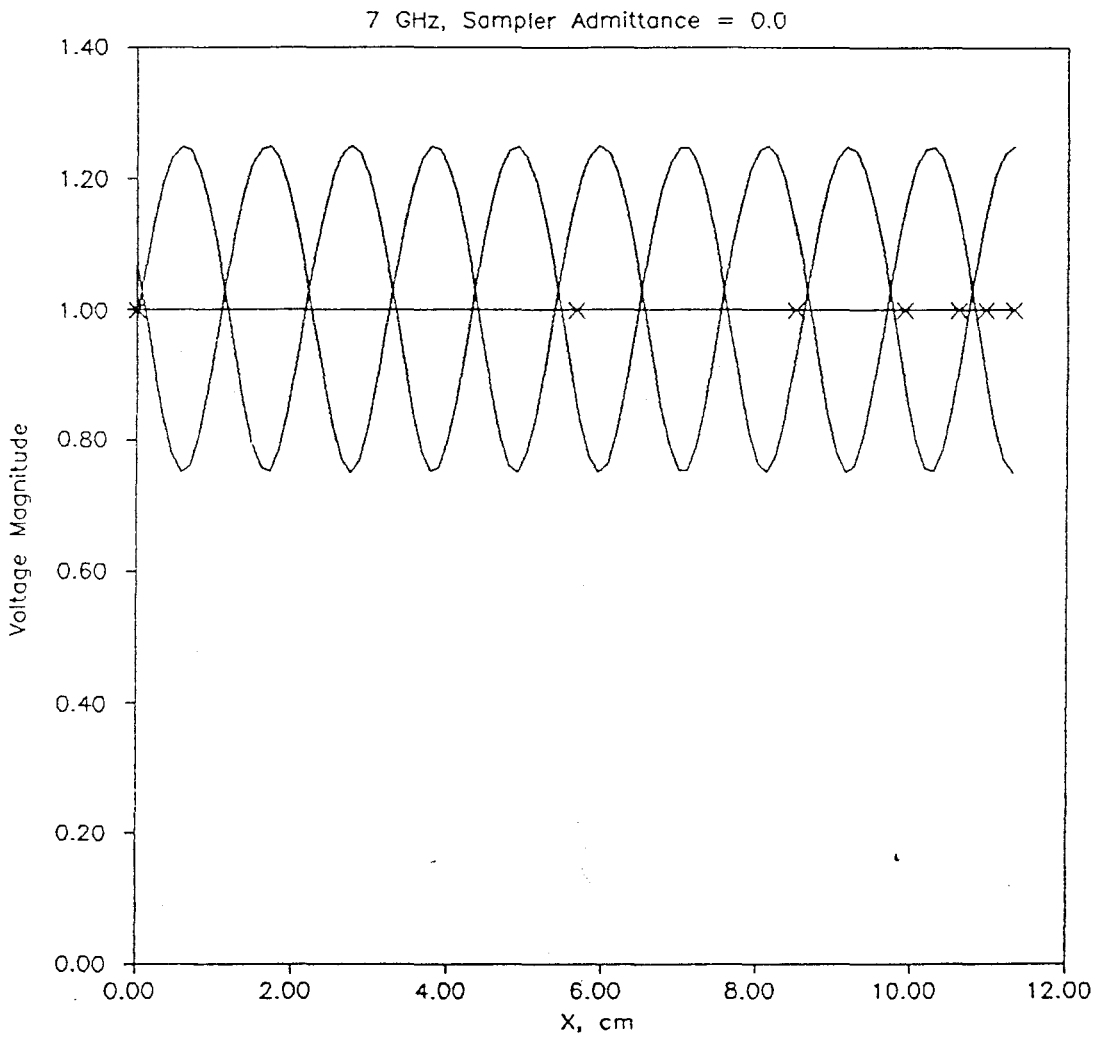

Figure 4.7 Standing wave patterns for a short, open and load connected to a sampled-line reflectometer. Sampler admittance is 0 in this plot.

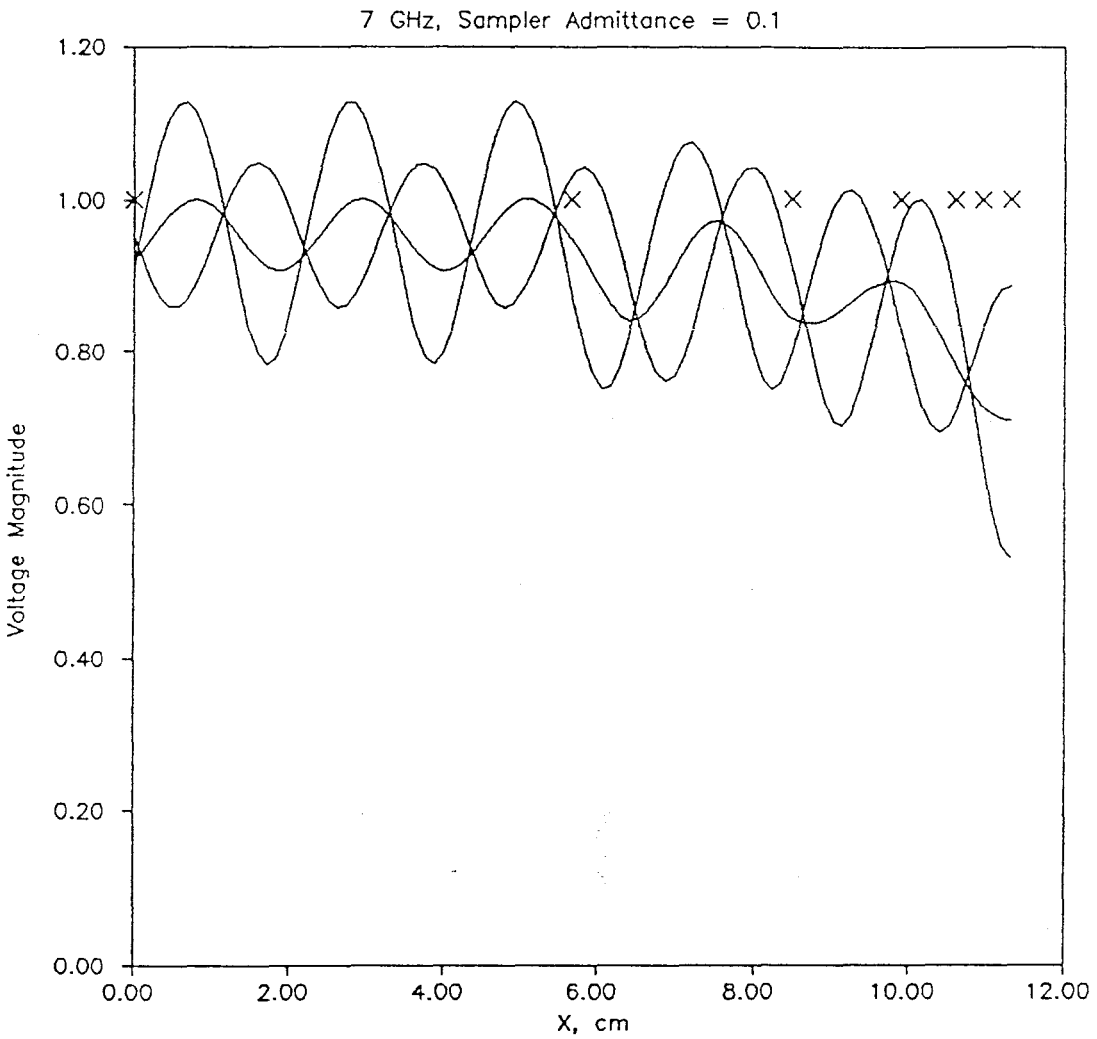

Figure 4.8 Standing wave patterns for a short, open and load connected to a sampled-line reflectometer. Sampler admittance is $0.1Y_0$ in this plot.

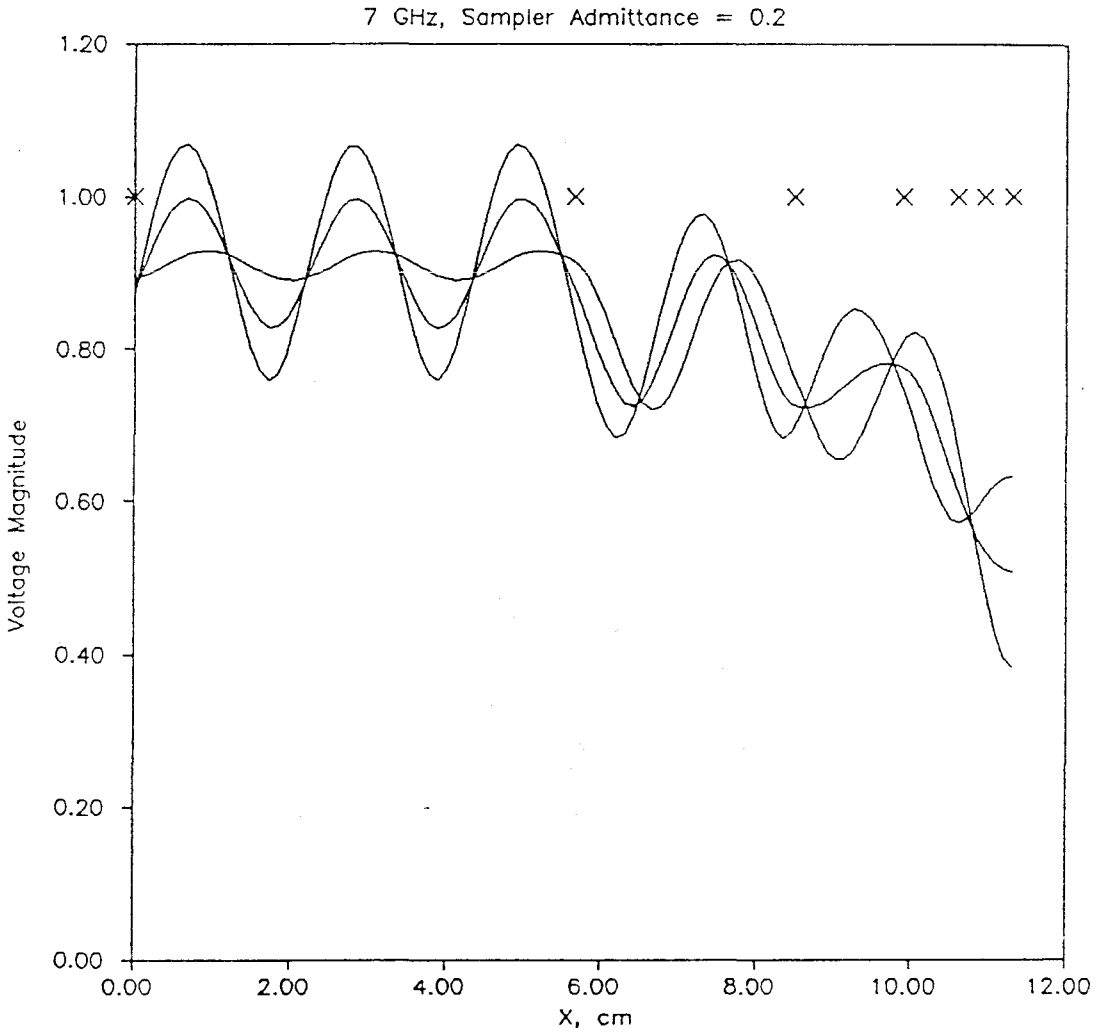

Figure 4.9 Standing wave patterns for a short, open and load connected to a sampled-line reflectometer. Sampler admittance is $0.2Y_0$ in this plot.

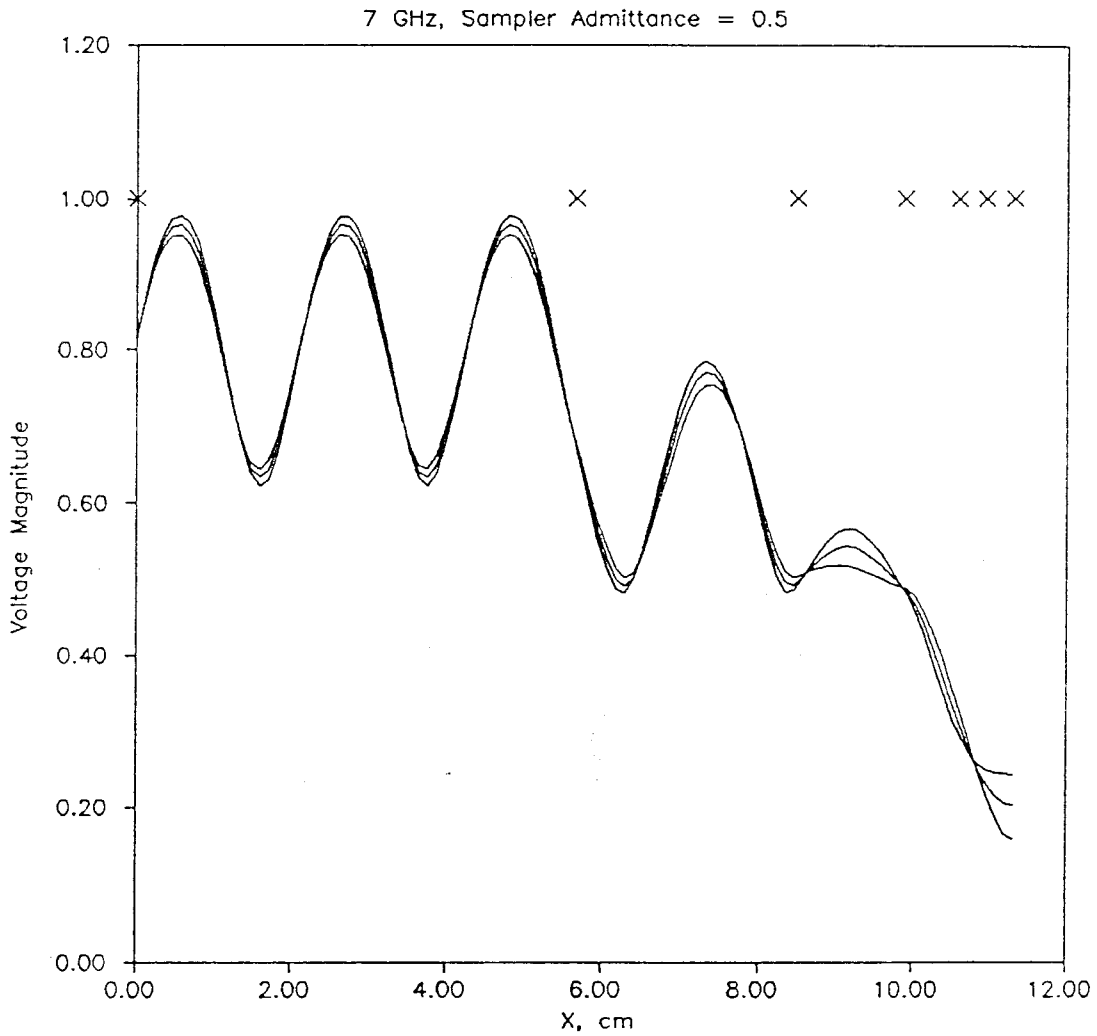

Figure 4.10 Standing wave patterns for a short, open and load connected to a sampled-line reflectometer. Sampler admittance is $0.5Y_0$ in this plot.

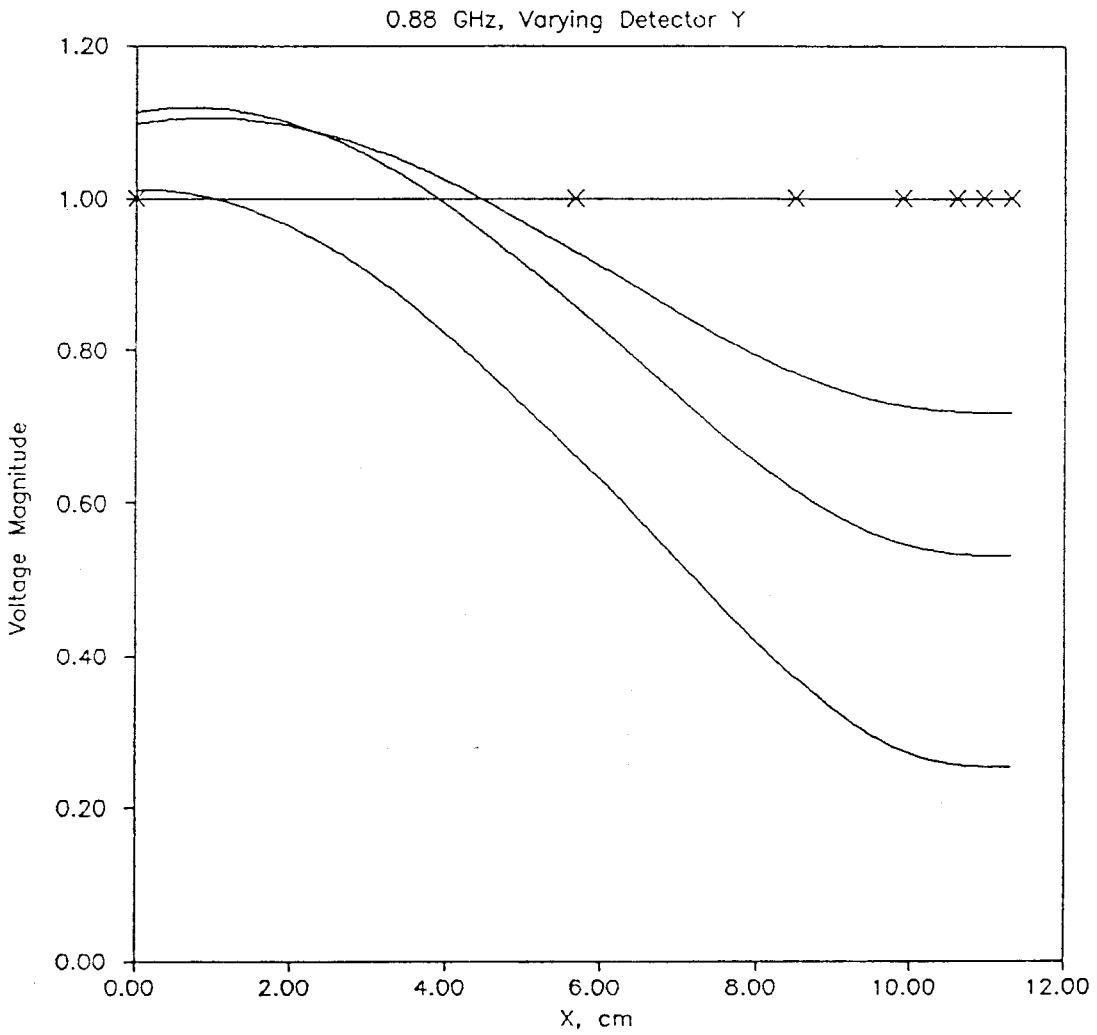

Figure 4.11 Standing wave pattern on the sampled line with a matched load connected to its test port. The detector admittance varies from 0 to $0.5Y_0$

Freq.	Y/Y_0	$\mathrm{Re}(w_1)$	$\mathrm{Re}(w_2)$	$\mathrm{Im}(w_2)$	R
0.875	0.0	0.982	0.495	0.00	0.459
0.875	0.1	0.973	0.493	0.04	0.184
0.875	0.2	0.948	0.488	0.08	0.098
0.875	0.5	0.816	0.461	0.15	0.027
1.250	0.0	5.572	0.848	0.00	0.531
1.250	0.1	4.075	0.678	0.50	0.313
1.250	0.2	2.643	0.549	0.63	0.145
1.250	0.5	1.209	0.530	−0.57	0.042

Table 4.1 Calibration coefficients for the n-port to 4-port conversion under various detector loading values. Y is the detector sampler admittance and w_1 and w_2 are the primary measurement center and a secondary center, respectively. R is the radius of the transformed $|\Gamma| = 1$ circle in the w-plane. For the frequency range of 0.625–1.25 GHz, the primary triple for the analyzer consists of the first, second and seventh diode, numbering from the generator. The secondary triple given as an example consists of the first, second and third diodes. 0.875 GHz is near the optimum frequency for the primary triple and 1.25 GHz is the worst case, at the extreme of the triple's frequency range.

reflects the fact that as diode admittance increases, the unknown load connected has a decreasing effect on the voltages observed by the detectors.

As the radius of the transformed $|\Gamma| = 1$ circle decreases, measurement accuracy degrades steadily. A given amount of noise on any of the measured voltages transforms into increasingly large errors in the determination of Γ.

Measurements made with sampled-line analyzers which have been built to date have indicated that a good upper bound on detector admittance is $0.1Y_0$. Above this value, unacceptable errors are generally observed at some frequencies.

References

[1] E.L. Ginzton, *Microwave Measurements*, New York: McGraw-Hill, 1957, pp. 303–307

[2] C-L. J. Hu, "Microwave automatic impedance measuring schemes using three fixed probes," *IEEE Trans. Microwave Theory Tech.*, vol. MTT-31, no. 9, pp. 756–762, Sept. 1983

[3] C-L. J. Hu, "A novel approach to the design of multi-probe high-power microwave automatic impedance measuring schemes," *IEEE Trans. Microwave Theory Tech.*, vol. MTT-28, no. 12, pp. 1422–1428, Dec. 1980

[4] E.H. Shively, "Electromagnetic wave characteristic display apparatus including multiple probe means," U.S. Patent no. 3,238,451, issued Mar. 1, 1966

[5] E. Martín, J. Margineda and J. Zamarro, "An automatic network analyzer using a slotted line reflectometer," *IEEE Trans. Microwave Theory Tech.*, vol. MTT-30, no. 5, pp. 667–669, May 1982

Chapter 5

The Elf Network Analyzer

The Elf network analyzer system is an example of a four-port network analyzer. It was constructed to meet a need for accurate microwave network measurements to support other research programs and the EE153 teaching laboratory. The system consists of a Hewlett-Packard HP 8410C network analyzer, an HP 8350B sweep oscillator, and an IBM personal computer. A 3000-line computer program, named Elf, runs on the PC performing calibration and measurement algorithms described in chapter 2 and providing a flexible, menu-oriented user interface. The system, when calibrated, achieves a worst-case measurement error vector of magnitude $\leq$0.02 for transmission and reflection coefficient measurements over the 0.5-to-12 GHz frequency range. The error magnitude is $\leq$ 0.04 from 12 to 18 GHz. Elf provides an inexpensive method for upgrading the HP 8410 to achieve the high accuracy of an automatic network analyzer.

In the following sections, the hardware and software of the Elf system will be described.

5.1 Hardware Description

Figure 5.1 shows a block diagram of the hardware of the Elf measurement system. The computer communicates with the rest of the system through two interface cards, a general purpose A/D-and-D/A card [1] and an IEEE-488 bus interface card [2]. In the configuration shown, the IEEE-488 card is used to set the frequency of the sweep oscillator, and the A/D card reads the value of the network analyzer measurement from the horizontal and vertical outputs of the HP 8414A polar display used with the analyzer. The vector voltmeter of the HP 8410B network analyzer is a phase-locked receiver, so it automatically tracks the frequency of the sweep oscillator.

It was necessary to modify the HP 8414A polar display for this application. The horizontal and vertical outputs of this unit, as it comes from the factory, are tapped off the outputs of emitter-follower stages in the horizontal and vertical deflection amplifier chains. There is no buffering between these taps and the outside world. It was found that a capacitive load on these terminals, such as a 3-meter coaxial cable connected to the computer's A/D input, would cause these emitter-followers to oscillate. When the computer interface was connected, then, what should have been a dot on the 8414A's CRT became an ellipse of varying size. To correct this problem, buffer amplifiers in the form of IC voltage followers were built into the 8414A.

The reflection-transmission test unit originally used was a Hewlett-Packard 8743B, which features 7-mm precision connectors, and couplers operating from 2 to 12.4 GHz. Since the original construction, a reflection-transmission unit built at Caltech, using directional couplers that cover the 0.5–18 GHz frequency range has been substituted for the HP unit. In addition to its broader frequency coverage, the new unit features flexible cables between the test unit and the device under test, making the measurement process less cumbersome physically. Schematics of this reflection-transmission test set are given in figures 5.2 and 5.3.

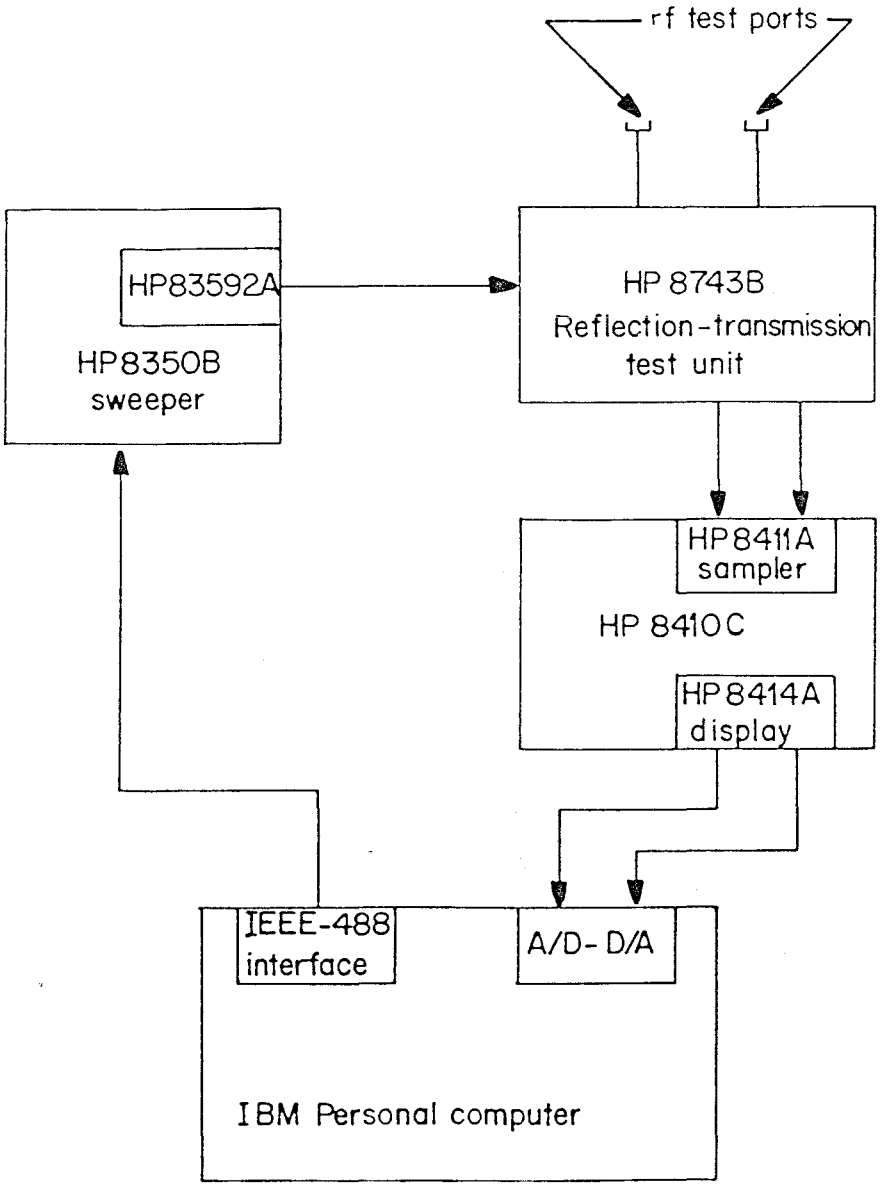

Figure 5.1 A block diagram of the Elf system. The computer controls the measurement by setting the sweeper frequency, and instructing the user to throw switches on the reflection-transmission test unit.

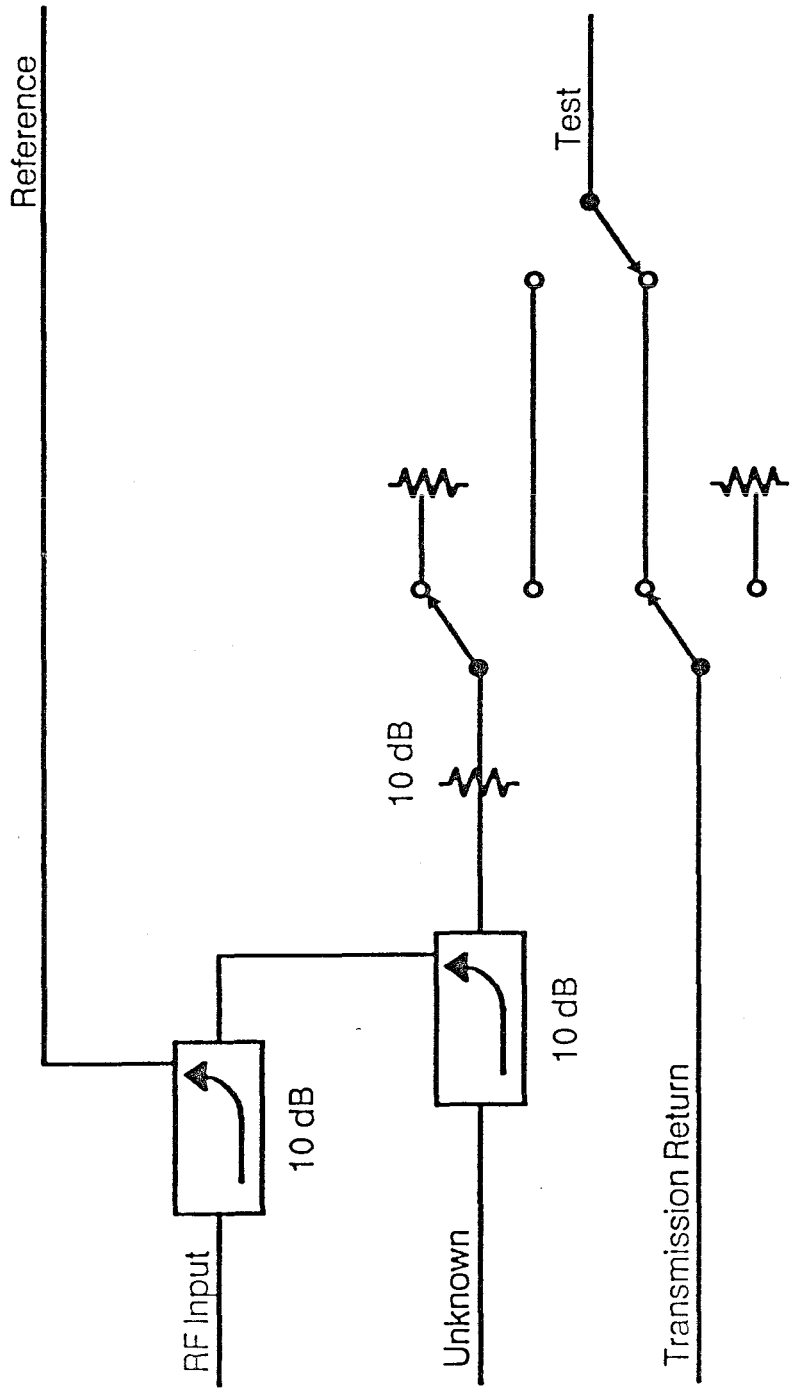

Figure **5.2** RF section of the reflection-transmission test set. Attenuators and directional coupler isolation are used to minimize the effects of the switches on the network, a requirement described in chapter 2.

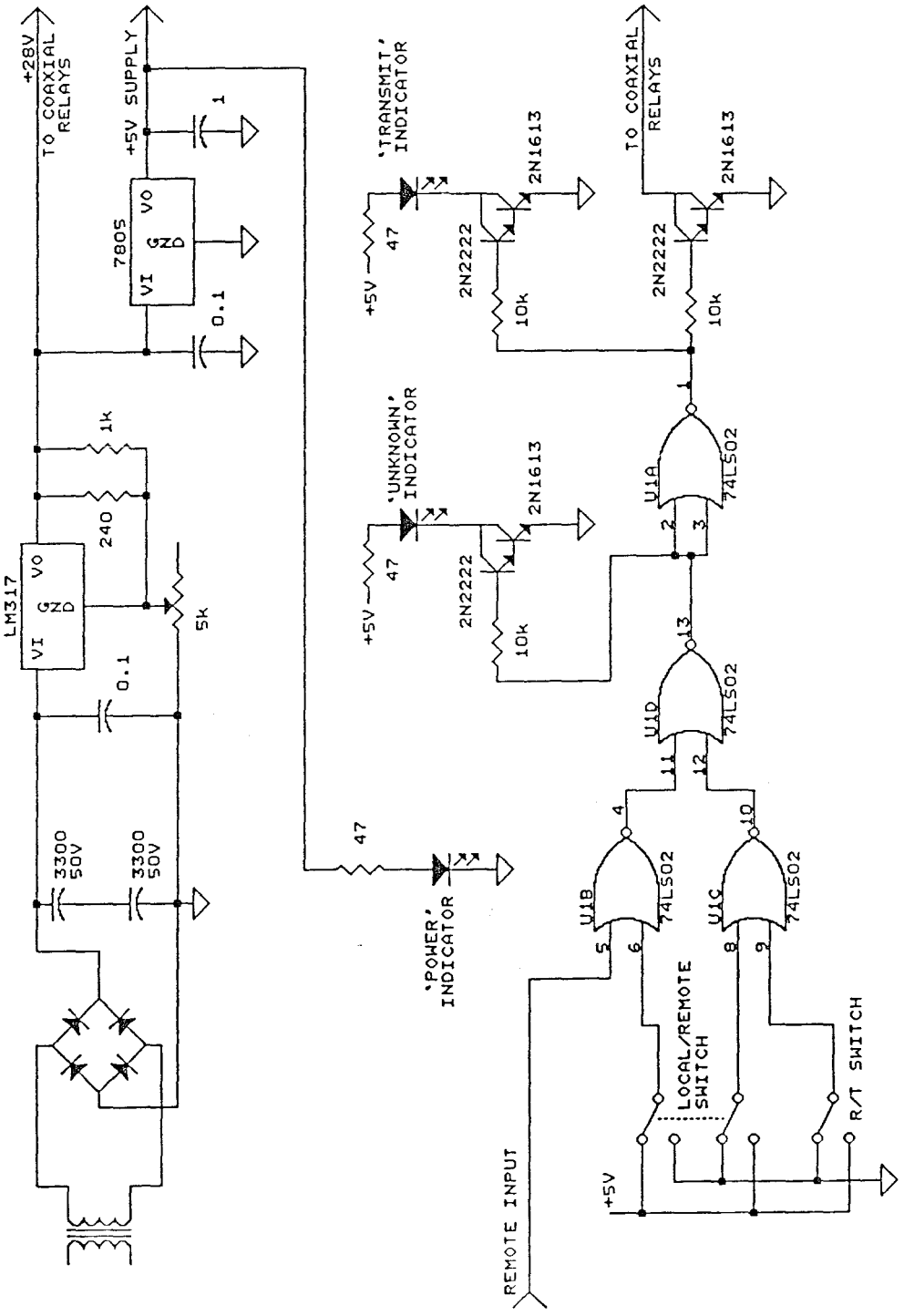

Figure 5.3 Power supply and control electronics for the reflection-transmission test set. The unit may be switched from transmission to reflection measurement mode, either manually, or by a TTL signal that allows the transmission-reflection test set to be computer-controlled.

When the system was initially constructed, an IEEE-488 compatible sweeper was not available, so there is another system configuration option that uses any frequency-proportional-to-voltage microwave source. In this configuration, a voltage from the computer's D/A board is used to set the sweeper frequency, assuming that this frequency is related linearly to voltage. The frequencies at the ends of the sweep are measured by an IEEE-488 compatible microwave counter (HP 5350A) to determine the constants of the linear relation between voltage and frequency.

5.2 Software Description

Elf is written in Pascal, using the Borland Turbo Pascal [3] compiler. It uses the 8087 numeric coprocessor in the IBM PC to increase calculation speed. As noted above, Elf is a menu-oriented program. Figure 5.4 shows the hierarchy of Elf's menus. At start-up, the main menu is displayed. Four options on the main menu select immediate actions to be performed and the remaining four select sub-menus from which additional options can be selected. The first half of the main menu controls the interactions of Elf with the hardware, dealing with mode selection, calibration and measurement. The second half is concerned with manipulation, storage and display of the data after measurement. Elf does not have a continuous measurement mode. After each swept-frequency measurement is made, the data are error-corrected and stored, and may then be saved or displayed in a number of formats.

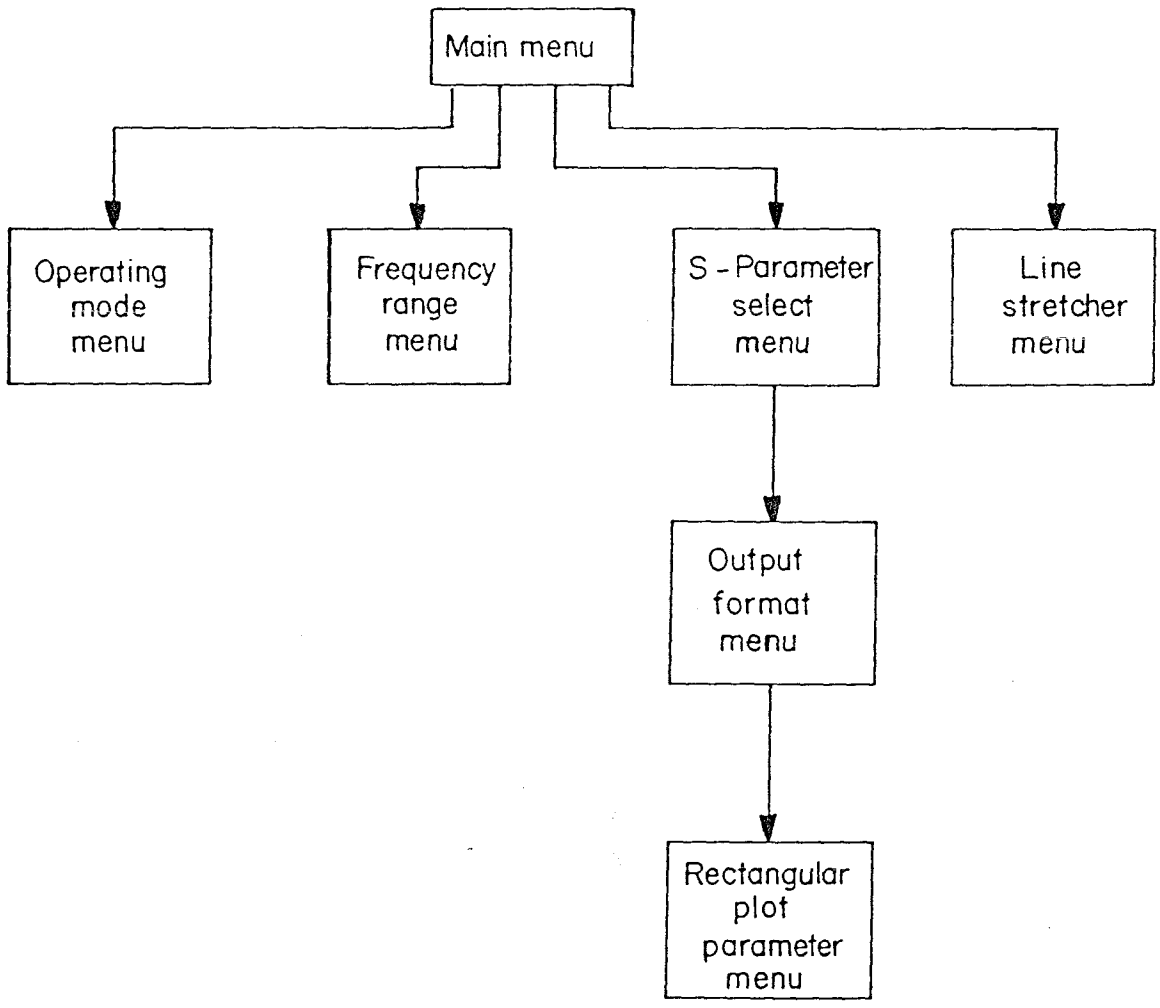

Figure 5.4 Elf's menu tree.

5.2.1 Mode Selection, Calibration, and Measurement

The main menu display shows the following:

```
                    MAIN MENU
1.  Select number of frequency points.
2.  Select operating mode.
3.  Select frequency range.
4.  Calibrate analyzer.
5.  Make measurement.
6.  Save data to disk.
7.  Line stretcher.
8.  Print data.
9.  Exit
```

From this starting point, a measurement can be made by going through the first five menu items in sequence. First, the number of measurement points is selected by pressing '1' and 'ENTER' and answering the resulting prompt. Calibration and measurement will be performed at this number of frequency points evenly spaced between the start and stop frequencies selected below.

Next, the operating mode must be selected. Selecting '2' will result in the following sub-menu:

```
                MODE SELECT MENU
1.  Reflection measurement
2.  Full s-parameter measurement
3.  Sliding load calibration
4.  Exit
```

The choice between reflection and full S-parameter measurements is offered because a full S-parameter calibration and measurement is unnecessarily time consuming when one only wishes to measure a reflection coefficient. The sliding load calibration option is offered for better accuracy in high frequency measurements. Imperfections in the precision 50-Ω load used as one of the calibration standards become more significant with increasing frequency, causing errors in the determination of the zero-reflection point. The locus of reflection coefficients of a sliding load as it moves is a small circle about the zero-reflection point, so the point can be determined even in the presence of imperfections in the load. The effect is to calibrate to the characteristic impedance of the line the load is sliding in, and not to the load itself.

The sliding load calibration may be used with either the reflection or the full S-parameter measurement. In using this sub-menu, then, one selects either '1' or '2' for the type of measurement, and then '3' if desired, for either. Entering '4' returns Elf to the main menu.

Having selected the measurement mode and returned to the main menu, '3' is entered to select the frequency range of the measurement. The following sub-menu results:

```
                FREQUENCY RANGE SELECTION MENU

Sweeper                          Frequency Range

1.  HP 8620C                     4.  Measure full range

2.  HP 694C                      5.  Select frequency sub-range

3.  HP 8350B

6.  Exit
```

The first two choices above were non-IEEE-488 sweepers that were modified to be voltage controlled sources. Choice three is the IEEE-488 controlled sweeper. Choice four is used with the voltage-controlled sweepers; it uses the counter to

measure the extremes of the frequency sweep of the source. Selection five can then be used to choose a sub-range of the frequency sweep of the source. When the IEEE-488 controlled sweeper is used, only step five is needed to select the frequency sweep range. Choice six returns to the main menu.

With the operating mode, frequency range, and number of points selected, the analyzer is ready for calibration. The question of choice of calibration standards then arises. Due to small nonlinearities which are not calibrated out by the procedure described in section 5.2.1, the network analyzer tends to be most accurate when measuring reflection and transmission coefficients close to those of the calibration standards used.

Since the only requirement for calibration is three known standards (six for full S-parameter measurement), the standards can be chosen to be close to the expected measurement values for maximum accuracy. For example, when measuring a high impedance device at the end of a transmission line, one might choose an open circuit on the same length of line as one of the calibration standards.

In Elf, a default general-purpose set of standards is programmed in. To choose another set of standards, a mathematical model of the new standards as a function of frequency must be entered. This involves changing Elf's Pascal source code, and recompiling it. The default set of standards is a short circuit, an open circuit, a matched load, and a straight through (the matched load and straight through are measured in both reflection and transmission to give the total of six standards). The matched load can be either fixed or sliding, as noted above. The shielded open is modeled as a frequency-dependent capacitance. The model used is from [4], $C = 0.079 + 4 \times 10^{-5} f^2$ where C is the capacitance in pF, and f is the frequency in GHz. The short circuit is assumed to be perfect.

When the calibration option is selected from the main menu, a series of instructions appears on the screen, and the operator follows these to the end

of the procedure. Since the procedure can involve several steps, and errors are possible, the option for bailout is provided at each step. A typical display is:

```
Place open circuit at reference plane.
Enter selection
1.  Re-do last step.
2.  Return to main menu.
<Rtn> to continue.
```

Upon successful completion of the calibration procedure, Elf returns to the main menu. The system is then ready to make measurements.

The result of selecting 'Make measurement' from the main menu depends on whether the system is in reflection or full S-parameter measurement mode. If in reflection mode, the measurement is performed immediately. A message, 'Measurement in progress,' appears on the screen while the sweep and error correction are performed, and the program returns to the main menu. The data may then be displayed or manipulated by selecting appropriate menu items.

If Elf is in full S-parameter measurement mode, the measurement process involves a series of instructions similar to those shown in the preceding box. These tell the user to switch the reflection-transmission test set to the proper position, and flip the device under test end-for-end as required. When the proper steps have been completed, the complex error correction is performed on the measured data, and Elf returns to the main menu.

5.2.2 Manipulation, Storage and Display

By stepping through the first five main menu items, the analyzer is calibrated and a measurement performed. The remaining menu items allow the measured data to be manipulated in a limited way, stored on disk, and displayed in several formats.

Item six on the main menu allows measured data to be saved in a data file on disk. Elf will write the data in an ASCII file with the s-parameters in polar format (phase in degrees). Appropriate headings and the date of the measurement are also included in the file. The file is a device file, compatible with the *Puff* computer-aided design program developed at Caltech.

Entering menu item seven calls up the software line stretcher. There are two line stretcher sub-menus. The one that comes up when '7' is entered from the main menu depends on the current mode selected. In reflection mode, the line stretcher sub-menu looks like:

```
                    LINE STRETCHER MENU
1.  Input line length.  Current value is 0.00 cm
2.  Auto-Stretch
3.  Exit
```

In full S-parameter mode there is one more port, so the menu looks like:

```
                    LINE STRETCHER MENU
1.  Input port 1 line length.  Current value is 0.00 cm
2.  Input port 2 line length.  Current value is 0.00 cm
3.  Auto-Stretch on port 1
4.  Auto-Stretch on port 2
5.  Exit
```

Data entry and operation of the line stretcher is the same in both cases. The line stretcher applies a phase shift to the measured data that is linear with frequency. This moves the phase reference plane by a specified amount (assuming the transmission line has no dispersion). The amount of shift can be entered manually by selecting item 1 in the reflection mode sub-menu, or 1 or 2 in the S-parameter sub-menu.

After selecting the menu item, the user is asked for the desired reference plane shift length. It is entered in centimeters of air-dielectric line. A positive shift moves the reference plane toward the unknown, and negative away from it.

The "auto-stretch" option computes a least squares linear fit of phase vs. frequency, and applies the resulting line stretch length to the data. In full S-parameter mode, the auto-stretcher looks only at the phase of S_{11} and S_{22} for sub-menu items 3 and 4, respectively.

Finally, item eight on the main menu allows the user to display the measured or line-stretched data in a variety of formats. Entering '8' gives access to a chain of up to three sub-menus, the largest number in the program. These sub-menus are used to select parameters for display of the measured data.

The first sub-menu is active only in full S-parameter mode. It is the s-parameter selection menu. The s-parameter selection menu looks like this:

```
                    DISPLAY MENU
1.  S11
2.  S12
3.  S21
4.  S22
5.  Print
6.  Exit
```

Only one S-parameter may be displayed at a time. A marker appears beside the selected parameter. Entering 5, 'Print', moves Elf down to the next sub-menu. The next sub-menu is:

```
                    PRINT MENU
Source                          Destination
1.  Measured data               3.  Screen
2.  Line-stretched data         4.  Printer
                                5.  Smith chart plot
                                6.  Rectangular plot
7.  Print
8.  Exit
```

In reflection mode, this menu is displayed immediately on selection of '8' from the main menu. Items 3 through 6 allow selection of the desired type of display. None of the actions selected in 3 through 6 occurs until item 7, 'Print' is entered, however. With the 'Screen' option, a table of the selected S-parameter in polar form scrolls down the screen. Item 4 produces the same table on the printer. Item 5 displays the data on a Smith chart.

If item 6, 'Rectangular Plot' is selected, followed by '7', another sub-menu appears. It is the rectangular plot parameter selection menu:

```
                    RECTANGULAR PLOT MENU
1.  Set Xmin.  Currently, Xmin = 0.000
2.  Set Xmax.  Currently, Xmax = 0.000
3.  Set Ymin.  Currently, Ymin = 0.000
4.  Set Ymax.  Currently, Ymax = 0.000
5.  Magnitude Plot
6.  dB Plot
7.  Phase Plot
8.  Plot
9.  Exit
```

Something other than zeroes will be displayed in the data areas of the menu in practice. The x-axis is always frequency, and on entering the menu for the first time, the limits of the x-axis will be set to the minimum and maximum frequencies that have been calibrated. As with the previous menu, this is a setup menu: nothing actually happens until item 8, 'Plot,' is entered. Then the rectangular plot appears. The resulting plot is of the type selected, linear magnitude, dB magnitude, or phase, plotted within the limits selected.

5.3 Sample Measurement

Figured 5.5 and 5.6 show magnitude plots of the measured values of S_{11} and S_{21} for a 10.35-cm length of precision air coaxial line (Hewlett-Packard model 11566A) over the frequency range of 0.5 to 18 GHz. The magnitude of the error in the $|S_{21}|$ plot is about 0.01 at the low frequencies, increasing to perhaps 0.02 above 12 GHz. Noise on the outputs of the network analyzer is the main source of this error. On the $|S_{11}|$ plot, errors increase steadily, beginning at ~ 0.01 for the low frequencies, increasing to 0.02 in the 6–12 GHz range, and increasing rapidly above 15 GHz. There are several possible sources of inaccuracy at high frequencies. The increased loss and reduced directivity of the directional couplers in the reflection-transmission test set make the system more sensitive to noise in the calibration measurements at high frequencies. Also, models used for all the calibration standards become less accurate with increasing frequency.

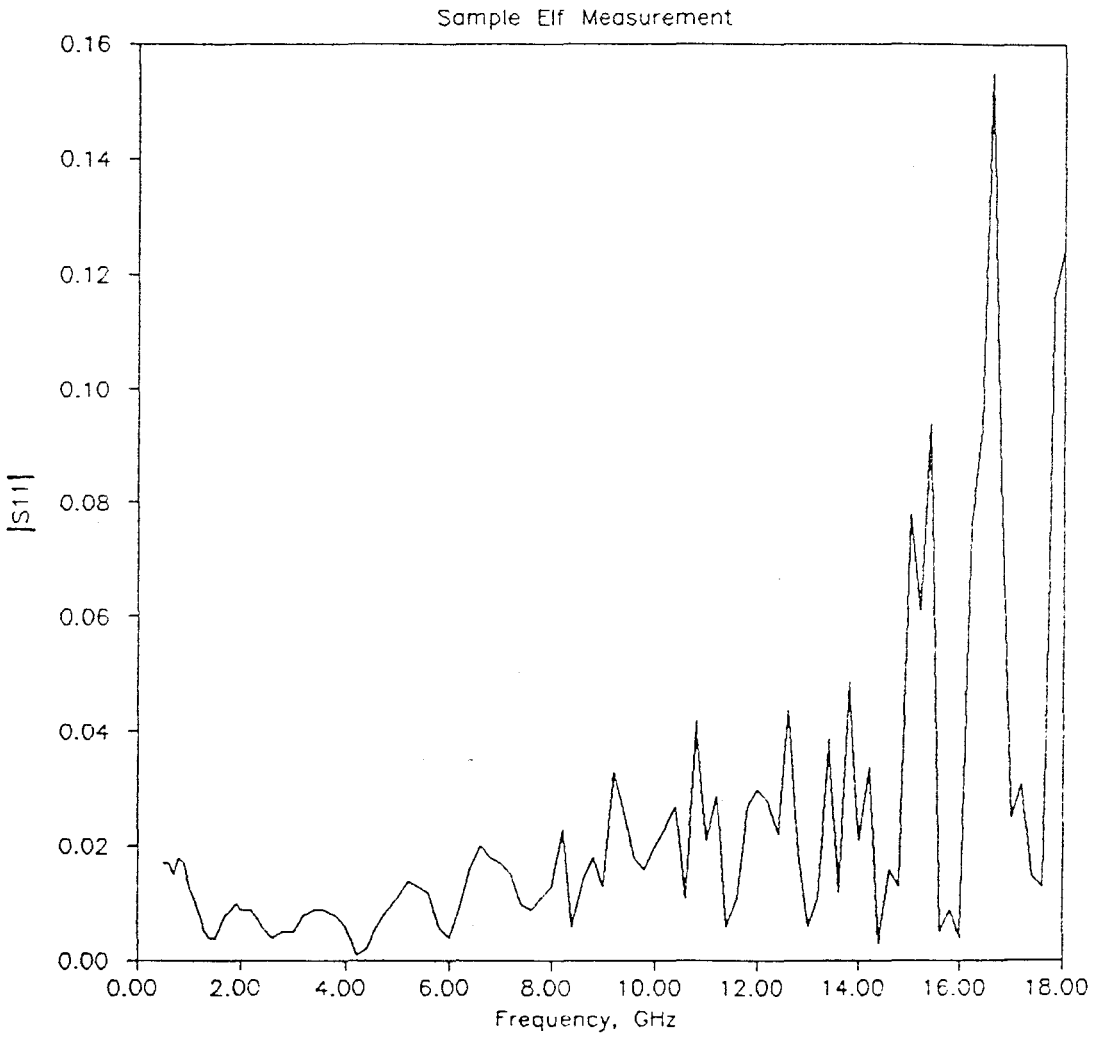

Figure 5.5 Elf measurement of S_{11} of a length of precision coaxial line.

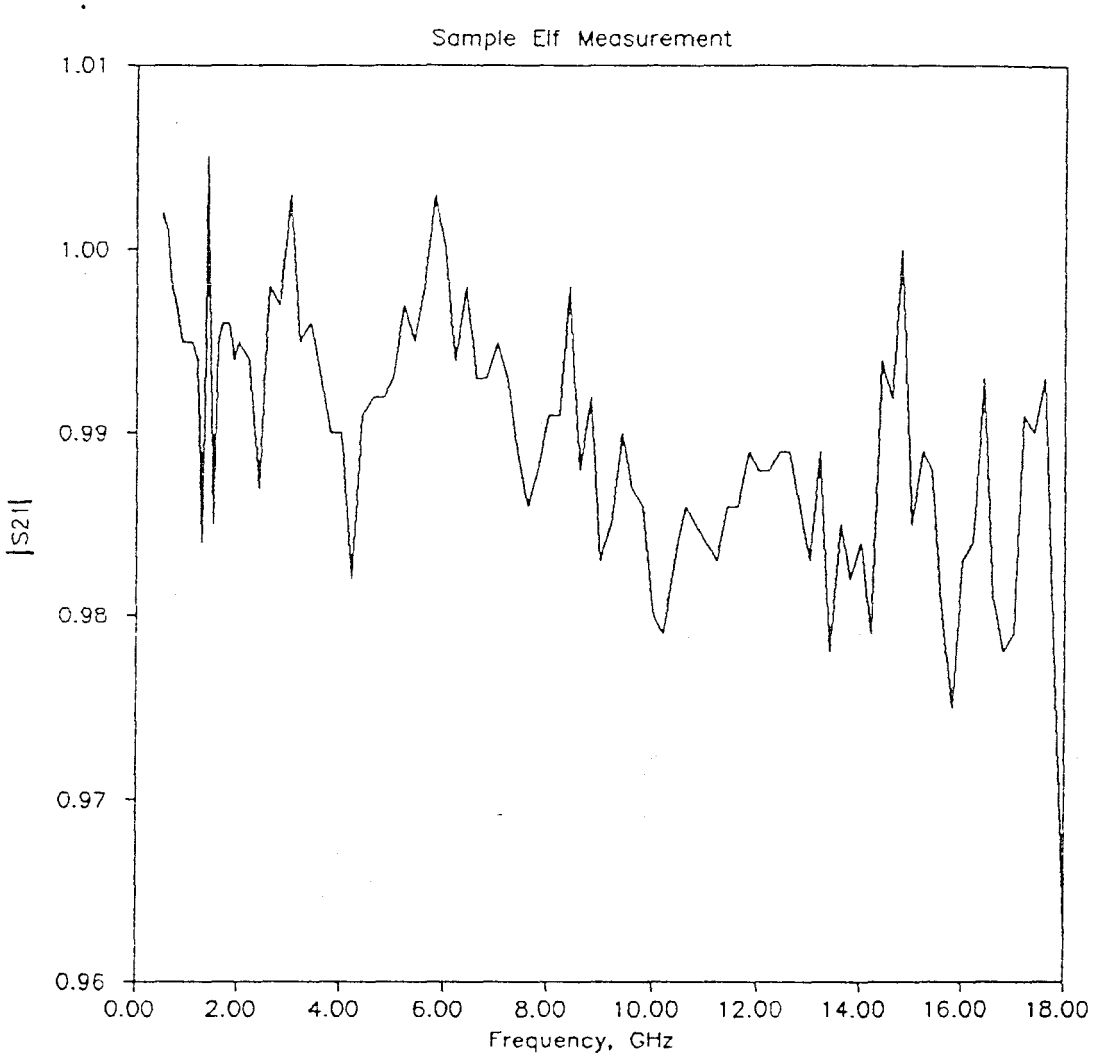

Figure 5.6 Elf measurement of S_{21} of a length of precision coaxial line.

References

[1] Model DT-2801A from Data Translation, Inc., 100 Locke Drive, Marlborough, Massachusetts 01752

[2] Model PC-488 from Capital Equipment Corporation, 10 Evergreen Ave., Burlington, MA 01803

[3] The Turbo Pascal compiler is a product of Borland International, 4585 Scotts Valley Drive, Scotts Valley, CA 95066

[4] Larry R. D'Addario, "Computer-corrected reflectometer using the HP-8410 and an Apple II," *National Radio Astronomy Observatory Electronics Division Internal Report*, no. 228, May 1982

[5] J.G. Evans, "Linear two-port characterization independent of measuring set impedance imperfections," *Proc. IEEE,*(Lett.), vol. 56, no. 4, pp. 754–755, Apr. 1968.

[6] A.A.M. Saleh, "Explicit formulas for error correction in microwave measuring sets with switching-dependent port mismatches," *IEEE Trans. Instrum. Meas.*, vol. IM-28, no. 1, Mar. 1979.

[7] W. Kruppa and K.F. Sodomsky, "An explicit solution for the scattering parameters of a linear two-port with an imperfect test set," *IEEE Trans. Microwave Theory Tech.*, vol. MTT-19, no. 1, pp. 122–123, Jan. 1971

[8] S. Rehnmark, "On the calibration process of automatic network analyzer systems," *IEEE Trans. Microwave Theory Tech.*, vol. MTT-22, no. 4, pp. 457–458, Apr. 1974

Chapter 6

The Sprite Sampled-Line Network Analyzer

Figure 6.1 shows the Sprite sampled-line network analyzer system schematically. The Sprite system consists of an IBM AT personal computer interfaced to two sampled-line reflectometer modules, a broad band phase shifter, and a signal generator. A control program, called Sprite, runs on the AT, coordinating the actions of these components, and performing the calibration and measurement routines. Sprite is written in C, with some assembly language routines. The Sprite program is presently about 110KB of code.

The Sprite system architecture is the same as that presented in chapter 3 for the six-port S-parameter measurement system, except that the Sprite system lacks the variable attenuators used in the NBS system. This simplifies the system somewhat, reducing the number of switch setting combinations that must be calibrated, and the number of conditions the software must test for. The system with just the phase shifter can gather enough information to calculate the full S-parameters of a two-port, and is adequate for measurement of passive two-ports. The switched attenuators improve the dynamic range of the analyzer, especially when measuring active devices. Future versions of the network analyzer will include the switched attenuators.

In the sections below, the various components of the hardware will be described. The Sprite software will then be presented briefly, and finally some sample measurements with the system will be presented.

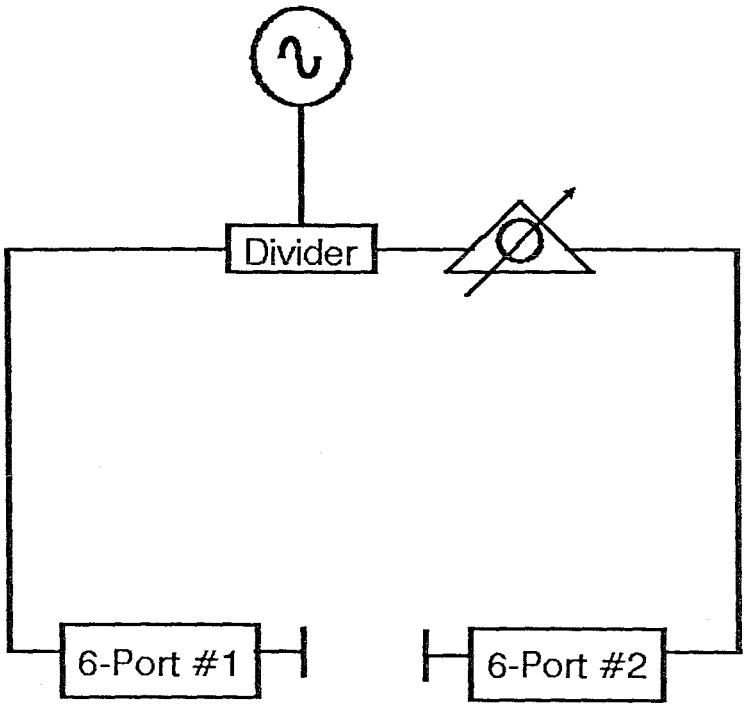

Figure 6.1 The Sprite sampled-line network analyzer system uses the same basic architecture as was described in chapter 3 for six-port network analyzers. The omission here of variable attenuators in the system simplify it but reduce the dynamic range over which S-parameters can be accurately measured.

6.1 Hardware Description

The hardware of the Sprite system is broken down into four subsystems. Two of these subsystems, the phase shifter and the reflectometer heads, are microwave circuit modules. The other two, the preamplifier bank and the synchronization circuitry are low-frequency signal processing systems. These subsystems will be described below.

6.1.1 The Reflectometer Heads

The reflectometer heads contain the actual sampled-line microwave circuitry. Each one consists of a microstrip transmission line with SMA connectors on either end. Sampling circuits with the prescribed spacing are connected to the microstrip line.

Four different versions of the sampled-line analyzer have been built to date. In each, a different configuration was used for the microwave sampling circuit. Arriving at a sampler design that works well over a broad bandwidth has been the most difficult part of the sampled-line analyzer hardware design.

Two problems are encountered in the sampler circuit. The first is the line loading problem. As was seen in Chapter 4, excessive loading of the sampled-line by the samplers destroys measurement accuracy. Thus, the samplers must provide a high impedance, preferably $|Z| > 500\,\Omega$, over the entire frequency range of operation.

The second problem is that of designing a sampling circuit with a fairly smooth frequency response. If the responsivities of the sampler circuits vary rapidly with frequency, and if they differ from sampler to sampler, then it is impossible to adjust the post-detection amplifier gains to keep all the sampler output voltages within the limited dynamic range of the A/D converters over a broad frequency sweep. If, on the other hand, each sampler's response is smooth, rolling off with increasing frequency, then gain settings can be adjusted

to approximately equalize the outputs from all the detectors, and the microwave test signal power can be increased with frequency to counter the roll-off.

To achieve this smooth frequency response, a good RF ground for the detectors must be established and parasitics in the sampling circuits must be controlled. Since microstrip is an unbalanced transmission line, the sampled signal is presented to one end of a detector diode, and the other end of the diode is grounded. In some circuit configurations, it is not practical to connect the diode detector directly to ground, so some type of capacitive connection to ground must be designed. Broad band operation can then become difficult. Parasitics in such a structure can cause unexpected resonances which, at some frequencies, reduce the voltages across the detectors to very small values.

These two problems, line loading and sampler frequency response, were not completely recognized in the first two network analyzers, giving rise to their rather poor performance. The third analyzer was designed with these difficulties in mind, but unexpected parasitics limited its performance at the higher frequencies. The fourth reflectometer was essentially the same design as the third, but with some minor modifications to reduce the parasitics in the sampling circuit. The fourth represents a fairly good implementation of the sampled-line analyzer.

The S-parameter measurement system uses the third and fourth reflectometer heads, so the performance of the system is limited by that of the third reflectometer. The four versions of the sampled-line reflectometer built to date will be discussed in turn below.

Figure 6.2 shows a photograph of the first sampled-line network analyzer. Here a microstrip line was fabricated on a 2.8cm-square, 1mm-thick RT/duroid 6010.2 circuit board. The duroid material has a dielectric constant of 10.2 ± 0.25 and a loss tangent of approximately 0.002 up to 10 GHz. The microstrip is fabricated from 0.03mm-thick copper cladding through an etching process.

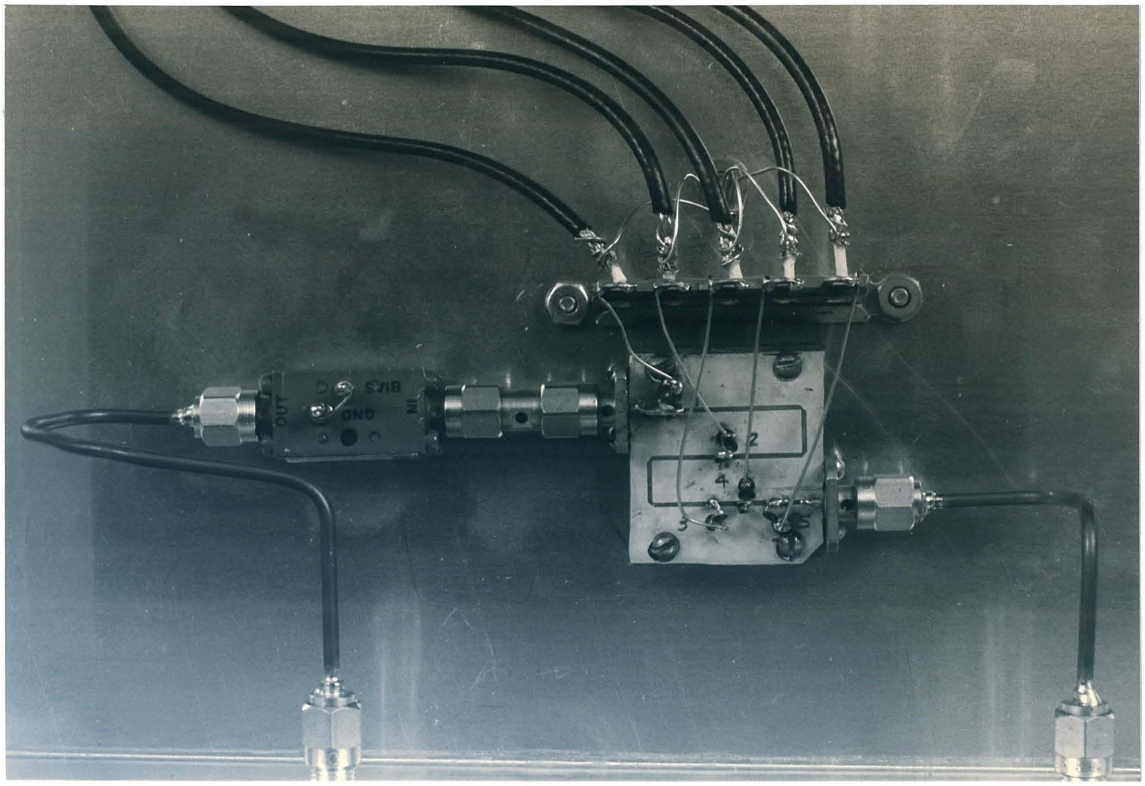

Figure 6.2 The first sampled-line network analyzer consisted of five detectors placed along an S-shaped microstrip line.

This analyzer used 5 detectors to cover 3 octaves. It was designed to cover the frequency range of 0.75 to 6 GHz.

The circuit was fabricated on a board of this size with the "S" turn in the line because an early version of the *Puff* [1] CAD program was used to lay it out and these were convenient values for it.

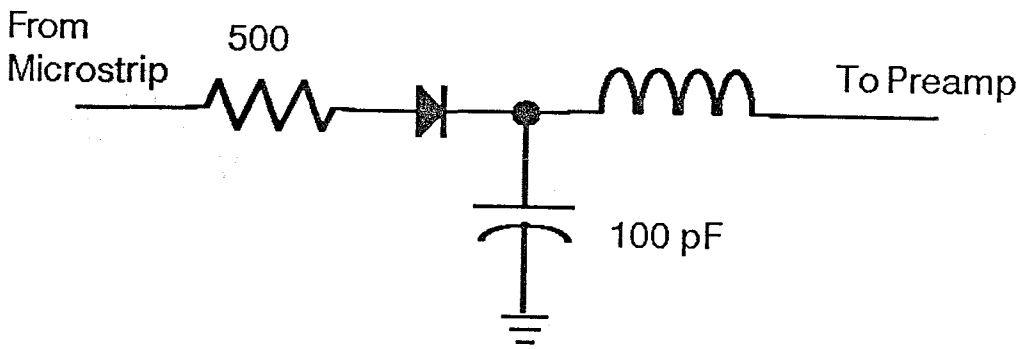

Figure 6.3 Schematic diagram of the sampling circuit used in the first network analyzer.

The sampler circuit used with this network analyzer is shown in figure 6.3. A drawing of the physical configuration of a sampler is shown in figure 6.4. The sampler was fabricated by soldering a 500 Ω chip resistor [2] directly to the microstrip, with the resistor standing up in the air. Close to the point where the resistor was attached, a hole was drilled through the circuit board to the ground plane, and a chip capacitor [3] was soldered to the ground plane. A packaged Schottky diode was then soldered between the tops of the chip resistor and chip

capacitor. The chip capacitor thus provides the detector's RF ground. Zero-bias detector diodes were used.

The RF ground at the chip capacitor provides fairly good isolation between the RF signals and the low-frequency portions of the circuit. To provide additional isolation, an inductor, fabricated by suspending a piece of #24 wire several millimeters above the circuit board, was placed between the chip capacitor and the instrumentation amplifier's input.

With this sampler circuit, an external bias tee was used to provide a path for the detector diodes' DC return current. This tee was placed on the generator side of the sampled-line and a DC block was placed between the line and the device under test. The DC block was used for two reasons. First, many microwave devices can be damaged by even small DC currents flowing on the transmission line. Also, there was concern that if the bias current were allowed to flow out of the test port, the device under test could change the indicated RF impedance just by a change of its DC impedance.

The detector circuit used in the first analyzer provided good isolation of the detectors from the microstrip line. Figure 6.5 shows a plot of $|S_{21}|$ for this analyzer from 0.5 to 18 GHz. There are no deep resonances or sharp cutoffs in this plot, indicating that the line does not suffer from any large discontinuities. The line is considerably lossier than would be expected were the samplers absent, however. $|S_{21}|$ was calculated using standard loss models for the microstrip, and the coaxial lines joining the sampled-line to the measurement ports. This calculation gave an $|S_{21}|$ which went from 0.99 at 200 MHz to 0.80 at 20 GHz. The additional loss observed in the sampled-line analyzer is attributed to effects of the samplers on the line.

Figure 6.6 shows the frequency response of the five sampling circuits of the first sampled-line analyzer. The vertical axis is on a logarithmic scale, $Y = 10 \log_{10} V_{\mathrm{A/D}} - P_{i,\mathrm{dBm}}$, where $V_{A/D}$ is the numerical value given by the computer's

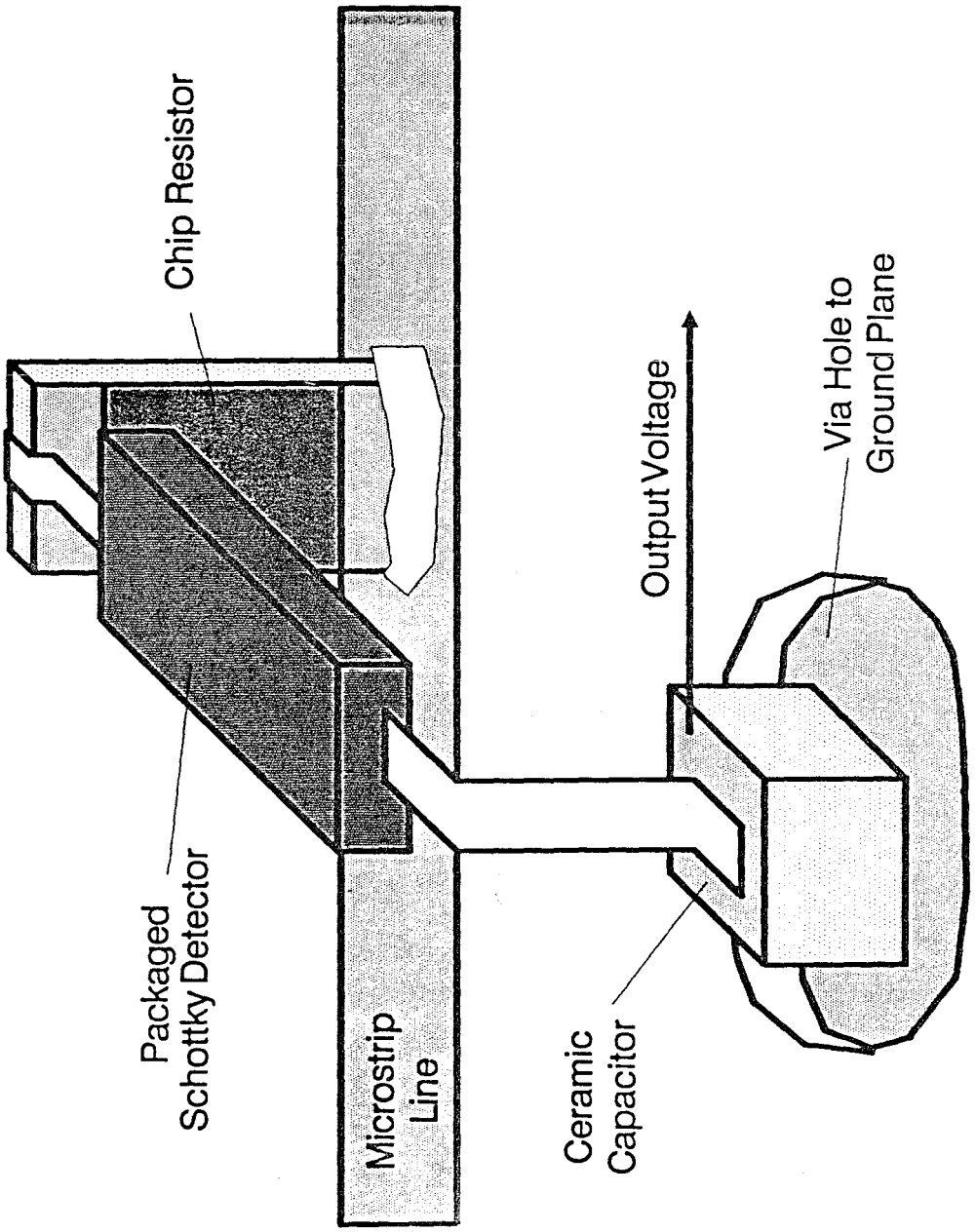

Figure 6.4 Physical configuration of the sampling circuit in the first network analyzer.

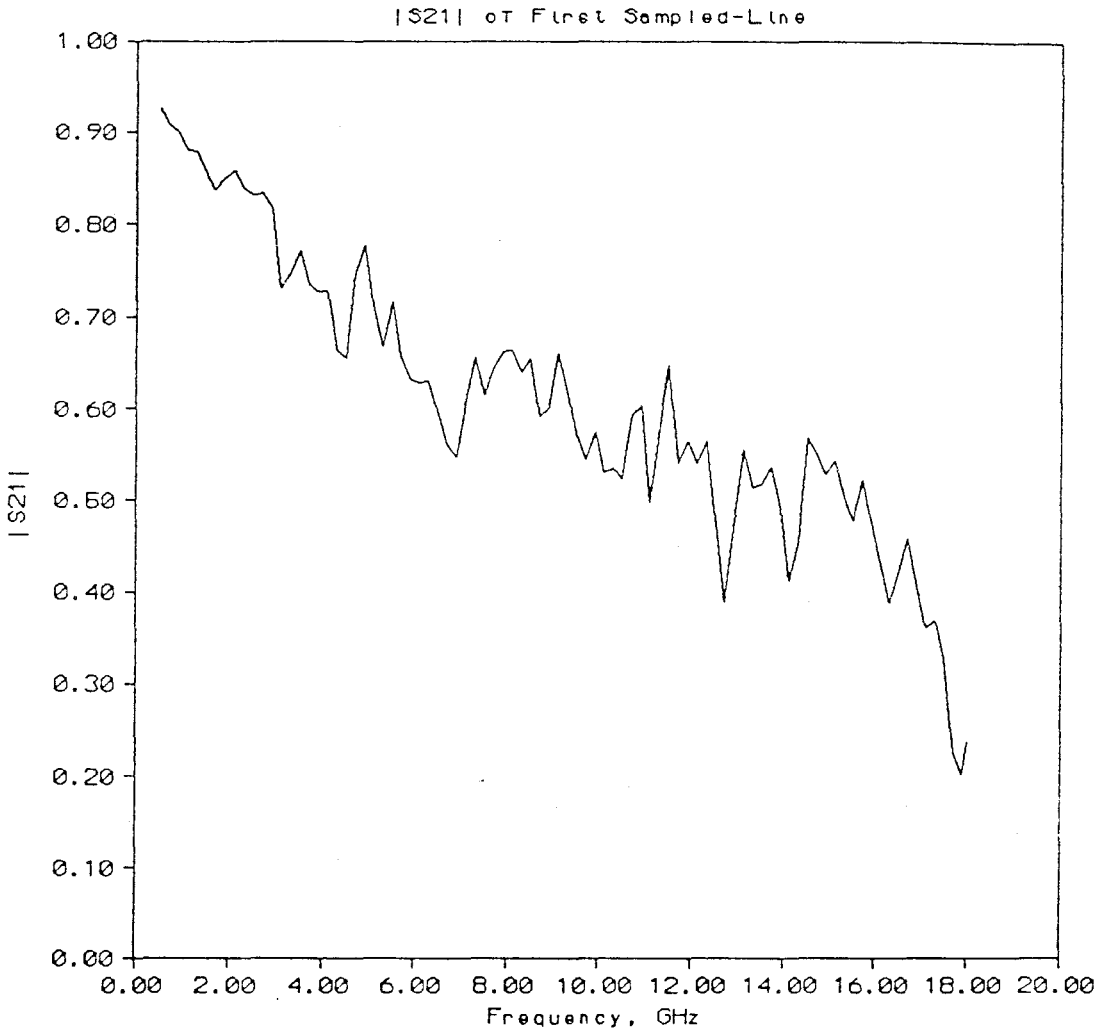

Figure 6.5 $|S_{21}|$ for the first sampled-line analyzer.

A/D converter and $P_{i,\mathrm{dBm}}$ is the output power of the signal generator in dBm used for the measurement. Y is thus a ratio of responsivities. It gives the ratio of a given detector's responsivity to the responsivity of a detector that would yield a voltage output equal to one least significant bit of the A/D for an output power of 0 dBm from the generator. This same, rather odd scale is used for all frequency response plots of the sampler circuits of the various analyzers, so comparisons can be made between them.

The sampler responses of the first sampled-line analyzer are smooth and well-behaved up to about 3 GHz. Between 3.5 and 4.0 GHz, all the outputs go through some rapid changes, indicating a resonance somewhere in the sampler circuits. The best candidate is the chip capacitor used for the diode's RF ground. Multi layer ceramic capacitors were used here, and specifications for these capacitors indicate that they may have a parallel resonance at some frequency greater than 2 GHz.

At this resonant frequency, the output signals diverge by as much as 12 dB. Fortunately, though, the greatest divergence is between the first and second samplers, which are spaced too far apart to be used as the primary measurement diodes at this frequency. The other detector responses stay fairly well-matched (within $\approx 5\,\mathrm{dB}$) up beyond 6 GHz, which is the maximum frequency the analyzer was designed for.

By the time 9 GHz is reached, however, the parasitics of the sampling circuit take over and render the circuit useless.

So from these data the first sampled-line analyzer looks good from 0.75 to 6 GHz, as designed. Unfortunately, however, a measurement error in fabrication of the analyzer led the first two diodes to be spaced further apart than intended. This led to a gap in the frequency range of measurement for the analyzer. Calibration tests showed that the analyzer gave accurate measurements

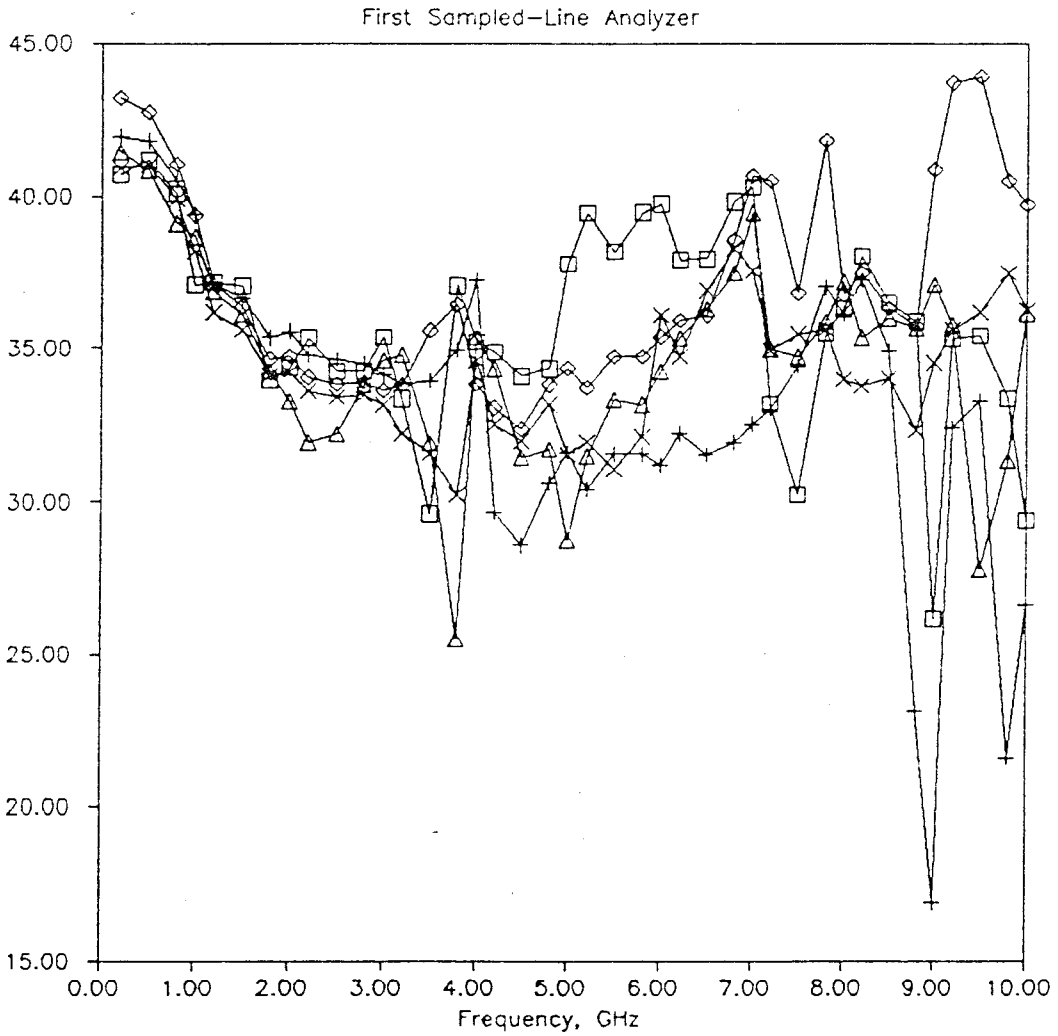

Figure 6.6 Frequency response of the detector circuits of the first sampled-line analyzer. Vertical scale is a somewhat arbitrary dB scale as described in the text.

over the frequency ranges of 0.4–1.4 GHz and 2.5–5.5 GHz. Over these ranges, the maximum magnitude of the error vector with this analyzer was about 0.02.

The first sampled-line network analyzer, though suffering from these frequency limitations, was used for network measurements by students in the EE153 Computer Aided Design of Microwave Integrated Circuits class during the 1986-87 academic year at Caltech. It was used in two modes. The first was a narrow band mode. Most of the student circuits were designed for the 3–5 GHz frequency range and the analyzer could be calibrated to give good measurements over this entire range. In the second or broad band mode, it was found that the analyzer could be calibrated from 0.5 to 5.5 GHz with 0.5 GHz spacing of the frequency points. These points just happened to fall at points where the calibration could be made to work. With the broad band data, a Fourier transform could be performed to observe such things as step discontinuities in the time domain.

The first network analyzer was a reflectometer only. It was used, however, to measure the full S-parameters of some of the students' projects. This was done through an indirect procedure: when it is known that a two-port network is reciprocal, then its S-parameters can be determined to within a sign of S_{12} and S_{21} by measuring the reflection coefficient observed at port 1 with three different known impedances connected to port 2. The procedure is identical in concept to the four-port calibration using three known impedance standards.

The first network analyzer's control program was written in Pascal [4]. The program implemented the sliding short six-port to four-port conversion procedure described in chapter 3, as well as a short-open-load four-port calibration procedure. No optimization or use of data from the secondary samplers were used in this program. It essentially treated the sampled-line analyzer as a five-port network analyzer and worked from there. This control program was about 80KB of Pascal code.

This first control program did not have a general-purpose user interface. When it was used in the EE153 class, it was interfaced to the *Puff* CAD program, which the students were using to lay out their circuits. Sections of the control program were rewritten as modules that *Puff* could call. The special version of *Puff* with these modifications ran on an IBM PC interfaced to the network analyzer. The special *Puff*'s user interface was the same as what the students were used to, but pressing the 'M' key, which did nothing in standard *Puff*, performed a measurement over the calibrated frequency range. The measured data could then be written to disk as a standard *Puff* file and taken away for further analysis. The students found this arrangement convenient and measurement accuracy was sufficient to allow them to evaluate their designs.

With the success of the first sampled-line analyzer, a second was designed. This new version was to have a wider frequency of operation, from 0.6 to 20 GHz, or five octaves. Several changes were made in the sampling circuitry. Among them, the packaged diode was replaced with a beam lead detector [5] diode to reduce package parasitics.

Figure 6.7 (a) shows the sampling circuit first used in the second sampled-line analyzer. The first change made to arrive at this circuit from that of the first analyzer was the removal of the resistor between the detector diode and the line. It was thought that the isolation functions of this resistor could be performed by an inductor. This inductor was fabricated as a short length of high-impedance microstrip line connected to the line to be sampled.

The sampling circuit of Figure 6.7 (a), however, had problems with RF grounding and with isolation between the high frequency and low frequency sections of the circuit. In this circuit the chip capacitor used in the first analyzer was replaced with parallel plate capacitors fabricated as microstrip patches. Two patches were used. A small one near the detector diode provided an RF ground for the higher frequencies, and a larger one connected to this by a short length of

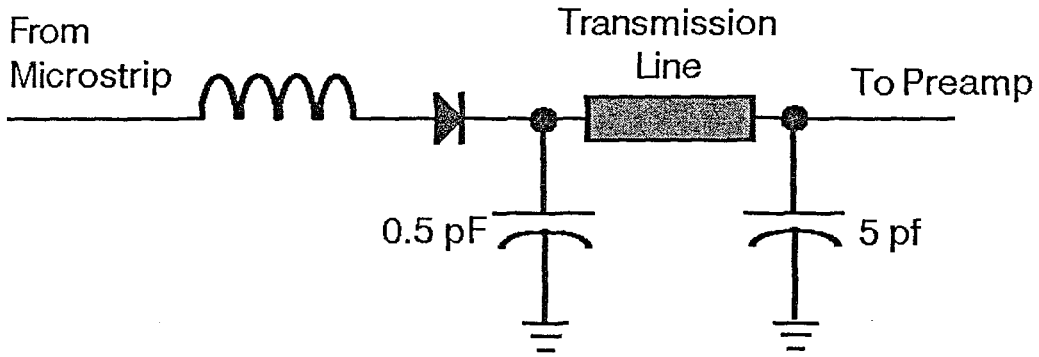

(a)

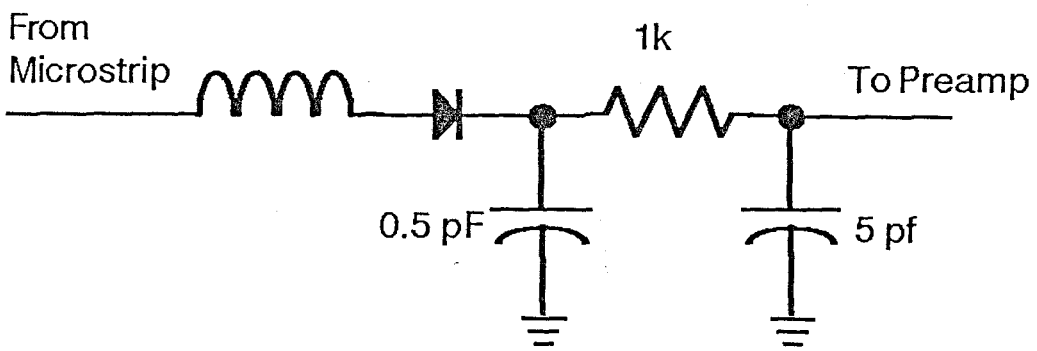

(b)

Figure 6.7 Detector circuit used in the second sampled-line analyzer, before and after modification.

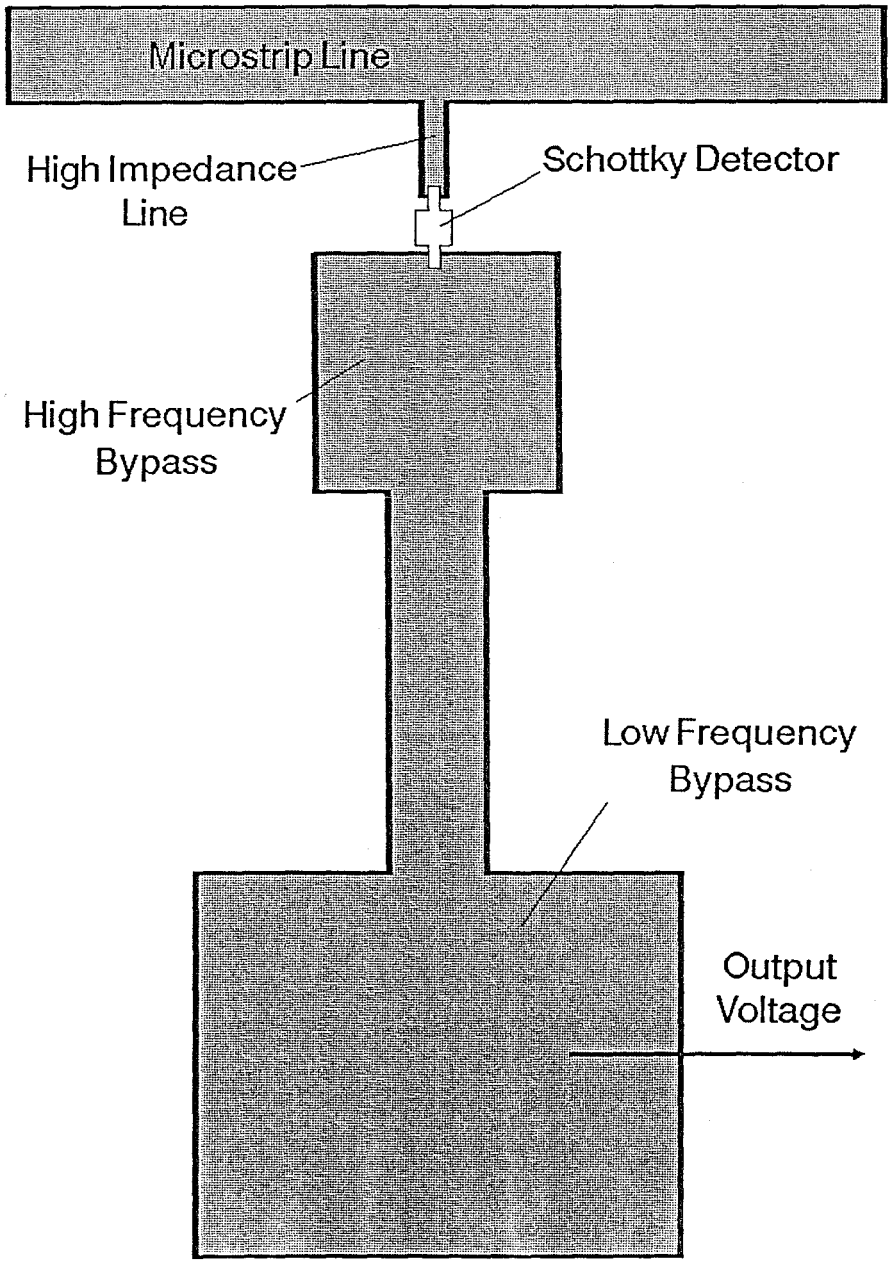

Figure 6.8 Physical configuration of the samplers in the second network analyzer as they were originally built.

transmission line did the same for the lower frequencies. The physical configuration of this sampler is shown in Figure 6.8. Unfortunately, these patch capacitors did not work as well as rough calculations had predicted and the microwave signals fed through the structure to the coaxial cables leading to the preamplifiers. The effect was that when the analyzer was connected to the microwave source, wiggling these cables caused the microwave detector outputs to change wildly. In an attempt to improve the RF-DC isolation, the lengths of line between the capacitor pads were replaced with resistors. This change is shown in figure 6.7 (b). The physical configurations of the sampler after this modification is shown in figure 6.9. Figure 6.10 shows two photographs of the second sampled-line network analyzer after this modification.

Figure 6.11 shows $|S_{21}|$ of the second sampled-line analyzer after modification. The roll-off of the magnitude of S_{21} with frequency is steeper than for the first analyzer. This is not unexpected, since the second analyzer has two more sampling diodes than the first.

The modification of the second analyzer did improve the RF-DC isolation, but the RF grounding problem persisted. The results are seen in figure 6.12, which shows the frequency responses of the samplers for the second network analyzer. Responsivity changes by 15 dB, a factor of 31 in output voltage for a given power, are observed over a frequency change of 500 MHz. This behavior makes things very tough for the processing circuitry that follows the sampling head.

The second sampled-line analyzer was a reflectometer like the first, and used the same Pascal control program. Calibration tests gave spotty results for this analyzer. Over a range of about 0.5 to 7 GHz, its measurement accuracy fluctuated, being good for a few hundred MHz, then suddenly going bad. Above 7 GHz it was unusable.

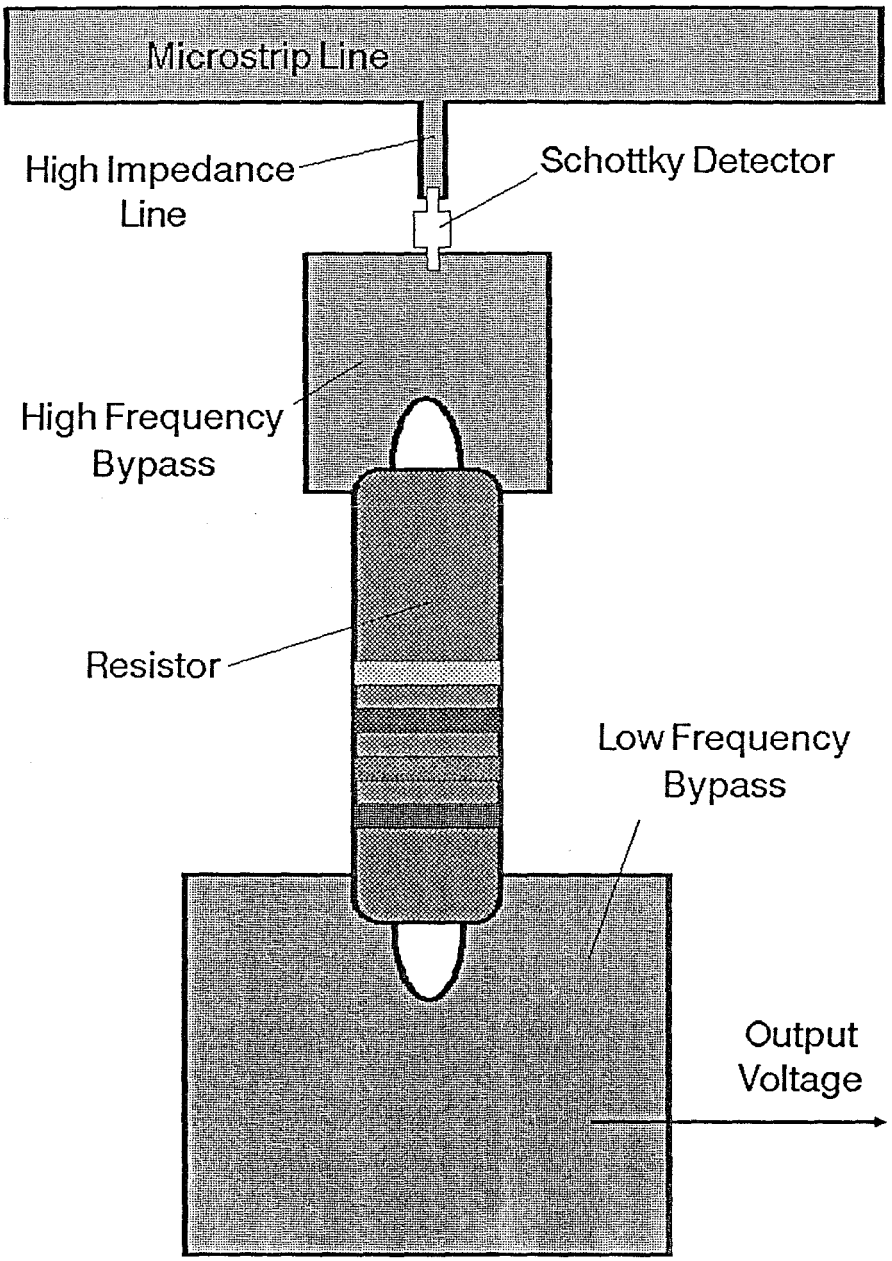

Figure 6.9 Physical configuration of the samplers in the second network analyzer after modification.

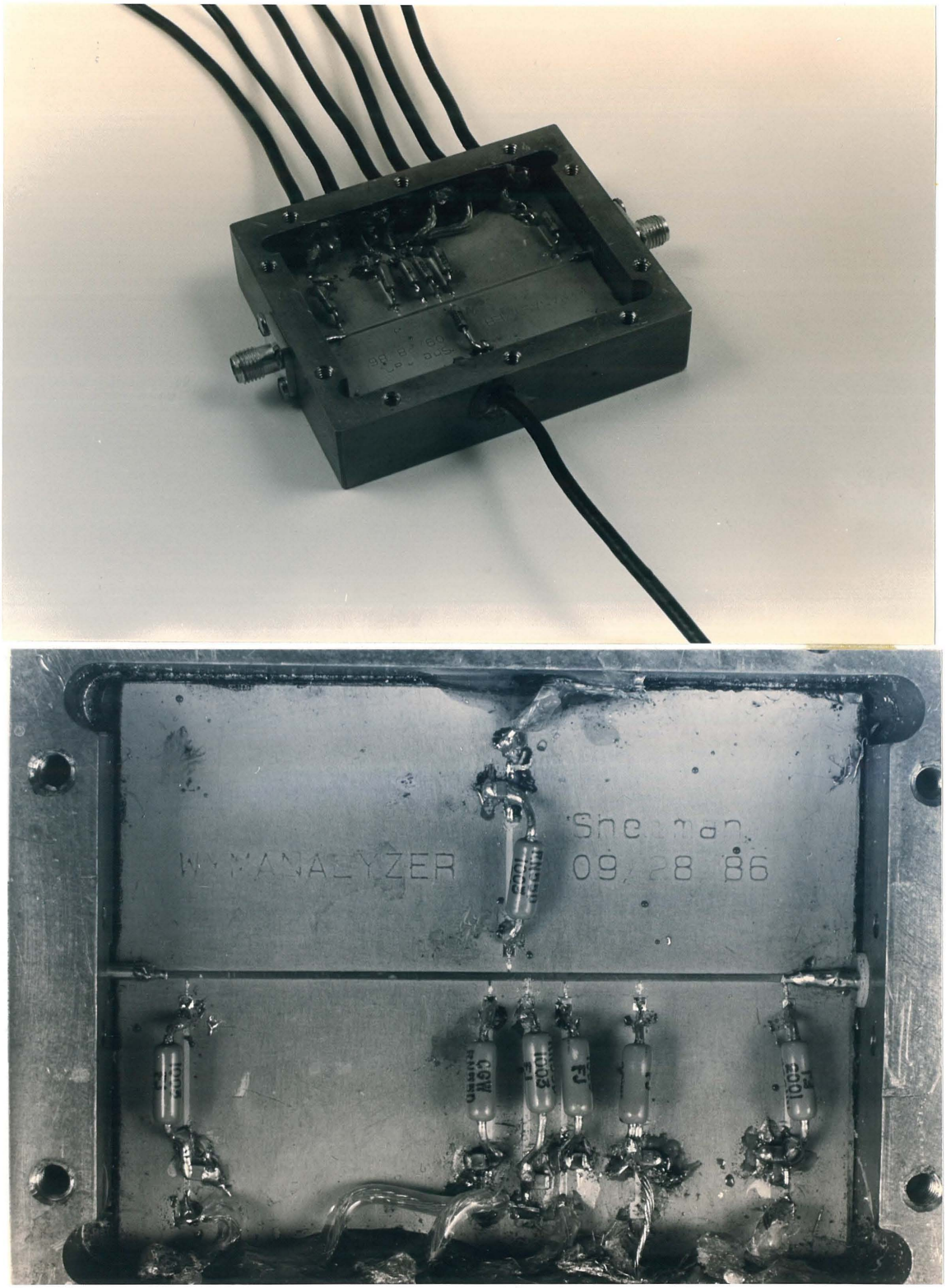

Figure 6.10 The second sampled-line network analyzer.

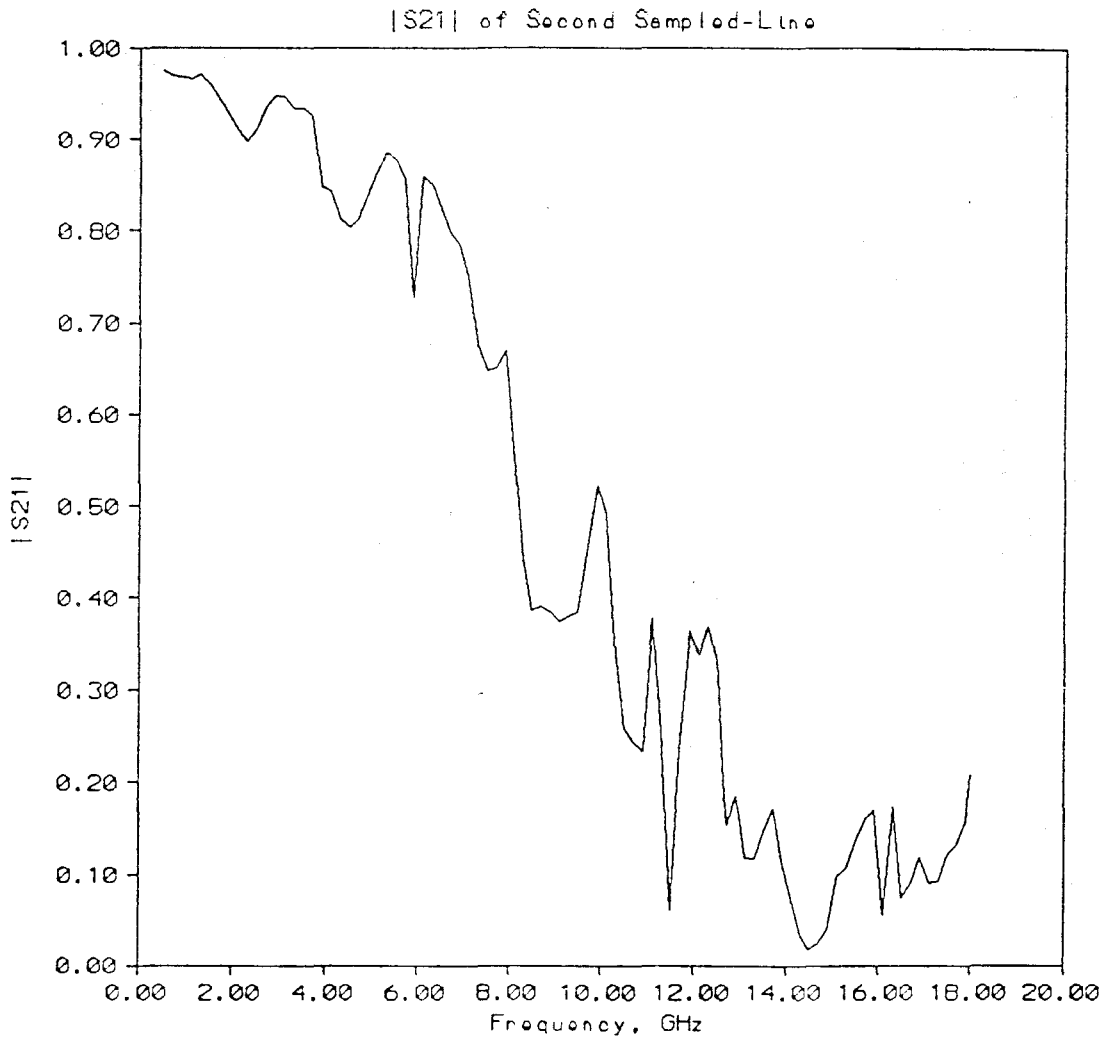

Figure 6.11 $|S_{21}|$ of the second sampled-line analyzer.

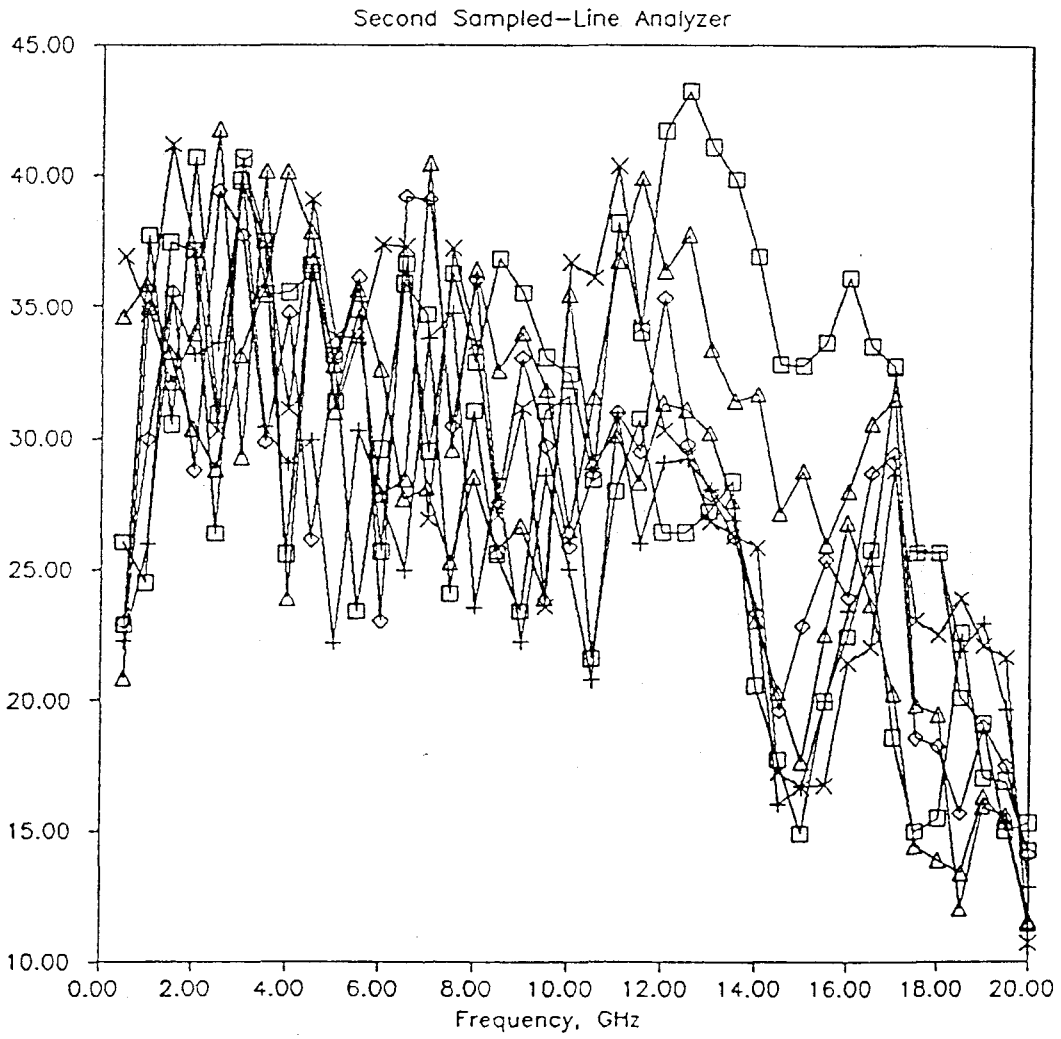

Figure 6.12 Frequency response of the sampling circuits in the second network analyzer after modification. Vertical scale is the same as that used in figure 6.6

The lessons learned from the first and second sampled-line reflectometers were valuable for the design of the third and fourth. Several things were recognized. First was that a direct ground connection for the detector diode is desirable for very broad band operation. In the third and fourth analyzers, then, the sampled line ran close to a parallel metal ridge, on which the sampler circuits were built. The diodes could then be connected directly to ground without the necessity of drilling through the substrate. As long as the metal ridge is at least two line widths away from the microstrip line it affects the line's characteristic impedance by only a few percent [6].

It was also realized that resistive networks are a good solution when very broad band isolation is required. In the last two analyzers, resistive isolation was used between the line and the detector, and between the RF and DC portions of the circuitry. In the third and fourth analyzers, also, the need for a bias tee was eliminated to reduce system complexity.

At the time the last two sampled-line reflectometers were constructed, the *Puff* CAD program was in good working order and it was used in the design process. A lumped-element sampling circuit was designed, which could be fabricated with standard hybrid-IC fabrication techniques. Figure 6.13 shows the circuit diagram of the sampler. It is fabricated with chip capacitors and resistors and beam lead detector diodes [7]. The chip capacitors used here were of a parallel plate ceramic type [8] which did not suffer from the resonance problems encountered in the first analyzer. Connections between the components were made with bond wires and conducting epoxy [9].

In the *Puff* simulation, the bond wires were modelled as lengths of $147\,\Omega$ transmission line. The bond wires are 0.001" in diameter and a $147\,\Omega$ microstrip line is 0.001" wide. Since the bond wire is actually up in the air instead of flat against the substrate, it is likely to be more inductive and thus provide better

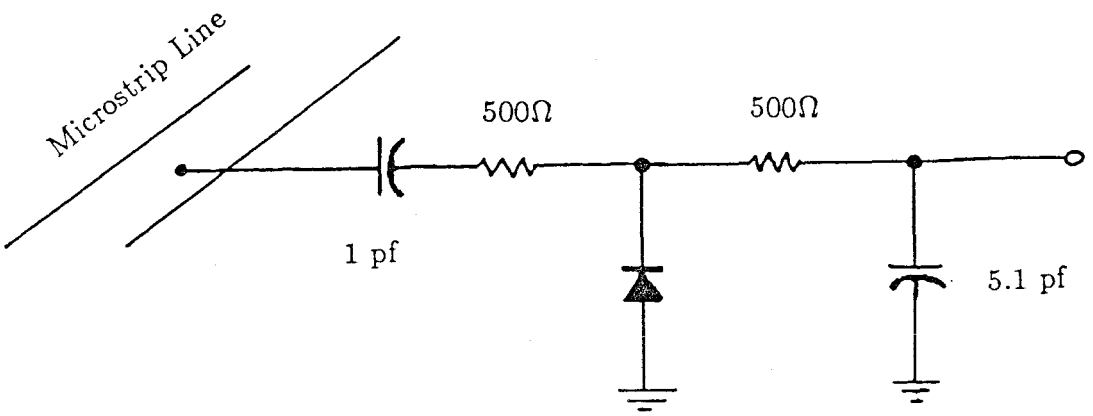

Figure 6.13 Sampling circuit used in the third and fourth sampled-line network analyzers.

isolation than the 147 Ω line. The line is thus a conservative model for the bond wire.

At low frequencies, the sampler of Figure 6.13 is an open circuit, and as frequency increases, its impedance approaches 500 Ω. Transmission line effects due to the bond wire on the circuit's input do not come into play until well above 20 GHz. Thus, this circuit's admittance goes to $Y \sim 0.1Y_0$, a safe value by the criteria established in chapter 4 for the sampled-line network analyzer.

Figure 6.14 shows a *Puff* analysis of a network analyzer consisting of seven such samplers connected to a line with the spacing discussed in chapter 4. *Puff* predicts very good performance for this analyzer. The insertion loss of the sampled-line is about 3 dB over most of its operating range, and its return loss is better than 10 dB over the range. Isolation between the RF and DC lines is better than 25 dB over the entire range and better than 40 dB above 3 GHz.

The detector response rolls off due to the diode capacitance as expected, indicating that about 25 dB more power will be needed at 20 GHz than at the low frequencies to get the same output reading.

Figure 6.15 shows a photograph of the third sampled-line network analyzer. Figure 6.16 shows the physical configuration of the samplers used in the third sampled-line analyzer. Unfortunately, when the analyzer was built, parasitic capacitances in the chip resistors used in the sampling circuit caused the analyzer's performance to be significantly worse than predicted. Figure 6.17 shows the value of $|S_{21}|$ for the third sampled-line analyzer as measured by Elf. Transmission through the unit essentially goes to zero at around 8 GHz, making it impossible to make measurements with the analyzer at these frequencies.

Having observed this poor performance, the search for its cause led to the chip resistors. The largest components in the circuit, these resistors have solder pads that are about 0.025" on a side. The bodies of the resistors are alumina and the resistors are epoxied to the metal ridge next to the microstrip line. The solder pads thus placed above the ground plane give rise to a shunt capacitance to ground not included in the model for the sampler. Using $C = \epsilon A/d$, the solder pad capacitance is estimated at 100 fF. When this shunt capacitance is included in the *Puff* simulation, the dip at 8 GHz is observed. The solder pad capacitance resonates with the bond wires at around 8 GHz, placing a short circuit on the line at each sampling point.

In an attempt to reduce the shunt capacitance of the resistor solder pads, the chip resistors between the line and the detector diodes were stood on end for the fourth version of the network analyzer. This new physical configuration is shown in figure 6.18. The fourth network analyzer was identical to the third in other respects. Standing the resistors on end simply moved the solder pads further away from the ground plane, reducing their shunt capacitance. The effect of this change is shown in figure 6.17, where $|S_{21}|$ of the fourth network analyzer

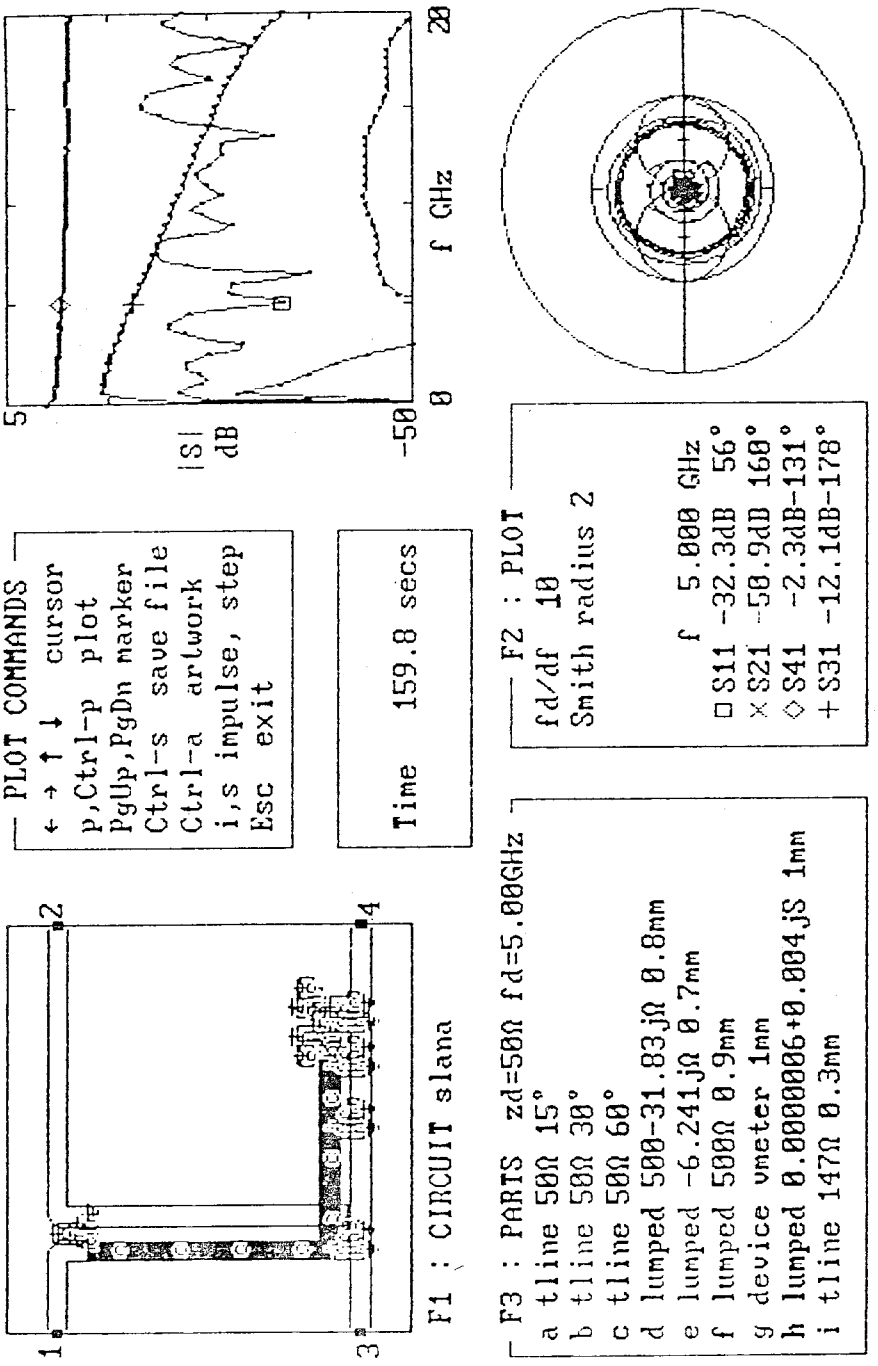

Figure **6.14** *Puff* analysis of the design used for the third and fourth sampled-line network analyzers.

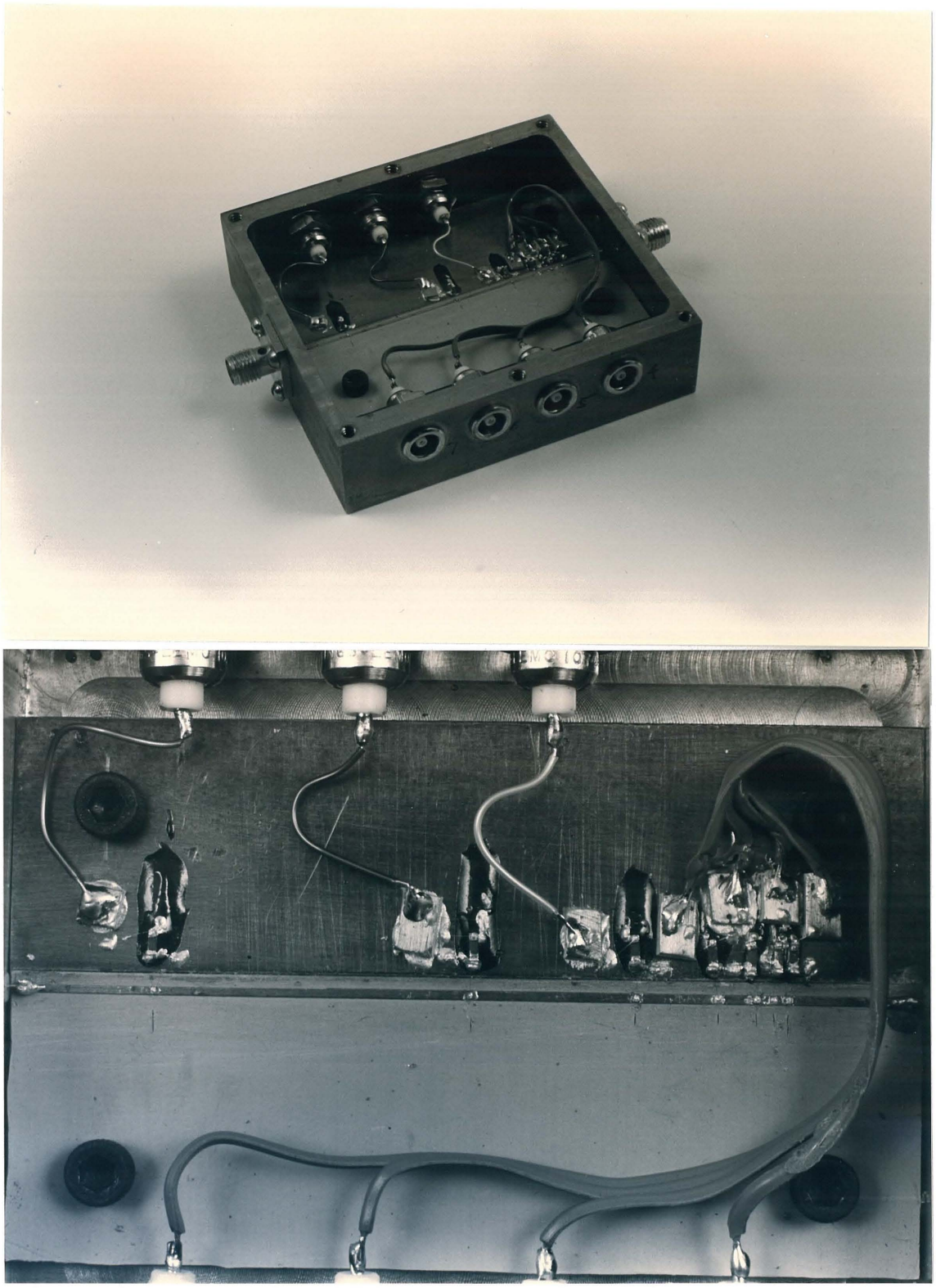

Figure 6.15 The third sampled-line network analyzer

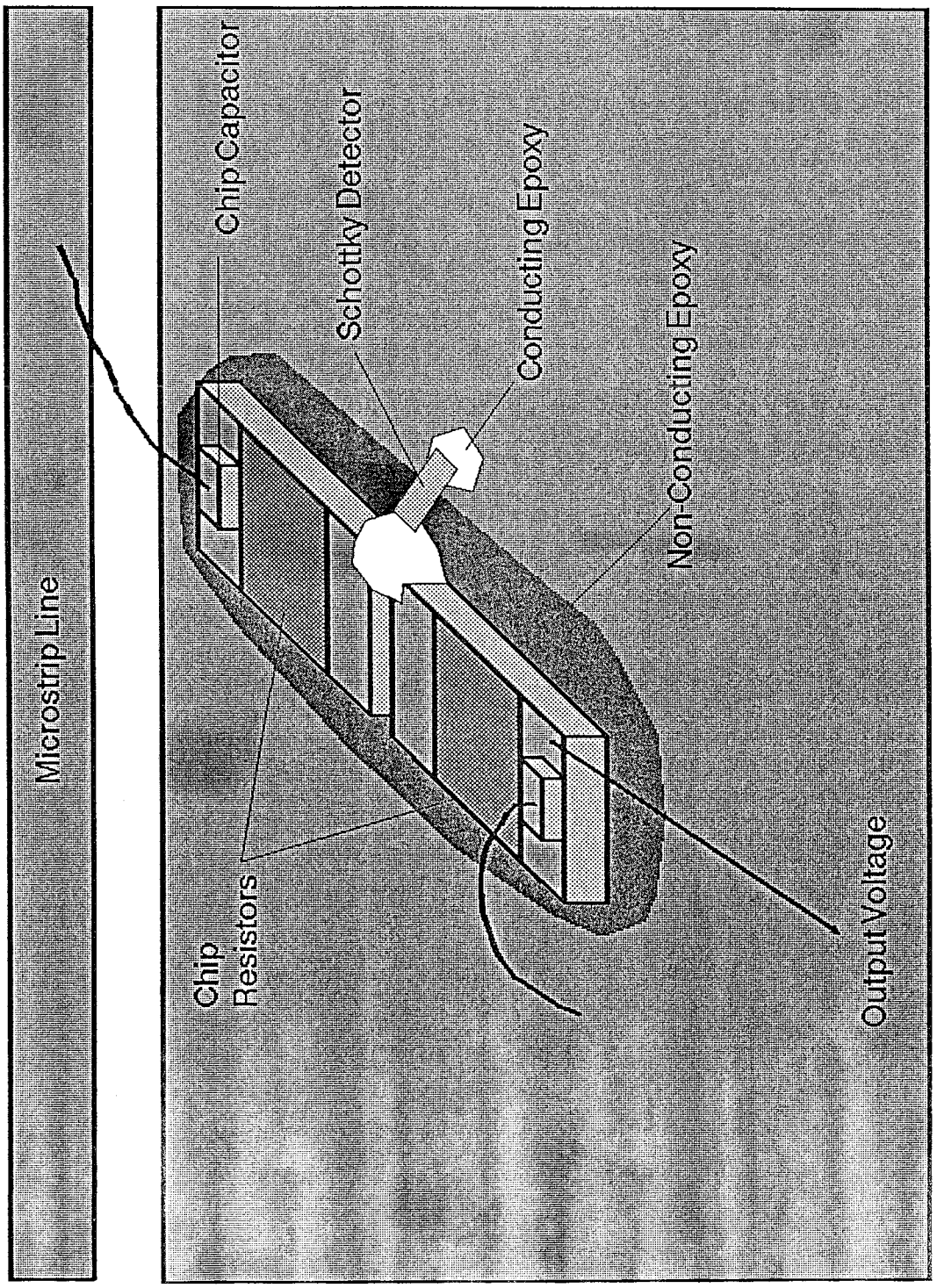

Figure 6.16 Physical configuration of the samplers used in the third network analyzer.

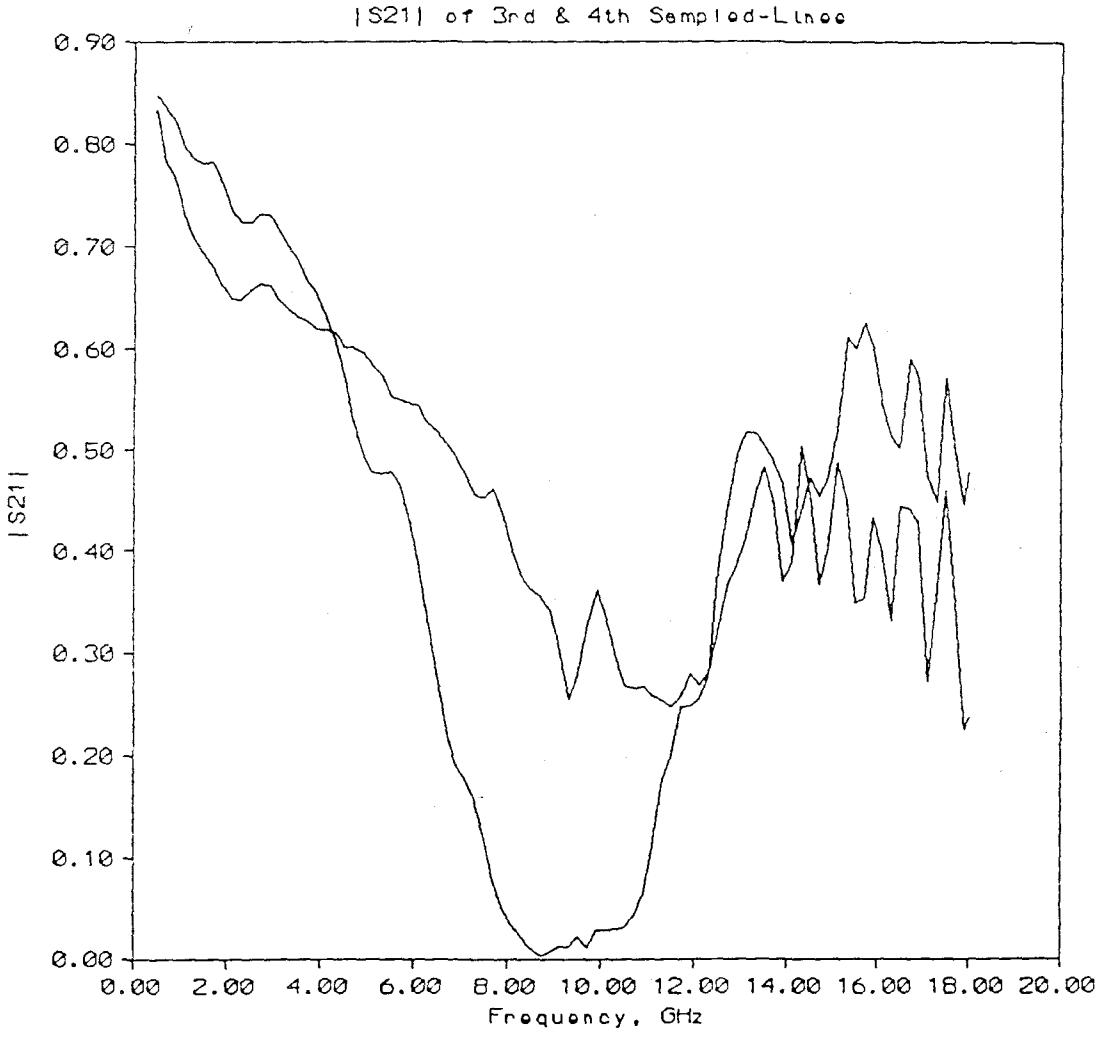

Figure 6.17 $|S_{21}|$ of the third and fourth sampled-line network analyzers.

is plotted on top of that of the third network analyzer. The resonance at 8 GHz has been removed.

Figures 6.19 and 6.20 show the diode response curves for the third and fourth network analyzers. The effects of the solder pad resonance are evident in the third analyzer's curves. The first diode on the line actually has a slightly increased response due to the resonance, but responses of the other diodes decrease steadily the further the diode is down the line due to the fact that at each diode, a fraction of the incident power is reflected back toward the generator.

Above the resonance, the diode responses of the third analyzer are somewhat erratic, indicating that it will not be of much use as an analyzer at frequencies above 7 GHz.

The fourth analyzer's diode responses go smoothly over the resonance seen in the third and do not become erratic until around 15 GHz. At this frequency, a number of things may be coming into play. The reduced parasitic capacitance of the chip resistors may be resonating with the bond wires, or other circuit parasitics may be showing up. Also, the fact that $|S_{21}|$ increases above about 14 GHz suggests that there may be some coupling to a hybrid or cavity mode inside the box enclosing the sampled-line. One would expect the loss of the microstrip and the effects of the samplers to keep $|S_{21}|$ going down with increasing frequency.

The fourth analyzer looks to be the best implementation of the sampled-line analyzer to date. By comparing the measured $|S_{21}|$ for the fourth analyzer with that predicted by *Puff* for an analyzer with $Y = 0.1Y_0$ loading, however, it is seen that the sampler admittance of the fourth analyzer is considerably greater than $0.1Y_0$ for frequencies of more than a few GHz. Parasitic capacitance is a good candidate for this problem as well. The solder pads on either end of the chip resistor give rise to a parasitic capacitance in parallel with the resistor, as

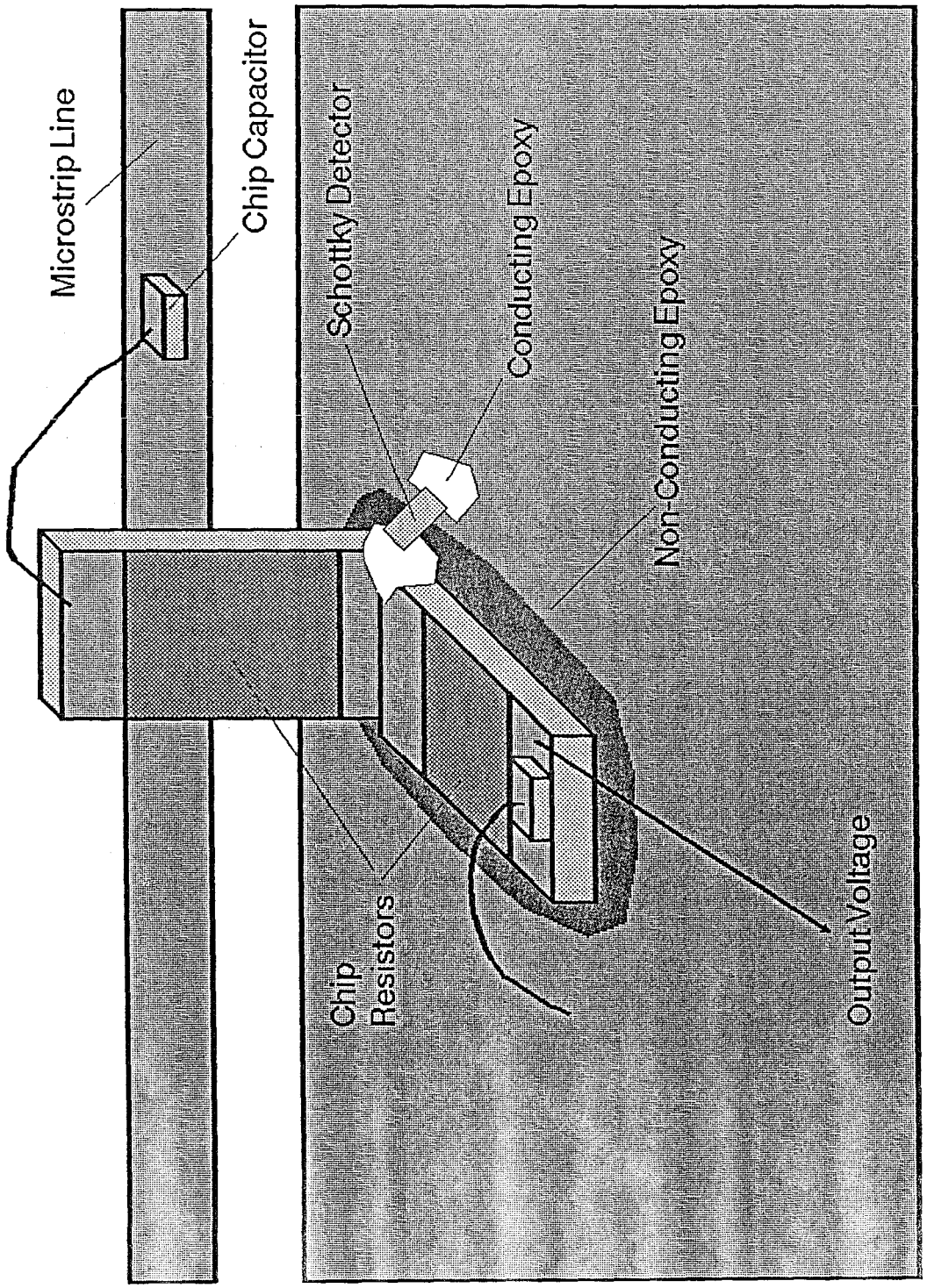

Figure 6.18 Physical configuration of the samplers used in the fourth network analyzer.

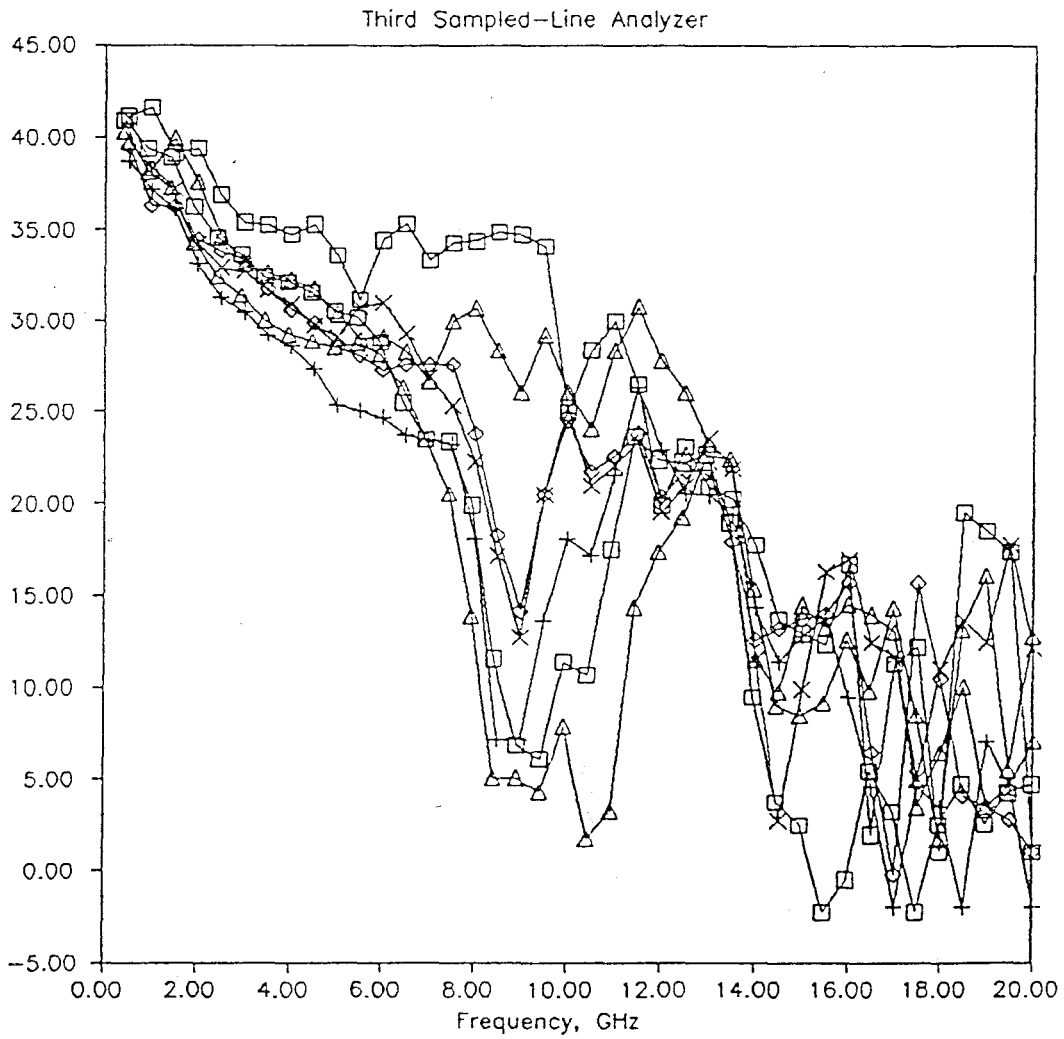

Figure 6.19 Frequency response of the sampling circuits in the third network analyzer. Vertical scale is the same as that used in figures 6.6 and 6.12.

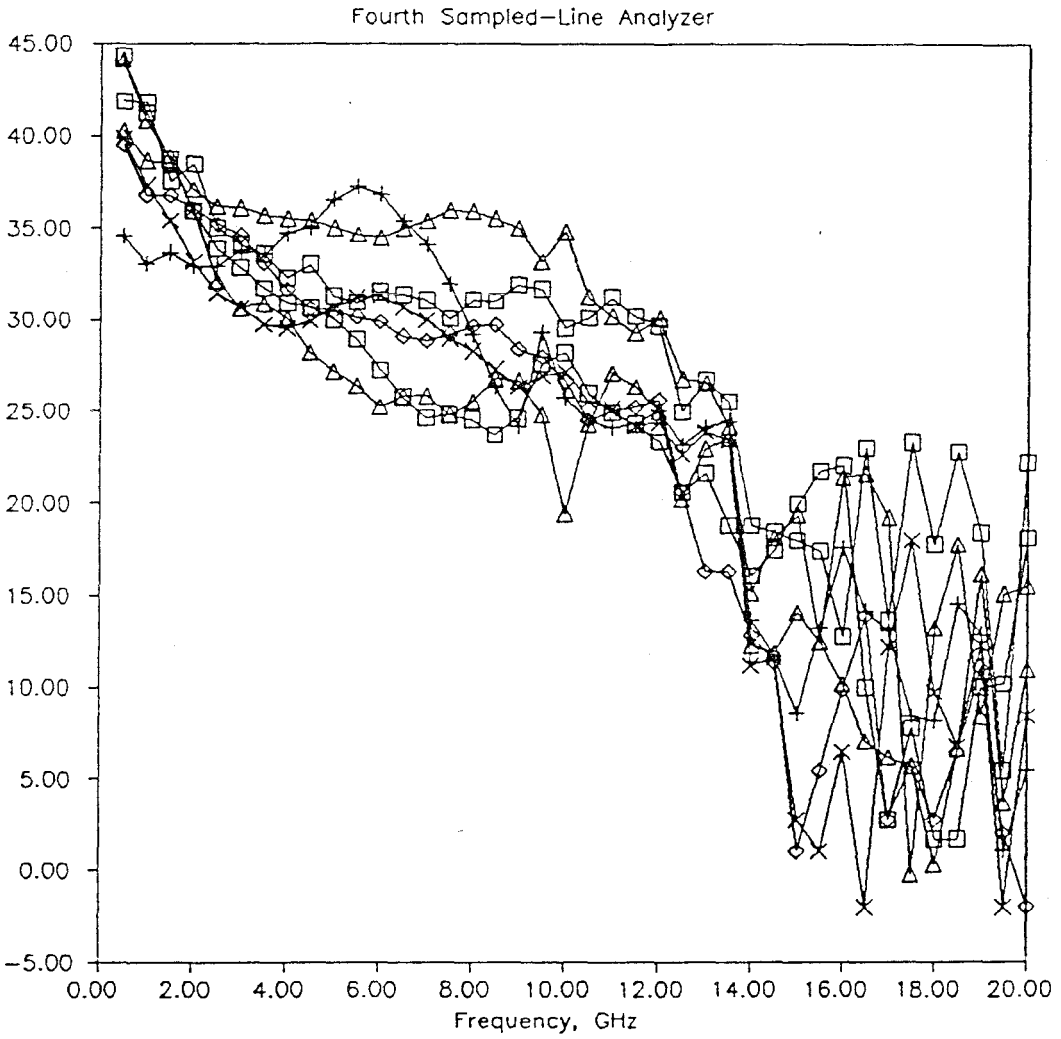

Figure 6.20 Frequency response of the sampling circuits in the fourth network analyzer. Vertical scale is the same as that used in figures 6.6, 6.12, and 6.19.

well as that to ground. This reduces the resistor's ability to isolate the diode from the line.

6.1.2 The Microwave Phase Shifter

As shown in figure 6.1, a microwave phase shifter is required for the Sprite system. The phase of the excitation of one reflectometer head with respect to the other must be changed in order to measure the full S-parameters of the device under test.

Ideally, the phase shifter would provide, at any frequency, a range of phase shifts spaced uniformly from 0° to 360°. It is also desirable to have a large number of available phases. These phases are used to calculate a least-squares estimate of the S-parameters.

Since the phase shifter must operate over a broad frequency range, a switched delay line design was selected. Coaxial switches that operate over a DC to 18 GHz frequency range are readily available. These switches are used to switch the signal through combinations of delay lines, which provide the desired phase shifts. This reduces the design problem to the selection of a set of coaxial line lengths that give a good spread of phase delays over the frequency range. Figure 6.21 shows the RF layout. A pair of six-way switches and a pair of two-ways were available at the time of the design, and since it was found that a viable phase shifter could be constructed with this combination, they were used. This design provides a total of twelve different phase shifts.

A computer program was written which could plot out the phase delays of the ensemble of delay lines as a function of frequency. This program was used to choose the delay line lengths. The results are given in table 6.1. Basically, the six-way switch selects between a set of delays with lengths that increase exponentially from the shortest to the longest. The two-way switch adds in a short delay, which only offsets things a small amount at the low frequencies, but at some higher frequencies mixes things up enough to improve the phase coverage

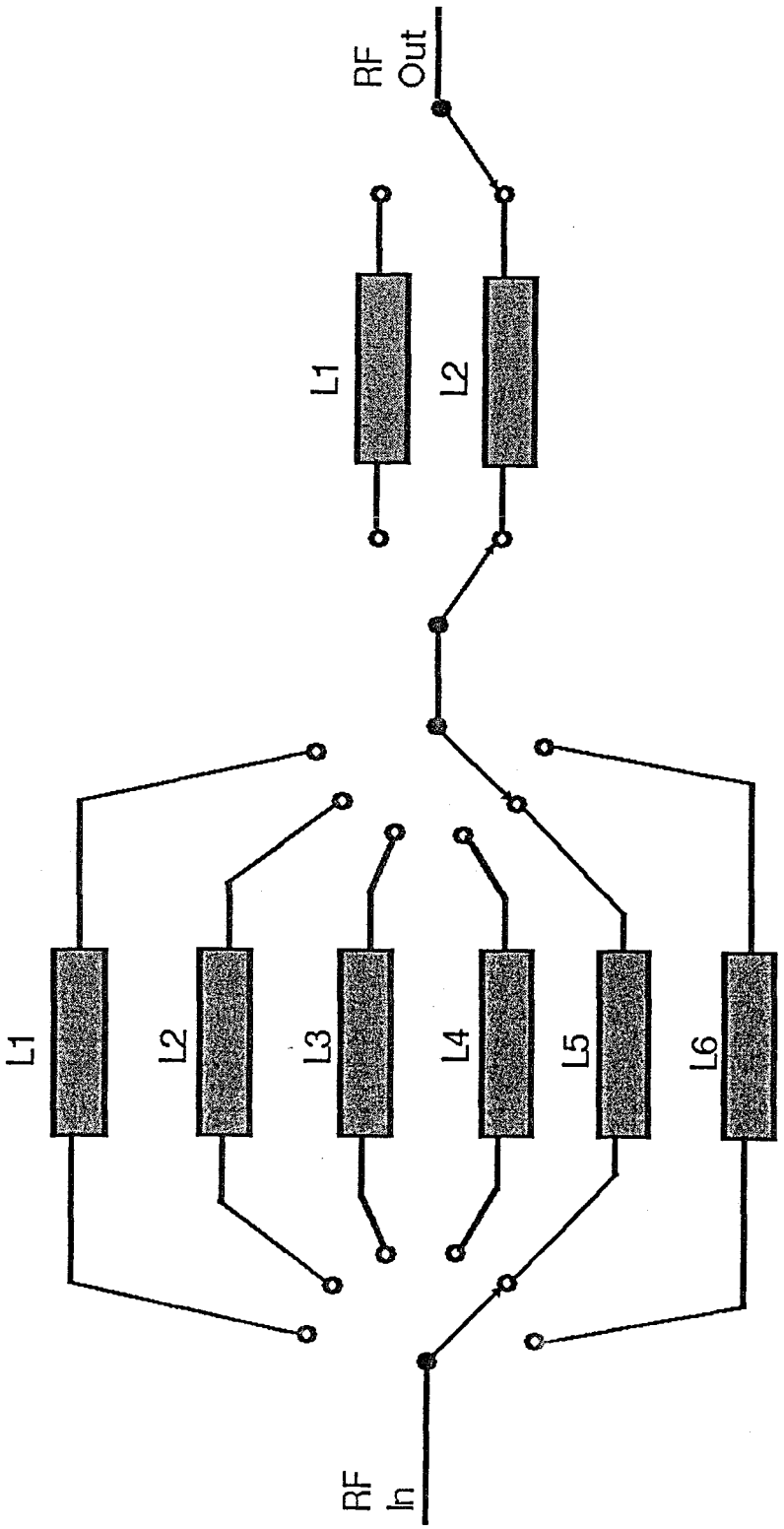

Figure 6.21 RF layout of the microwave phase shifter.

significantly. A fixed delay line in the second arm of the network analyzer is adjusted such that when the L_1's are selected by both switches (shortest delay), the signal path through the phase shifter arm is 1.06 cm longer than through the other arm. This is why L_1 is nonzero in the first list.

Six-Way Switch Delay Lines	
L_1:	1.06 cm
L_2:	2.02 cm
L_3:	3.84 cm
L_4:	7.32 cm
L_5:	13.93 cm
L_6:	26.52 cm
Two-Way Switch Delay Lines	
L_1:	0.0 cm
L_2:	1.06 cm

Table 6.1 Delay line values for the microwave phase shifter. Lengths given are in cm of teflon-dielectric ($\epsilon_r = 2$) coaxial line.

The delay lines were cut from 0.085"-diameter semirigid coaxial line. Connectors were attached to the lines and they were attached to the coaxial switches. A simple computer interface circuit was designed and built. The interface allowed a four-bit word from the computer's laboratory interface card to select any of the twelve phases.

Figure 6.22 shows the transmission through the phase shifter for a typical delay setting. The dip at 9.5 GHz is thought to result from too tight a bend in one of the semirigid coaxial lines used in the construction. The extra 1.5 dB of loss is acceptable for use in the network analyzer system.

The delays of the various settings of the phase shifters were measured using a vector voltmeter. The signal from a microwave generator was split equally. One half of it went through a fixed delay line and the other half through the phase shifter. The two emerging signals were applied to an HP 8410A network analyzer which, without the reflection-transmission test set, is just a vector voltmeter. The

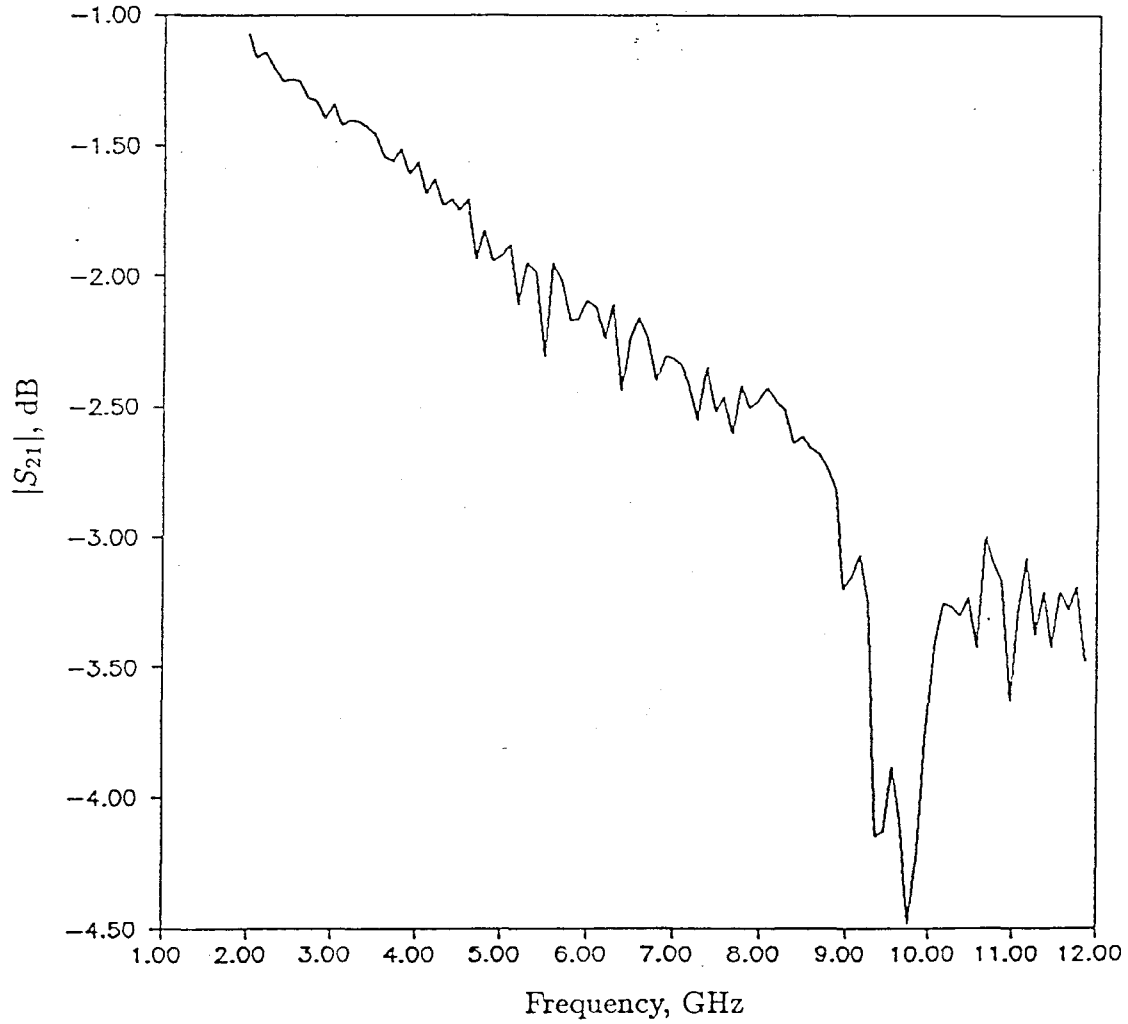

Figure 6.22 $|S_{21}|$ of the microwave phase shifter for a typical phase setting.

frequency of the test signal was swept, and a linear regression was applied to the resulting phase data. A frequency counter was used to get accurate frequency information. The frequency was swept from 0.6 to 2.6 GHz.

The lengths of the delay lines were found to be within a few percent of the design values. However, systematic errors were noted due to dispersion in the coaxial delay lines. Dispersion was neglected in the computer program used to design the phase shifter. The relatively large number of phases in this phase shifter seems to have allowed it to tolerate phase errors due to dispersion as far as the network analyzer's operation is concerned. As long as the phase coverage is good, the particular values are not important. Errors due to dispersion will increase with frequency, however. The fact that dispersion was large enough to be seen in these tests indicates that future phase shifter design programs will need to include dispersion effects.

6.1.3 The Preamplifier Bank

The preamplifier bank consists of a set of fourteen identical AC-coupled amplifiers, one for each diode detector in the Sprite system. The output voltages of the diode detectors with the power levels typically used in Sprite are in the range of a few millivolts. The A/D converter used with Sprite has an input range of ± 2.5 volts, and 12-bit resolution. Hence the need for the preamplifier. The preamplifier must be AC-coupled due to the large offset voltages that result from the diode bias currents. A $20\,\mu$A bias current gives a DC offset voltage of 0.2V with these diodes. The AC-coupled preamplifier rejects this offset and amplifies the response to the microwave signal, which is chopped at a 1 kHz rate.

Figure 6.23 shows a schematic diagram of the preamplifier, and its frequency response. These preamps pass a 1 kHz square wave with little distortion.

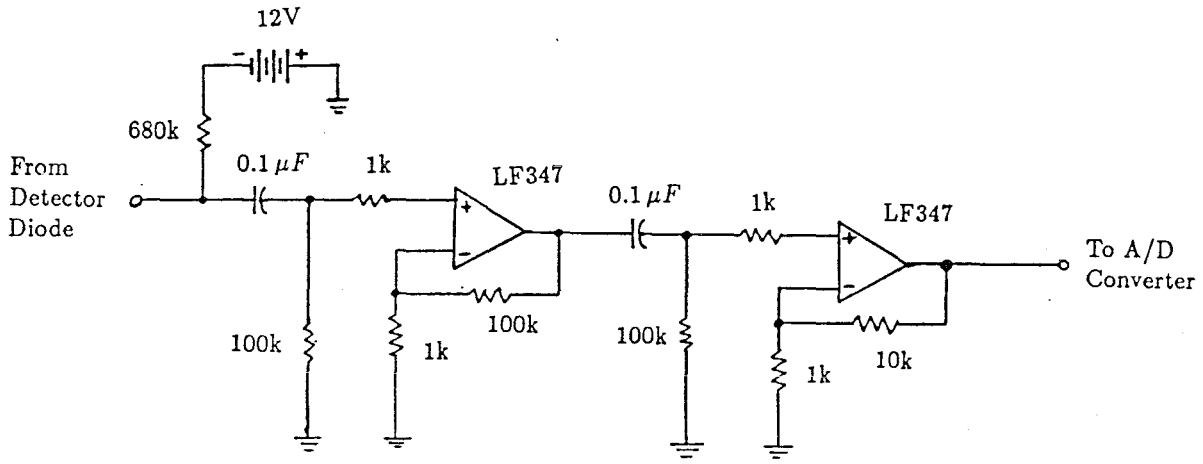

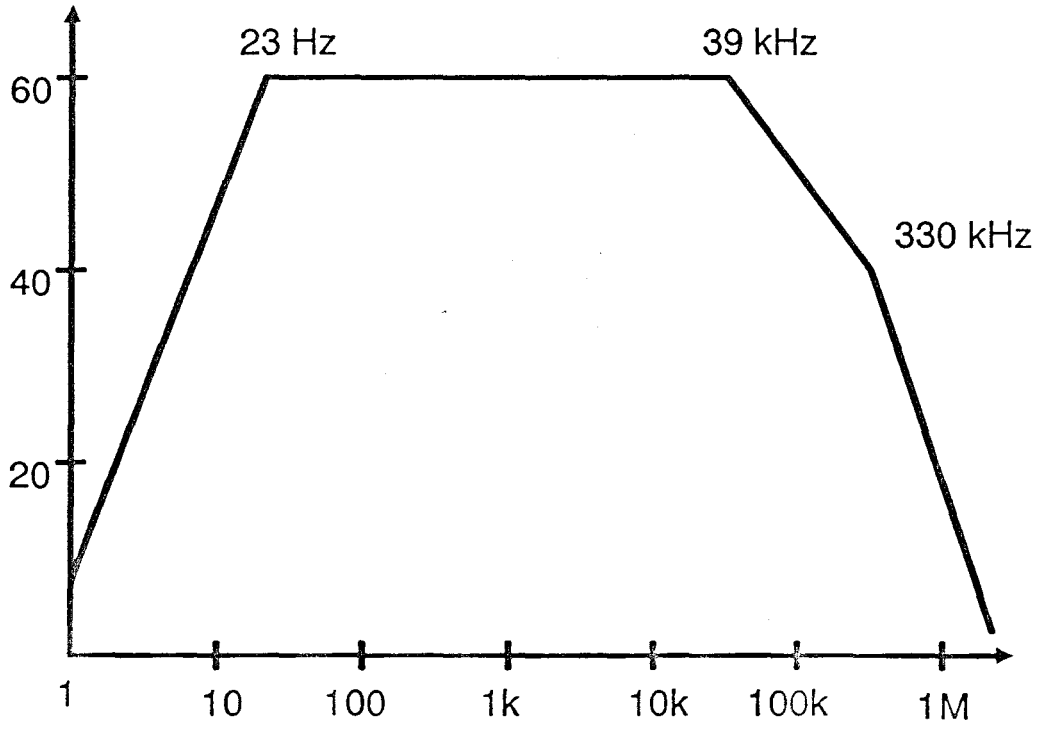

Figure 6.23 AC coupled preamplifiers boost the signals from the diode detectors to levels compatible with the A/D converters in the computer. Here a schematic and a frequency response for a typical channel of the preamplifier bank is given.

6.1.4 The Synchronization Circuitry

The sampling of the computer's A/D converter is synchronized to the signal which chops the output of the microwave signal generator. Each diode's output is thus sampled at the same point on the AC waveform for every measurement. This minimizes the amount of averaging required in software to achieve a given noise level.

Figure 6.24 shows the circuitry used to achieve the synchronized sampling. The 555 timer, in free running mode, is used to generate a clock with a frequency of 27.4 kHz. The first stage of the first 74LS93 divides this down to 13.7 kHz and yields a clean square wave (the 555 timer output does not have a 50% duty cycle). This signal is used as the external clock for the A/D converter. All A/D conversions will be performed on the rising edge of this clock signal. The frequency of 13.7 kHz is the specified maximum external clock frequency for the DT2801.

The external clock signal is further divided down by the LS93's to yield an 856 Hz signal. This signal serves two functions. It is used to clock a pair of D flip-flops, which synchronize the computer's measurement requests. To initiate a measurement, the computer pulls the trigger request (TRQ) line high, and sets itself up for a block A/D conversion with external clock and external trigger. The delay of at least one clock cycle guaranteed by the two flip-flops assures that the A/D board has sufficient time to set itself up. The computer then receives the external trigger signal from the circuit and begins making A/D conversions synchronized with the external clock.

The 856 Hz signal also modulates the microwave source. A transistor inverter increases its amplitude to the $\pm$14V level required for this function. Thus microwave signal modulation, A/D conversion and conversion triggering all take place synchronously.

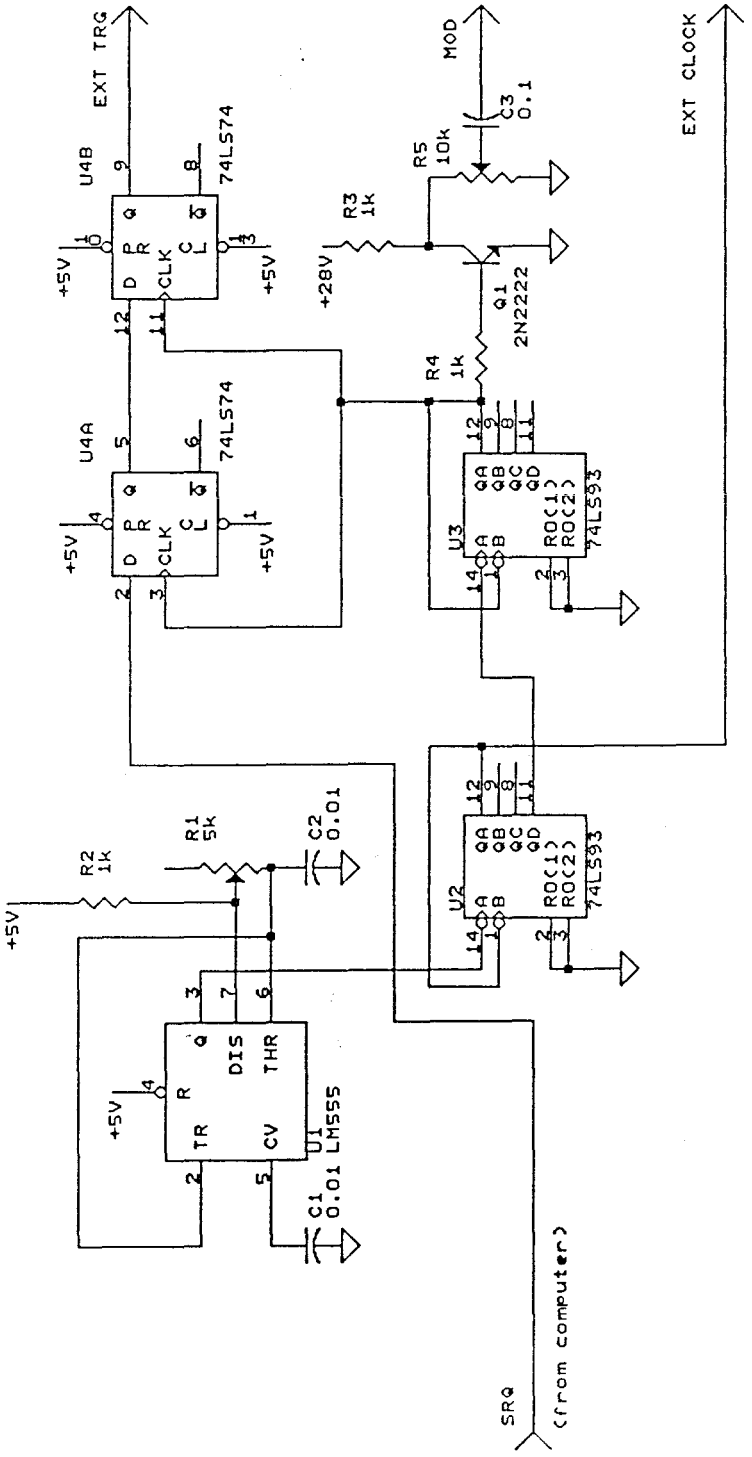

Figure 6.24 Schematic of the synchronization circuitry used with the sampled-line network analyzer.

6.2 Software Description

Elf and the first sampled-line reflectometer calibration program were written in Turbo Pascal, version 3.0. This version of Pascal restricted the size of a compiled program to a 64KB segment. If the program were larger, overlay files would have to be used, which quickly becomes unwieldy. Both Elf and the first sampled-line analyzer program pushed this limit. Since the full S-parameter calibration program promised to be more complex than either of these, an alternative was sought.

The Turbo C [10] compiler became available during this time. It did not suffer from the code size limitations of Turbo Pascal 3.0 and offered C's greater flexibility and power in the structure and control of data. Turbo C was chosen as the compiler for the current version of the sampled-line network analyzer program.

The change to the C language brought about changes in the data structures used in the program. In Elf, the data were stored in arrays. This is somewhat cumbersome and error-prone; in doing a frequency sweep, care must be taken that all the indices of all the arrays move together.

With C, the data structure was changed to a linked list of records. Each record contains values of all the system variables at a given frequency. Sweeping in frequency is accomplished by simply moving along the linked list. Memory for each record is dynamically allocated to match the number of frequency points desired by the user. Each record in the linked list also contains the root element of another linked list. These linked lists – one for each frequency – contain the values of the diode voltages read at each slide position during the sliding short circuit calibration procedure. These sliding short circuit linked lists are also dynamically allocated, to match the number of sliding short positions used.

Sprite actually holds two data structures like that described above, one for each reflectometer head. This approach was taken, instead of having one data

structure with information on both heads, in the interest of designing a data structure that could later be expanded in a natural way to include analyzers with more than two heads.

Sprite is currently about 108KB in size when compiled. It performs all the interface, calibration, measurement and display functions required to implement the sampled-line network analyzer. At present, however, unlike Elf, its user interface is not well-developed. A description of the program from a user's point of view, as was given in chapter 5, is thus impractical. Instead, the following paragraphs present a brief description of the algorithms that are implemented, and how they are used in a typical calibration and measurement with the Sprite system.

As with the Elf system, or with any vector network analyzer, Sprite's first task is calibration. Calibration is a multi-step process in Sprite, with several options that may be used or omitted as the user chooses. In Sprite's calibration procedure, the user is stepped through the entire calibration procedure and all the calibration data are taken and saved to disk before the calibration algorithms themselves begin to process the data. In case of a crash, then the data can be read back in and the calibration algorithms restarted. Sprite can thus save and restore calibrations for later use. Since calibration drift with this system is small, even over multi-day time periods, this is a useful feature.

At each frequency there is one triple of diodes within each head, which is known as the primary triple. As noted in chapter 4, with the sampled-line analyzer, a set of three detectors is sufficient to find w, the complex ratio between the voltages at two of the detectors. The primary triple is the set of diodes known *a priori* to have the best spacing for that frequency. The first step in Sprite's calibration procedure is to calibrate the primary triple at each frequency of the measurement in each reflectometer head. The sliding short circuit method

described in chapter 4 that gives values for the calibration coefficients for a triple in closed form is used here.

Under some circumstances, such as a resonance in one of the detector circuits, this primary triple calibration procedure can fail. The calibration procedure consists of fitting an ellipse to P_3/P_4 vs. P_5/P_4. This ellipse must lie entirely in the first quadrant. At bad frequencies, however, the ellipse can be quite eccentric and noise in the measurements can cause the best fit conic section to be a hyperbola, or an ellipse that crosses out of the first quadrant. When this occurs, the calibration coefficients cannot be extracted through this method. It also indicates that measurement accuracy would be very poor at that frequency. Consequently, in the event of a primary triple failure, Sprite marks the frequency as bad for that head, and no further calibration is attempted on that head at that frequency.

Assuming success in the primary triple calibration, the secondary triples are calibrated. A secondary triple consists of the first two diodes in the primary triple, and a new third diode. This is so because the final desired result is w, the complex ratio between the voltages at two of the detectors. Thus these two must be included in all triples so all calibrations are performed in the same w-plane. The same diode voltage, that of the first diode in all triples, is the denominator for all the ratios used in the calibration procedures.

Failures in calibration of the secondary triples are much more common than primary triple failures, but they are not catastrophic. In the event of such a failure, the secondary triple is marked bad for that particular frequency, so data from one diode cannot be used in the determination of w in that reflectometer head. The other secondary triples and the primary triple are still usable, so w can be found, perhaps with slightly reduced accuracy, and the remainder of the calibration and measurement algorithms can proceed.

With the primary and secondary triples calibrated in both reflectometer heads, each head can find its value of w, but these w's are not calibrated to the reference planes of the heads. Values of $(n-2)$ centers and scale factors in the w-plane are known for each reflectometer head, where n is the number of detectors in each.

At this point, an optimization routine can be run to improve the estimates of the centers and scale factors, as described in chapter 4. The code for this procedure still exists in Sprite, but it is seldom used. The optimization routine converges, but it is slow and does not greatly improve estimates of the calibration coefficients. For the current network analyzer, it involves a fourteen parameter optimization at each frequency point for each sampling head. A greater improvement in accuracy is achieved by taking more calibration points on the sliding short circuit during that phase of the calibration procedure.

At this point there are two possibilities as to how w is determined in each head. The primary triple alone may be used, or data from all the triples may be brought into play. The tradeoff is one of speed versus accuracy. If only the primary triple is used, the value of w is found through simple trigonometry. If all the triples are used, the value of w is found by finding the value of w that minimizes an error function ξ where

$$\xi = \sum_{i=1}^{(n-2)} \left(\frac{|w - w_i|^2 - \zeta_i P_i / P_4}{\zeta_i} \right)^2 \tag{6.1}$$

where w_i and ζ_i are, respectively, the centers and scale factors associated with all the calibrated triples and the P_i's are the observed powers.

Minimization of the above error function is done iteratively, by a downhill simplex method, so solution of (6.1) takes considerably more computing time than does the trigonometric solution using only the primary triple. The accuracy improvement, however, can be large, especially at the edges of a primary triple's frequency range. Solution of (6.1) takes around half a second per frequency point

in the current Sprite system. In a reflectometer mode for a modest number of frequency points, this is not too bad a wait, but in the S-parameter mode, where w's must be found for twelve phases of excitation at each frequency point, the wait becomes quite noticeable. In future versions, a faster method for solving (6.1) must be implemented.

In the next stage of Sprite's calibration, the two reflectometer heads are calibrated to read the true reflection coefficients at their reference planes. A short-open-load type calibration is performed first. The results from this calibration are used to resolve root ambiguities in the thru-reflect-line calibration, which is performed next. The TRL calibration currently uses a set of five precision delay lines of various lengths, selecting at each frequency the one closest to an odd number of quarter wavelengths for the TRL procedure at that frequency.

At this point the Sprite system is calibrated as a pair of reflectometers. As noted in chapter 3, this is sufficient for the measurement of reciprocal two-ports. In the final stage of the calibration procedure, the C's are found as described in chapter 3, which allows the determination of a_2/a_1 from the observed reflection coefficients. Nonreciprocal two-ports may then be measured by Sprite, and the calibration procedure is complete. This final calibration step uses data from the same five delay lines as are used in the TRL calibration. Instead of selecting one best line, as is necessary in the TRL process, however, data from all the delay line measurements are used to form a least-squares estimate of the C's.

With calibration complete, the Sprite system operates in a continuous measurement mode. It cycles through the twelve phases of the phase shifter, measuring the reflection coefficient at each head's reference plane at each phase. These results are summed into a matrix that is solved as described in chapter 3 for S_{11}, S_{22}, and Δ. The C's are then used to extract S_{12} and S_{21} from Δ.

The results are displayed graphically as they are calculated. Currently a two-window display of the measured S-parameters is used. One window shows a

Smith chart plot of the data, and the other a rectangular plot. The rectangular plot may show in dB magnitude, linear magnitude, or phase.

At any point in the measurement, the measurement procedure may be paused and the measured data written to disk as a *Puff*-compatible device file.

This output file, as well as the calibration files used by Sprite, are ASCII files that may be printed out or read with a text editor. This makes examination of the measured data easy, and looking at the calibration data is often useful in diagnosing problems in the Sprite hardware.

6.3 Sample Measurements

Sample measurements using the Sprite network analyzer system are shown in figures 6.25 and 6.26. The analyzer is used in two different modes here. In figure 6.25, the analyzer is used as a dual reflectometer. This allows the properties of the two network analyzer heads to be seen individually. Figure 6.26 shows a full S-parameter measurement. In both, the frequency axis is on a log scale. Since each triple of diodes is expected to work over about an octave of frequency, this allows the performance of all triples to be observed equally well.

In the dual reflectometer measurement, both reflectometers measure a 15-cm length of precision coaxial line terminated in an open circuit. Thus, a reflection coefficient with unity magnitude and phase that varies linearly with frequency is expected. In the S-parameter measurement, the 15-cm length of line is connected between the reflectometer heads. The expected S-parameters are then $S_{11} = S_{22} = 0$ and S_{12} $(= S_{21})$ would have unity magnitude and linearly varying phase.

Examining figure 6.25, it is seen that the third sampled-line analyzer, when used as a reflectometer, performs well over the first octave, from 0.625 to 1.25 GHz, except for a couple of bad points at the low end. Apparently the frequency range of the diode triple has been stretched too far here. Otherwise, the magnitude of the measurement error vector over this range is about 0.05.

Over the next octave, from 1.25 to 2.5 GHz, the analyzer continues to perform fairly well. There is a glitch at the high end of the range, again probably due to a triple being stretched too far in frequency. The error vector has magnitude 0.1 at 2.125 GHz, but elsewhere over this range the error vector magnitude holds at 0.05.

The third analyzer falls apart in the 2.5–5 GHz octave. There are primary triple failures at 4, 4.25, and 5.0 GHz, and the error levels make the analyzer unusable above about 3 GHz.

The analyzer has another small range of reasonable accuracy around 5 GHz, but it is unusable above that frequency, with primary triple failures for all frequencies above 7.5 Ghz

The fourth sampled-line analyzer is considerably better. It does not begin to show any significant problems until 5 GHz, and after a rough spot at 5–5.5 GHz, it is fairly good up to 10 GHz. Again there is the problem below 750 MHz indicating that the first triple cannot be stretched to this low a frequency. The glitches at 5 and 9.5 GHz show that, as detector loading increases, triples lose the ability to cover an entire octave with good accuracy.

Over most of the first octave, the magnitude of the error vector of the fourth analyzer is about 0.02. In the second it increases to about 0.04, and is about 0.06 in the center regions of the third and fourth octaves.

Figure 6.26 shows a full S-parameter measurement using the sampled-line system. Due to the poor performance of the third sampled-line analyzer, which is used as one of the heads in the S-parameter measurement system, calibrations and measurements can only be performed reliably up to 3.5 GHz or so. Even here, the error in the determination of S_{22} is large due to the problem with the third reflectometer head.

So the Sprite system can currently perform reflectometer measurements from about 750 MHz to 10 GHz with a few bad frequency intervals, and can do full

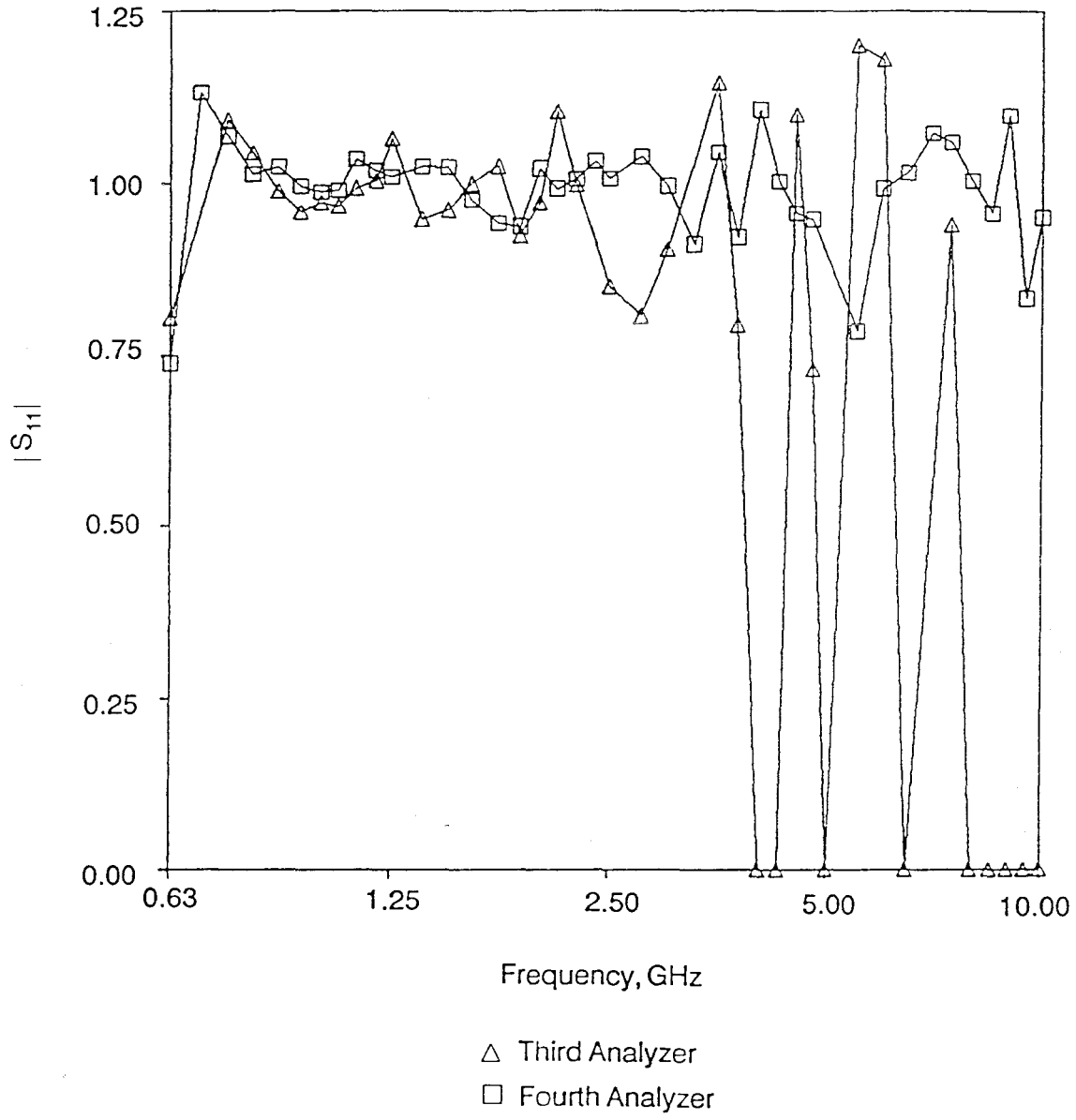

Figure 6.25 Dual reflectometer measurement with the sampled-line network analyzer.

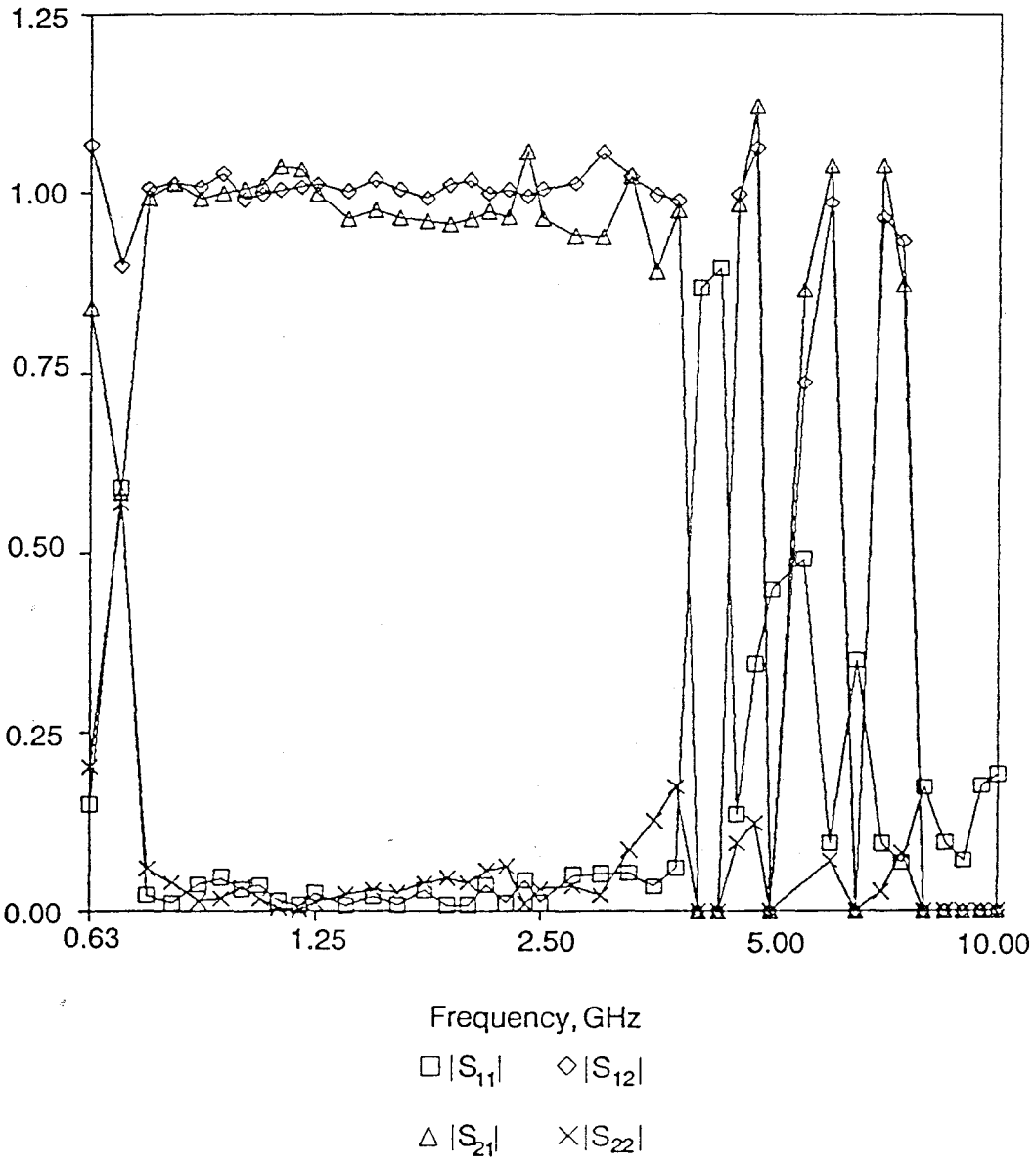

Figure 6.26 S-parameter measurement with the sampled-line network analyzer.

S-parameter measurements from 750 MHz to a little over 3 GHz. It is expected that constructing another sampling head with the resistors standing on end, as in the fourth version, would allow the full S-parameter measurements to be made up to 10 GHz, with a small gap at 5 GHz.

References

[1] R.C. Compton and D.B. Rutledge, *Puff: Computer Aided Design for Microwave Integrated Circuits,* Pasadena: Calif. Inst. of Tech., 1987

[2] KDI Electronics, Pyrofilm Division, 60 S. Jefferson Rd., Whippany, NJ 07981

[3] Johanson Dielectrics, Inc., 2220 Screenland Dr., Burbank, CA 91505

[4] The Turbo Pascal compiler is a product of Borland International, 4585 Scotts Valley Drive, Scotts Valley, CA 95066

[5] Hewlett-Packard model HSCH-5336

[6] K.C. Gupta, R. Garg and I.J. Bahl, *Microstrip Lines and Slotlines,* Dedham, MA: Artech House, 1979

[7] Hewlett-Packard model HSCH-5336

[8] Republic Electronics Corp., 575 Broad Hollow Rd., Melville, NY 11747

[9] Epo-Tek H20E, Epoxy Technology, Inc., 14 Fortune Dr., Billerica, MA 01821

[10] The Turbo C compiler is a product of Borland International, 4585 Scotts Valley Drive, Scotts Valley, CA 95066

Chapter 7

Conclusions and Suggestions for Future Work

The work to date has shown that it is feasible to apply an extended six-port network analyzer theory to a sampled transmission line with an attenuator on one end, and thereby construct an accurate microwave network analyzer. The requirements on sampler admittance and spacing have been investigated and are fairly well-understood. Several sampler design configurations have been tried, and a fairly good one for frequencies up to 10 GHz has been found. In the following sections, possible avenues for further research into the sampled-line network analyzer are presented.

7.1 Thin Film Sampler Design

It was seen in chapter 4 that for a sampled-line analyzer with seven detectors, the admittance of each detector must be less than $0.1Y_0$. For analyzers with more detectors, this requirement would become more stringent. The chip components, particularly the resistors, used in the present sampled-line analyzer have parasitic capacitances too high to meet these requirements at frequencies much above 10 GHz. A thin film design might solve these parasitic problems.

Alumina substrates are available with special metallizations, which can be used to fabricate thin film resistors on the substrates through an etching process. One such metallization has a layer of titanium tungsten on the substrate, covered by a layer of gold. Two masks are used to fabricate the circuit. The first mask places photoresist wherever a conducting path or a resistor is to be placed. Both layers of metallization are then etched away wherever there is no photoresist. The second mask places photoresist everywhere except where resistors are to be placed. The gold layer is etched away wherever a resistor is to be placed, exposing the TiW. The substrate is then baked and the exposed TiW oxidizes to form a $100\,\Omega/\square$ resistive layer.

Since lines 2 mils or less in width can be achieved with thin film etching techniques, resistive sampling circuits with very low parasitic capacitances could be fabricated in this way. Sampling circuits constructed in this way should be able to provide acceptable line loading and RF-DC isolation at least up to 20 GHz.

7.2 Monolithic Fabrication Options

To extend the sampled-line analyzer into the millimeter wave frequency range, the best approach might be to move to a monolithically fabricated version. Several options would be available here.

The monolithic analyzer would be built on silicon or gallium arsenide, so the Schottky diode detectors could be integrated with the microstrip line. The fact that a low loss microstrip line cannot be built on Si or GaAs is not a hindrance, since attenuation is already placed between the line and the device under test.

A sampler design similar to that discussed above could be further miniaturized with monolithic techniques, reducing parasitic capacitances to a desired level, or a different approach might be taken. Instead of trying to isolate the sampling diodes from the transmission line, the diode can effectively be made part of the transmission line. If a series inductance is added to the shunt capacitance of the diode, as shown in Figure 7.1, and the inductance is chosen such that $\sqrt{L/C} = Z_0$, then this combination looks like an incremental section of transmission line with characteristic impedance Z_0.

As long as the frequency is well below the resonant frequency of the LC network ($\omega \ll 1/\sqrt{LC}$), reflections from this structure are very small. For the beam lead diodes used in the current analyzer, with a capacitance of 130 fF, this resonant frequency would be about 25 GHz. Monolithic diodes could have considerably smaller junction capacitances. A 50 fF diode, with its associated inductance, would have a resonant frequency of 64 GHz.

The diode has an equivalent shunt resistance as well, but the resistor's effect is not significant in this structure as long as $R \gg 1/\omega C$. For typical detector diodes, even when biased, the equivalent resistance is in the kΩ region, so that on a 50 Ω line, its effect is not seen until well above the LC circuit's resonant frequency.

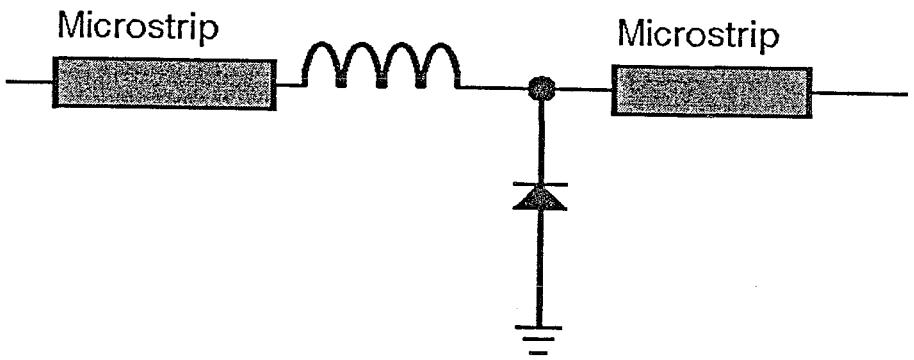

Figure 7.1 A series inductor and the shunt capacitance of the diode detector are used to construct a short segment of synthetic 50 Ω transmission line. Reflections from such a structure are small for frequencies below resonance of the LC combination.

The inductance for this structure might be implemented as a narrowing of the microstrip line in the neighborhood of the diode. Some careful modelling would be required for this design, especially if the design is to extend into the millimeter wave region.

With monolithic fabrication, it might also be desirable to use something other than microstrip for the sampled transmission line. Planar transmission lines, such as coplanar waveguide, slot line or coplanar strips keep all the conductors of the waveguide on the same side of the substrate, removing the need for via holes to make connections to the ground plane. Figure 7.2 shows two possible sampling configurations that might be fabricated, respectively, on coplanar waveguide and coplanar strip transmission lines.

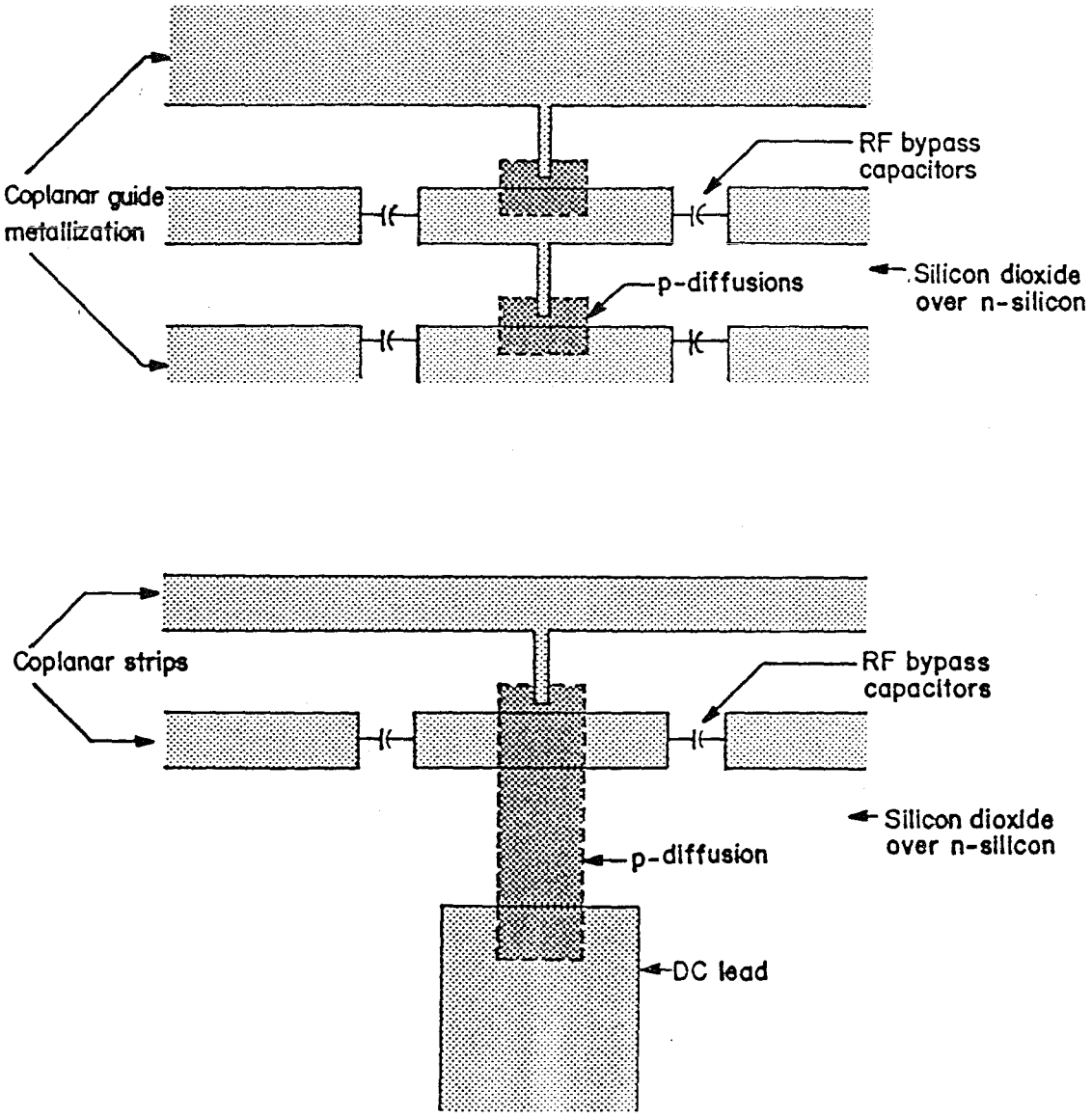

Figure 7.2 Possible sampler configurations for use with coplanar waveguide and coplanar strip transmission lines.

7.3 Measurement of Multi-Port Networks

Since the sampled-line reflectometer heads can be fabricated inexpensively, it is reasonable to consider a network analyzer that would have more than two reflectometer heads. Such an analyzer could be used to measure the scattering parameters of networks with more than two ports. Measuring such networks with a two-port network analyzer requires multiple measurements and some data reduction.

Multi-port networks of practical interest in microwave circuits include directional couplers, hybrids, and circulators.

Consider the case of a three-port measurement system. The configuration is shown in figure 7.3. It is assumed that each reflectometer head is calibrated to read the true reflection coefficient, Γ at its reference plane. When the three-port is connected to the reflectometers, then, the reflectometers read

$$\Gamma_1 = S_{11} + S_{12}\frac{a_2}{a_1} + S_{13}\frac{a_3}{a_1} \tag{7.1}$$

$$\Gamma_2 = S_{21}\frac{a_1}{a_2} + S_{22} + S_{23}\frac{a_3}{a_2} \tag{7.2}$$

$$\Gamma_3 = S_{31}\frac{a_1}{a_3} + S_{32}\frac{a_2}{a_3} + S_{33} \tag{7.3}$$

where Γ_i is the reflection coefficient read by the ith reflectometer and the S_{ij}'s are the S-parameters of the two-port being measured.

In (7.1–7.3) there are only two independent ratios of the a's. The values of a_2/a_1, and a_3/a_1 for instance, are sufficient to calculate all the required a ratios. Through some lengthy algebra, these ratios can be eliminated from (7.1–7.3), yielding a relationship between the observed Γ's and the S-parameters being measured:

$$\begin{aligned}&\Delta - \Gamma_1\Delta_{23} - \Gamma_2\Delta_{13} - \Gamma_3\Delta_{12} \\ &\quad + \Gamma_1\Gamma_2 S_{33} + \Gamma_1\Gamma_3 S_{22} + \Gamma_2\Gamma_3 S_{11} - \Gamma_1\Gamma_2\Gamma_3 = 0\end{aligned} \tag{7.4}$$

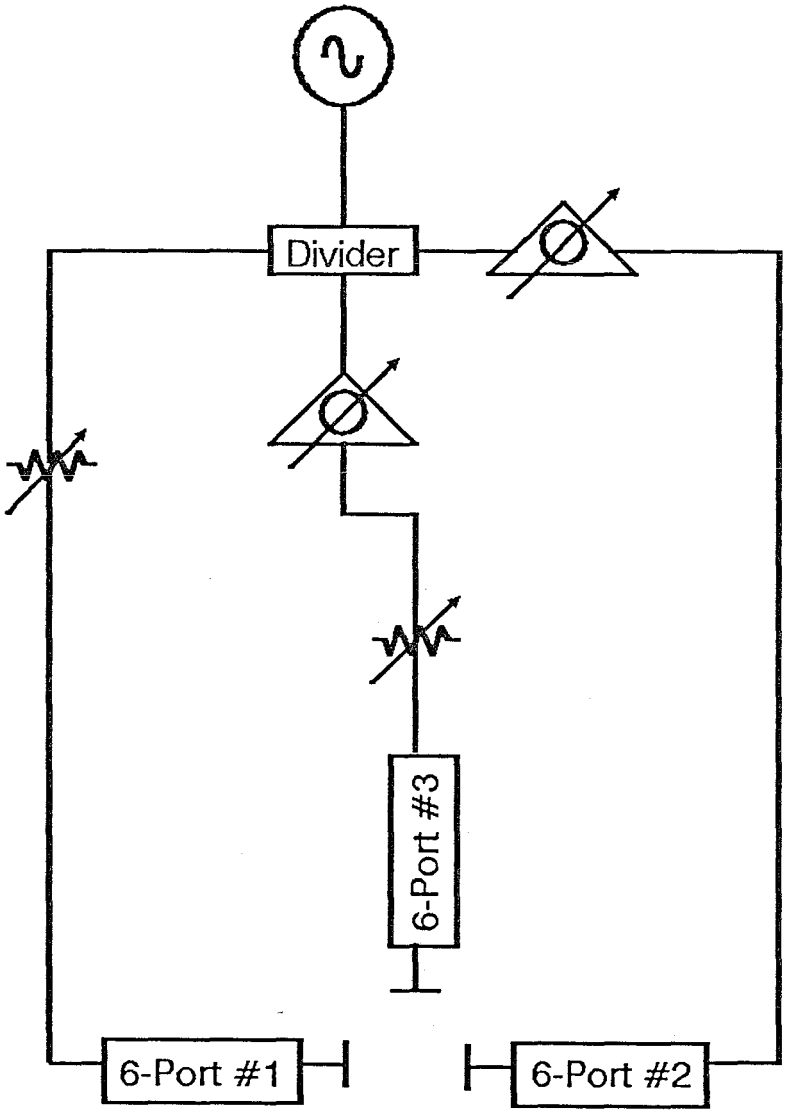

Figure 7.3 Architecture for a 3-port measuring system using sampled-line network analyzers.

where Δ is the determinant of the S-matrix and $\Delta_{ij} = S_{ii}S_{jj} - S_{ij}S_{ji}$.

This equation is analogous to equation (3.52) for the two-port case. It shows that three reflectometers can measure the full S-parameters of a reciprocal three-port network to within a sign ambiguity. The procedure is as follows. Equation (7.4) is seen as a linear equation in Δ, Δ_{12}, Δ_{13}, Δ_{23}, S_{11}, S_{22}, and S_{33}. By measuring the Γ's for at least seven different measurements of the a's, a set of linear equations is formed, which can be solved for $\Delta, \ldots, S_{33}$. In making these measurements, at least two of the a's must be varied. If only one changes then the columns of the resulting matrix will not be linearly independent. This is the reason for the two phase shifters shown in figure 7.3.

Solution of the set of linear equations gives S_{11}, S_{22}, and S_{33} directly. S_{12}, S_{23}, and S_{13} can then each be found to within a sign from Δ_{12}, Δ_{23}, and Δ_{13}. Of the eight possible combinations of signs for S_{12}, S_{23}, and S_{13}, only two give the correct value of Δ, the system determinant. Thus there is a single sign ambiguity in the determination of the S-parameters of reciprocal three-ports, as was the case in the two-port measurement system. If this ambiguity can be resolved through knowledge of the device under test, then the S-parameter measurement is complete.

If an independent way of resolving the sign ambiguity is required, or if the device under test is nonreciprocal, then an expression similar to (3.99) must be found, which gives a_2/a_1 and a_3/a_1 as a function of the observed Γ's. Equation (3.99), for the two-port case, gave

$$\frac{a_2}{a_1} = \frac{C_3 + C_1\Gamma_1}{1 + C_2\Gamma_2} \tag{7.5}$$

For the three-port case, the expression is similar, but the C's become bilinear transforms of Γ_3. The result for a_2/a_1 is

$$a_2/a_1 = \frac{\frac{K_1+K_2\Gamma_3}{1+K_3\Gamma_3}(K_4 + K_5\Gamma_1)}{1 + \frac{K_6+K_7\Gamma_3}{1+K_3\Gamma_3}\Gamma_2} \tag{7.6}$$

$$= \frac{\alpha_1 + \alpha_2\Gamma_1 + \alpha_3\Gamma_3 + \alpha_4\Gamma_1\Gamma_3}{1 + \beta_1\Gamma_2 + \beta_2\Gamma_3 + \beta_1\Gamma_2\Gamma_3} \tag{7.7}$$

There is a similar relationship for a_3/a_1. Each equation has seven coefficients that must be found in a calibration procedure and stored. A different set of these fourteen coefficients must be found and stored for each combination of positions of the phase shifters in the system. A set of at least seven reciprocal three-port calibration networks would be needed for this procedure.

So it is seen that as the number of ports on the device under test increases, the complexity of the calibration and measurement algorithms increase steeply. There is no fundamental theoretical problem in this extension, however, and a multi-head network analyzer, even with its more complex software, could perform measurements on multi-port networks much more quickly than a two-port network analyzer could. In situations where large numbers of multi-port networks must be measured, the added complexity might be justified.

APPENDIX :
INVERSION OF S-PARAMETER EQUATIONS

The desired result is a set of expressions for the true S-parameters of the device under test in terms of the measured values and the six calibration constants. The starting point is equations (2.20) and (2.29), which give the measured values in terms of the true values and the constants. The two equations of the same form that result from the reverse direction measurement complete the set. We begin the inversion by making the following definitions:

$$X_1 = \frac{S_{11} - \Gamma_L \Delta}{1 - S_{22}\Gamma_L} \tag{A1}$$

$$X_2 = \frac{S_{21}}{1 - S_{22}\Gamma_L} \tag{A2}$$

$$X_3 = \frac{S_{22} - \Gamma_L \Delta}{1 - S_{11}\Gamma_L} \tag{A3}$$

$$X_4 = \frac{S_{12}}{1 - S_{11}\Gamma_L} \tag{A4}$$

$$\Delta = S_{11}S_{22} - S_{12}S_{21} \tag{A5}$$

Then equations (2.20) and (2.29) can be rewritten, respectively, as

$$S'_{11} = \frac{X_1 + A}{BX_1 + C} \tag{A6}$$

$$S'_{21} = D + \frac{EX_2}{BX_1 + C} \tag{A7}$$

and similarly for the S'_{12} and S'_{22} equations,

$$S'_{12} = D + \frac{EX_4}{BX_3 + C} \tag{A8}$$

$$S'_{22} = \frac{X_3 + A}{BX_3 + C} \tag{A9}$$

These equations can be inverted:

$$X_1 = \frac{A - CS'_{11}}{BS'_{11} - 1} \tag{A10}$$

$$X_2 = \frac{S'_{21} - D}{E}(C + BX_1) \tag{A11}$$

$$X_3 = \frac{A - CS'_{22}}{BS'_{22} - 1} \tag{A12}$$

$$X_4 = \frac{S'_{12} - D}{E}(C + BX_3) \tag{A13}$$

So the quantities $X_1, \ldots, X_4$ can be expressed in terms of the measured quantities. It remains to solve for the S-parameters in terms of the X's. Expanding equations (A1) through (A4) gives

$$X_1(1 - S_{22}\Gamma_L) - S_{11} + \Gamma_L\Delta = 0 \tag{A14}$$

$$X_2(1 - S_{22}\Gamma_L) = S_{21} \tag{A15}$$

$$X_3(1 - S_{11}\Gamma_L) - S_{22} + \Gamma_L\Delta = 0 \tag{A16}$$

$$X_4(1 - S_{11}\Gamma_L) = S_{12} \tag{A17}$$

Using the expressions for S_{12} and S_{21} in equations (A15) and (A17) to expand Δ in equation (A14),

$$X_1(1 - S_{22}\Gamma_L) - S_{11} - \Gamma_L X_2 X_4(1 - S_{11}\Gamma_L)(1 - S_{22}\Gamma_L) + \Gamma_L S_{11} S_{22} = 0 \tag{A18}$$

$$X_1(1 - S_{22}\Gamma_L) - S_{11}(1 - S_{22}\Gamma_L) - \Gamma_L X_2 X_4(1 - S_{11}\Gamma_L)(1 - S_{22}\Gamma_L) = 0 \tag{A19}$$

$$X_1 - S_{11} - \Gamma_L X_2 X_4(1 - S_{11}\Gamma_L) = 0 \tag{A20}$$

$$S_{11} = \frac{X_1 - \Gamma_L X_2 X_4}{1 - \Gamma_L^2 X_2 X_4} \tag{A21}$$

which can be expanded to give

$$S_{11} = \frac{E^2(A - CS'_{11})(BS'_{22} - 1) - \Gamma_L(AB - C)^2(S'_{12} - D)(S'_{21} - D)}{E^2(BS'_{11} - 1)(BS'_{22} - 1) - \Gamma_L^2(AB - C)^2(S'_{12} - D)(S'_{21} - D)} \quad (A22)$$

And similarly for the other S-parameters:

$$S_{12} = \frac{E(AB - C)(S'_{12} - D)[(BS'_{11} - 1) - \Gamma_L(A - CS'_{11})]}{E^2(BS'_{11} - 1)(BS'_{22} - 1) - \Gamma_L^2(AB - C)^2(S'_{12} - D)(S'_{21} - D)} \quad (A23)$$

$$S_{21} = \frac{E(AB - C)(S'_{21} - D)[(BS'_{22} - 1) - \Gamma_L(A - CS'_{22})]}{E^2(BS'_{11} - 1)(BS'_{22} - 1) - \Gamma_L^2(AB - C)^2(S'_{12} - D)(S'_{21} - D)} \quad (A24)$$

$$S_{22} = \frac{E^2(A - CS'_{22})(BS'_{11}) - \Gamma_L(AB - C)^2(S'_{12} - D)(S'_{21} - D)}{E^2(BS'_{11} - 1)(BS'_{22} - 1) - \Gamma_L^2(AB - C)^2(S'_{12} - D)(S'_{21} - D)} \quad (A25)$$